Studying the application of lignin for the fabrication of high-performance membranes

by

Laleh Shamaei

A thesis submitted in partial fulfillment of the requirements for the degree of

Doctor of Philosophy

Department of Mechanical Engineering
University of Alberta

Abstract

Lignin is one of the most plentiful natural polymer on the earth, produced on a large scale as the waste of pulp and paper industries. The inherent properties of lignin, such as nontoxicity, cost-efficiency, and biocompatibility, make it suitable for the green modification of bulk and surface characteristics of membranes to mitigate the fouling phenomenon. Fouling is the major drawback to the widespread application of membrane technology for wastewater treatment. Among multiple approaches that have been employed to minimize membrane fouling, enhancing the surface hydrophilicity of membranes is found to be indispensable. Herein, an industrial waste derivative of lignin, sulfonated kraft lignin (SKL), was used as a hydrophilic modifier for the synthesis of microfiltration (MF), ultrafiltration (UF), and thin-film composite (TFC) forward osmosis (FO) membranes with improved antifouling and permeation performance.

In the first stage, SKL was used as a bulk modifier to synthesize antifouling polyethersulfone (PES) UF membranes using the phase inversion technique. Different SKL concentrations (1-3 wt%) were employed to tune the physicochemical properties of PES membranes. The fabricated membranes were employed to treat the steam-assisted gravity drainage (SAGD) produced water. The SKL-modified membrane containing the highest SKL additive content (3 wt%) provided the maximum flux recovery ratio of 98.2% compared to the 52.2% flux recovery ratio of the pristine PES membrane. The enhanced antifouling property of the SKL-modified membranes was primarily ascribed to their improved hydrophilicity and more negative surface charge. By adding 3 wt% SKL, the underwater oil contact angle increased by 14°, and the surface charge of the membrane became 3 times more negative under the operating pH (>8) of SAGD produced water, confirming the results of the antifouling tests. The water flux increased significantly from 25.3 LMH/psi (L m^{-2} hr^{-1} psi^{-1}) for the pristine membrane to 68.6 LMH/psi for 3 wt% SKL-blended

membrane, while the rejection of the organic matter slightly decreased from 61.7% to 56.1%.

In the second stage of this research, hydrophilic SKL was coated on the surface of PES membranes by layer-by-layer (LbL) assembly technique using SKL as a polyanion and poly (diallyldimethylammonium chloride) (pDAC) as a polycation. The effect of the polyelectrolyte concentrations (0.1-2 wt%) and the number of polyelectrolyte bilayers (1, 2, and 3) were investigated to fabricate UF membranes with improved antifouling property. The membrane made by 3 pDAC/SKL bilayers and 2 wt% concentration of the individual polyelectrolyte solution possessed the highest antifouling performance against the n-hexadecane-in-water emulsion as synthetic oily wastewater. This membrane exhibited a low total flux decline ratio (DR_t) of 23.1% and a high flux recovery ratio of 93.8% compared to 44.2% DR_t and 75.9% flux recovery ratio of the pristine membrane. The improved antifouling propensities of the LbL-assembled membrane could be related to the significantly higher underwater oleophobicity of this membrane (oil contact angle of 157°) compared to the pristine membrane (oil contact angle of 109°).

In the last stage, SKL was used as a hydrophilic modifier for the fabrication of TFC FO polyamide membranes with enhanced permeation performance and antifouling propensities. TFC membranes were fabricated by interfacial polymerization reaction between m-phenylenediamine (MPD) and trimesoyl chloride (TMC). The effect of SKL concentration was examined by dispersing different contents of SKL (1, 3, and 6 wt.%) in MPD-aqueous solution. The SKL-embedded membranes provided higher water flux and lower specific solute flux compared to the pristine TFC membrane. The membrane, modified with the highest content of SKL, possessed 33.5 LMH water flux when tested in FO setup using 2 M NaCl solution as draw solution and deionized water as feed solution. The antifouling property of the membranes was tested for the filtration of SAGD boiler feed water. The DR_t of the TFC membranes decreased from 36.5% for the pristine

membrane to 21.9% for the 6 wt% SKL membrane. The enhanced antifouling performance of the SKL-modified membranes was attributed to their improved hydrophilicity. The water-in-air contact angle decreased from 88.7° for the pristine TFC membrane to 70.6° for the TFC membrane modified with 6 wt% SKL.

The present study created wealth from waste, sulfonated kraft lignin, and showed the tremendous potential of lignin for green and value-added applications. This work opens up a new paradigm to develop high-performance membranes using industrial waste lignin.

Keywords: Agro-industrial waste; Lignin; Membrane filtration; ultrafiltration; forward osmosis; Fouling; Surface modification; Layer-by-layer (LbL) assembly; Thin-film composite; Interfacial polymerization; Oil sands produced water; Oily wastewater treatment; SAGD

Preface

This dissertation is the original work by Laleh Shamaei. The majority of the content in chapters 2, 3, and 4 were published in the following journals:

1. L. Shamaei,P. Karami, B. Khorshidi, M. Sadrzadeh, Novel lignin-modified Thin Film Composite Forward Osmosis Membranes: Waste Material for Wastewater Treatment, Submitted to J. Memb. Sci. (Under review)
2. L. Shamaei, B. Khorshidi, M.A. Islam, M. Sadrzadeh, Development of antifouling membranes using agro-industrial waste lignin for the treatment of Canada's oil sands produced water, J. Memb. Sci. 611 (2020) 118326.
3. L. Shamaei, B. Khorshidi, M.A. Islam, M. Sadrzadeh, Industrial waste lignin as an antifouling coating for the treatment of oily wastewater: creating wealth from waste, J. Clean. Prod. 256 (2020) 120304.

Acknowledgement

Finishing my PhD studies at the University of Alberta had always been one of my dreams and my wish would not have come through without the support and help of some incredible persons to whom I would like to express my deep appreciation.

Foremost, I would like to thank my supervisor, Dr. Mohtada Sadrzadeh. You have always been more than a supervisor for all of us. Your endless support, motivation, enthusiasm and guidance in academic and personal life always inspired me and made me persevere. I feel so proud to have the opportunity to work with you and learn from you.

My gratitude extends to my committee members, Dr. Marc Secanell and Dr. Cagri Ayranci for their guidance and support. I would like to take the opportunity and thank Dr. Behnam Khorshidi for his treasured support, mentorship, tremendous encouragement and understanding.

My sincere thanks also goes to my friends and colleagues at the Advanced Water Research Laboratory (AWRL) and the University of Alberta. I owe a special thanks to Dr. Amirreza Sohrabi for his constant encouragement throughout my PhD life. My deep appreciation goes to Dr. Mohammad Amirul Islam for his endless scientific and spiritual support. I also appreciate all the support that I received from Pooria Karami, Behnam Sadri, Amin Karkooti, Hassan Hosseini, Farhad Ismail, Masoud Rastgar, Asad Asad, Sadegh Aghapour Aktij, Parmiss Mojir Shaibani, Sadaf Noamani, Shirin Niroomand, Nusrat Helali, Kavya Suresh, Nandini Debnath, Ishita Biswas, Farshad Mohammadtabar, Ali Mohammadtabar, and Zayed Almansoori; thank you all.

I cannot express enough thanks to my family. Above all, I am extremely grateful to my parents for their unconditional love, caring and support. You have always been there for me and I feel secure knowing that you will always have my back.

Finally, I would like to express gratitude to the following agencies for the funding opportunity to undertake my studies: Natural Resources Canada (NRCan), The Natural Sciences and Engineering Research Council of Canada (NSERC), and Canada's Oil Sands Innovation Alliance (COSIA).

Table of Contents

Chapter 1 Introduction **1**

1.1 Water demand 2

1.2 Treatment of SAGD produced water 2

1.3 Membrane technology for wastewater treatment 4

1.4 Synthesis techniques of porous and dense membranes 6

1.5 Separation and transport mechanisms 8

1.5.1 Porous membranes 8

1.5.2 Dense membranes 9

1.5.3 FO membranes 10

1.6 Membrane Fouling 16

1.6.1 Surface modification of membranes 18

1.6.2 Modification of membrane bulk properties 24

1.7 Lignin, an agro-industrial waste 30

1.8 Research objectives 34

1.9 Thesis structure 35

Chapter 2 - Development of Antifouling Membranes using Agro-industrial Waste Lignin for the Treatment of Canada's Oil Sands Produced Water **36**

2.1 Introduction 37

2.2 Materials and methods 37

2.2.1 Chemicals and reagents 37

2.3 Characterization of kraft lignin 38

2.3.1 Fabrication of PES membranes 39

2.3.2 Evaluation of viscosity of the dope solution 40

2.3.3 Evaluation of the surface topography of the membranes 40

2.3.4 Evaluation of surface wettability of membranes 40

2.3.5 Evaluation of the surface potential of the membranes 41
2.3.6 Evaluation of hydraulic permeability of the membranes 41
2.3.7 Evaluation of molecular weight cut-off (MWCO) of the membranes 41
2.3.8 Evaluation of antifouling properties of the membranes 42
2.4 Results and discussion 43
2.4.1 Chemical characterization of the kraft lignin 43
2.5 Evaluation of the morphology of the membranes 46
2.5.1 Evaluation of the surface wettability of the membranes 50
2.5.2 Evaluation of the surface charge of the membrane 50
2.5.3 Evaluation of permeation performance and MWCO of the membranes 52
2.5.4 Separation performance and antifouling characteristics of the membranes 53
2.6 Conclusion 56
Chapter 3 Industrial Waste Lignin as an Antifouling Coating for the Treatment of Oily Wastewater 57
3.1 Introduction 58
3.2 Materials and methods 59
3.2.1 Materials 59
3.2.2 Preparation of LbL-assembled membranes 59
3.2.3 Probing the presence of lignin on coated membranes 61
3.2.4 Evaluation of pure water flux and hydraulic permeability of membranes 61
3.2.5 Evaluation of anti-fouling properties of the membranes 61
3.2.6 Evaluation of surface wettability of membranes 62
3.2.7 Evaluation of MWCO of membranes 62
3.2.8 Analysis of the surface topography of membranes 63
3.3 Results and discussion 63
3.3.1 Probing the presence of lignin on the coated membranes 63
3.3.2 Permeation performance and fouling properties of LbL-assembled membranes 64
3.4 Conclusion 70

Chapter 4 Novel Lignin-modified Thin Film Composite Polyamide Osmosis Membranes: Waste Material for Wastewater Treatment 71

4.1 Introduction 72

4.2 Materials and methods 73

4.2.1 Chemicals and reagents 73

4.2.2 Synthesis of TFC PA membranes 73

4.2.3 Characterization of physicochemical properties of membranes 74

4.2.4 Evaluation of membrane performance in FO 75

4.2.5 Evaluation of fouling performance of the membranes 78

4.3 Results and discussion 79

4.3.1 Chemical composition of the synthesized PA layer 79

4.3.2 Surface morphology and wettability of the TFC membranes 79

4.3.3 Characterization of the membrane transport properties 81

4.3.4 Evaluation of the fouling resistance of the membranes 84

4.4 Conclusion 85

Chapter 5 Conclusion and future work 87

5.1 Conclusion 88

5.2 Future work 91

5.3 List of contributions 92

5.3.1 Journal papers 92

5.3.2 Conference presentations 93

References 94

List of Tables

Table 1.1: Summary of the membrane separation technologies.....5

Table 1.2: Summary of the previous works on various surface modification techniques employed for modification of membrane properties 18

Table 1.3: Summary of the previous studies, employed organic materials for the bulk modification of membranes.24

Table 1.4: Summary of the previous studies, employed inorganic materials for the bulk modification of membranes 25

Table 1.5: Summary of the previous studies, employed agro-industrial wastes for the surface modification of membranes.....28

Table 1-6: Summary of the previous studies, employed agro-industrial wastes for the bulk modification of membranes 29

Table 2-1: Properties of SAGD BFW at 25 °C. The BFW was employed as the feed solution for evaluating the antifouling propensities of the synthesized membranes 38

Table 2-2: The concentration of the constituents employed for the synthesis of the membranes 39

Table 3.1: PE concentrations and number of PE BLs employed for the preparation of LbL-assembled membranes.60

Table 4-1: the values of μ, ρ, and D_S at 22 °C, employed for the calculation of the membrane's intrinsic properties [39–41] 76

List of Figures

Figure 1-1: Schematic diagram of conventional SAGD produced water treatment 4

Figure 1-2: Classification of polymeric membranes according to the bulk morphology, fabrication techniques, internal free volume, and application [17,21]. 7

Figure 1-3: Schematic diagram of the solute concentration profiles across TFC membranes in (a) AL-FS concentration and (b) AL-DS configuration at steady-state condition [24]. 16

Figure 1-4: Schematic presentation of fouling on the surface of membranes 17

Figure 2-1: Schematic diagram of the blending procedure for the fabrication of SKL-modified PES membranes. ... 40

Figure 2-2: (a) and (b) FESEM surface images and EDX compositional analysis of the as-received dry SKL powders; (c) ATR-FTIR spectrum of the SKL powders, revealing the presence of absorption bands corresponding to hydrophilic functionalities including aliphatic carboxylates, alcohols, phenols, and sulfonates in SKL; (d) Surface zeta potential of the SKL powders. Negative surface potential with no isoelectric point was observed over the pH range of 4 to 9. 45

Figure 2-3: Schematic representation of the predicted substructure of sulfonated kraft lignin 45

Figure 2-4: Cross-sectional FESEM images of pristine (M0), and the modified M1, M2, M3 membranes prepared with 1, 2, and 3 wt.% of SKL. 46

Figure 2-5: Variation of polymer solution viscosities versus shear rate for pristine (M0), and the modified M1, M2, M3 membranes prepared with 1, 2, and 3 wt.% of SKL additive. 47

Figure 2-6: FESEM surface morphology, AFM surface topography images, and surface roughness data of the pristine (M0), and the modified M1, M2, M3 membranes prepared with 1, 2, and 3 wt.% of SKL concentration 49

Figure 2-7: Underwater surface oleophobicity of pristine PES support (M0) and the modified membranes with 1 to 3 wt.% (M1-M3). The wettability analysis was performed applying the underwater captive n-hexane bubble. The higher oil contact angle represents the higher oleophobicity of the membranes. Photographs of the fabricated membranes acquired 24 hr after fabrication are also presented in this figure. 51

Figure 2-8: Surface zeta potential of the pristine PES and the modified M1, M2, M3 membranes prepared with 1, 2, and 3 wt.% of SKL concentration. 51

Figure 2-9: Pure water flux vs. TMP and hydraulic permeability of the prepared membranes. The modified membranes M1, M2, and M3 were synthesized, applying different SKL concentrations of 1, 2, and 3 wt.%, respectively. 52

Figure 2-10: MWCO and average pore size of the pristine (M0), and modified membranes (M1 to M3) synthesized with various SKL concentrations of 1, 2, and 3 wt.%. Dextran solutions were filtered using a dead-end filtration setup to determine the MWCO of the membranes. 53

Figure 2-11: (a) Permeation flux of pristine (M0) and modified membranes M1, M2, and M3, during filtration of SAGD BFW, (b) the respective fouling parameters of the synthesized membrane. The TMP for each modified membrane was adjusted to yield the same initial flux as M0 membrane. The modified membranes M1, M2, and M3 were synthesized, applying different SKL concentrations of 1, 2, and 3 wt.%, respectively. 55

Figure 3-1: Schematic diagram of LbL-assembly of pDAC and lignin over the PES substrate. The LbL technique relies on the alternative deposition of cationic (pDAC) and anionic (sulfonated kraft lignin) polyelectrolytes on the surface of the membrane.....60

Figure 3-2: XPS survey spectra and elemental composition of pristine PES support and the LbL-modified membranes with 1 BL (M1) and 3 BLs (M3) of the pDAC and lignin. 64

Figure 3-3: Pure water flux vs. TMP and hydraulic permeability of the prepared membranes. The modified membranes M2, M4, M5, and M6 were prepared with different polyelectrolyte concentrations of 2.0, 1.0, 0.5, and 0.1 wt.%, respectively. 65

Figure 3-4: (a) Permeation flux and (b) anti-fouling characteristics of pristine PES membrane and the LbL-modified membranes. The LbL-coated membranes, denoted as M2, M4, M5, and M6, were prepared with 2 BLs of pDAC/lignin using polyelectrolyte concentrations of 2.0, 1.0, 0.5, and 0.1 wt.%, respectively. TMP for each LbL-coated membrane was adjusted to yield the same initial flux as the pristine PES membrane (M0). 66

Figure 3-5: Pure water flux at different TMP on the membranes. The hydraulic permeability of the membranes was measured from the slope of the flux versus TMP plot. The modified membranes M1, M2, and M3 were fabricated by LbL-assembly of 1, 2, and 3 BLs of pDAC/lignin, respectively. The polyelectrolyte concentration was kept constant at 2 wt.%. 67

Figure 3-6: (a) Cyclic permeation flux of pristine (M0) and LbL-coated membranes M1, M2, and M3, during oil emulsion filtration, and (b) the respective fouling parameters of the membrane. The TMP for each LbL-membrane was adjusted to yield the same initial flux as M0 membrane. 67

Figure 3-7: Underwater surface wettability of pristine PES support (M0) and the LbL-modified membranes with 1 to 3 BLs (M1-M3). The wettability analysis was conducted using the captive n-decane bubble under water. The reported values in the figure are the water contact angle (CA), which is the complementary angle of the n-decane contact angle with the surface of the membrane.....68

Figure 3-8: MWCO of the pristine (M0), and LbL-modified membranes (M1 to M3) prepared with 1 to 3 BLs. PEG was used to determine the MWCO of the membranes. 69

Figure 3-9: FESEM surface images of pristine (M0), and the LbL-modified M1, M2, M3 membranes prepared with 1, 2, and 3 BLs of pDAC/lignin. The parameters r_a and r_q are the average roughness and root mean square roughness, respectively. 70

Figure 4-1: Schematic diagram of the fabrication of the TFC membranes via IP between MPD and TMC using SKL as an additive over the PES substrate. 74

Figure 4-2: ATR-FTIR spectra of the PES support and the synthesized TFC membranes (M0, M1, M2, and M3). .80

Figure 4-3: Top surface FESEM photos of the (a) M0 (pristine TFC), and SKL-incorporated TFC membranes (b) M1, (c) M2, and (d) M3. TEM cross-section images of the (e) M0, (f) M1, (g) M2, and (h) M3. Surface wettability of (i-l) the pristine (M0) and the SKL-modified (M1-M3) membranes. 80

Figure 4-4: AFM 3D and 2D images and the surface roughness results of the unmodified membrane (M0) and SKL-embedded TFC samples (M1, M2, and M3).....81

Figure 4-5: (a) Water fluxes versus effective osmotic pressure gradient in AL-DS mode; (b) Water permeability coefficient (A), and salt permeability coefficient (B). NaCl concentrations of 0.5, 1, 1.5, and 2 M were applied as the draw solutions. DI water was used as the feed solution and the cross-flow velocities of the feed and the draw sides were adjusted at 1 LPM. 82

Figure 4-6: (a) Permeation performance in AL-DS configuration, (b) reverse salt passage and specific solute flux in AL-DS configuration for 2 M draw solution; (c) Water flux in AL-FS operation mode; (d) Reverse salt flux and specific salt flux in AL-FS configuration for 2 M draw solution 83

Figure 4-7: Permeation flux and fouling parameters of the membranes during the filtration of (a) 1000 ppm of sodium alginate and (b) SAGD BFW in AL-FS configuration. The normalized water flux was calculated by dividing the corrected water flux by the initial water flux ($J_{cw,f}/J_{w,i}$). A, B, and C correspond to the initial sharp flux decline region, gradual flux decline region, and steady-state region, respectively. 84

Abbreviation

AFM	Atomic force microscopy
AL-DS	Active layer facing the draw solution
AL-FS	Active layer facing the feed solution
ATR-FTIR	Attenuated total reflectance-Fourier transform infrared
BBD	Boiler blow-down
BFW	Boiler feed water
BL	Bilayer
BSA	Bovine serum albumin
CP	Concentration polarization
DI	Deionized
DOM	Dissolved organic matters
ECP	External concentration polarization
EDL	Electric double layer
EDX	Energy-dispersive X-ray
FESEM	Field emission scanning electron microscopy
FO	Forward osmosis
HA	Humic acid
ICP	Internal concentration polarization
ICP-OES	Inductively coupled plasma-optical emission spectroscopy
IX	Ion exchanger
IP	Interfacial polymerization
LbL	Layer-by-layer
LMH	L m^{-2} hr^{-1}
MBR	Membrane bioreactor
MF	Microfiltration
MPD	M-phenylenediamine
MW	Molecular weight
MWCO	Molecular weight cut-off
NIPS	Nonsolvent induced phase separation
NMP	N-Methyl-2-Pyrrolidone

NP	Inorganic nanoparticles
OTSG	Oilfield-style once-through steam generator
PA	Polyamide
pDAC	Poly (diallyldimethylammonium chloride)
PE	Polyelectrolyte
PEG	Polyethylene glycol
PES	Polyethersulfone
PSF	Polysulfone
PVDF	Polyvinylidene fluoride
PVP	Polyvinylpyrrolidone
QCM	Quartz crystal microbalance
RO	Reverse osmosis
SAGD	Steam-assisted gravity drainage
SKL	Sulfonated kraft lignin
SDS	Sodium dodecyl sulfate
TDS	Total dissolved solids
TEA	Triethylamine
TEM	Transmission electron microscopy
TFC	Thin film composite
TMC	Trimesoyl chloride
TMP	Transmembrane pressures
TOC	Total organic carbon
UF	Ultrafiltration
VIP	Vapor induced phase separation
WLS	Warm lime softener
XPS	X-ray photoelectron spectroscopy

Nomenclature

A	Water permeability coefficient of FO membranes
A_m	Effective filtration area of membrane
B_s	Draw solute permeability coefficient

$C_{D,b}$	Bulk concentration of draw solution
$C_{D,m}$	Solute concentration at the interface of the draw solution-membrane active layer
C_f	Total organic carbon concentration of feed
$C_{F,m}$	Solute concentration at the interface of the membrane active layer-sublayer
C_i	Concentration of component i across a porous membrane
C_p	Total organic carbon concentration of permeate
dC_i/dx	Concentration gradient of component i across a dense membrane
d_h	Hydraulic diameter of the flow channel
D_i	Diffusion coefficient of component i across a dense membrane
d_p	Pore diameter of a membrane
dP/dx	Pressure gradient across a porous membrane
Dr_{ir}	Irreversible fouling ratio
DR_r	Reversible fouling ratio
DR_t	Total flux decline ratio
D_s	Salute diffusion coefficient
FRR	Flux recovery ratio
$J_{cw,f}$	Final corrected water flux in FO fouling experiments
J_f	Permeation flux during filtration of foulants
J_i	Transfer rate of component i across a membrane
J_s	Reverse solute flux of FO membranes
J_w	Pure water flux
$J_{w,b}$	Water flux of the baseline experiment of FO fouling tests
$J_{w,f}$	Final water flux of FO fouling experiment
J_{wf}	Recovered pure water flux after washing step of FO fouling test
J_{wi}	Initial pure water flux of fouling tests
k	Mass transfer coefficient
K	Resistivity of solute for diffusion across the porous sublayer of FO TFC membranes
L_c	Length of the flow channel
M	Permeate mass
n	Number of ionic species that each solute molecule can dissociate into
R	TOC rejection
R	Universal gas constant
Re	Reynolds number

RFD	Relative fouling degree
S	Structural parameter
Sc	Schmidt number
Sh	Sherwood number
T	Absolute temperature
ΔP	Hydraulic pressure difference applied across FO membranes
Δt	Measurement time interval
R_a	Average roughness
R_q	Root mean square roughness

Greek Letters

κ	A coefficient that reflects the nature of the porous medium
$\pi_{F,m}$	Feed osmotic pressure on the interface of the active layer and the porous sublayer
$\pi_{F,b}$	Osmotic pressure of the feed bulk solutions
$\pi_{D,b}$	Osmotic pressure of the draw bulk solutions
$\pi_{D,m}$	Osmotic pressure at the interface of the active layer and the draw solution
$\Delta\pi_e$	Effective osmotic pressure difference across the selective layer of FO membranes
$\pi_{D,e}$	Effective osmotic pressure
ρ	Water density
μ	Dynamic viscosity
v	Flow velocity
τ	Tortuosity of the sublayer of TFC membranes
δ	Thickness of the sublayer of TFC membranes
ε	Porosity of the sublayer of TFC membranes

Chapter 1

Introduction

1.1 Water demand

The most obvious manifestation of the water crisis is that 2.1 billion people lack access to safely managed-drinking water, and more than half of the water, sanitation, and hygiene-related deaths are due to unsafe drinking water [1]. Over the past few decades, urbanization, industrial expansion and agricultural developments have led to the consumption of a large volume of freshwater, as well as the production of a massive volume of wastewaters [2]. Therefore, it has been reported that the global water demand has increased twice as fast as the global population and will grow by 55% from 2000 to 2050 [3,4]. Thus, the produced wastewater must be treated to facilitate safe disposal into the environment and promote efficient reuse to minimize fresh water uptake. To that end, recently, immense efforts have been urged toward the development of efficient technologies for reclamation and recycling of wastewaters to preserve freshwater resources [2].

The oil sands industry in Canada is one of the sectors that cause concerns regarding water consumption. It uses between 0.4 to 5.5 barrels of water to produce one barrel of bitumen in in-situ operation [5,6]. The water uptake varies between facilities depending on the employed technology for bitumen recovery and water treatment methods [5]. In terms of fresh water consumption, in-situ extraction uses roughly 0.6 to 0.9 barrels of fresh water to produce one barrel of bitumen [7]. Due to the concerns regarding the treatment of the produced water and fresh water consumption in the oil sands industry, Alberta Environment and the Energy Resources Conversation Board (ERCB) obliged the in-situ operations to lessen the use of brackish and fresh water and maximize the recycling and reuse of the process-affected water [5]. Accordingly, in-situ extraction should reduce the fresh water and brackish groundwater uptakes to a maximum of 10% and 25% of the total make-up water, respectively [5]. Therefore, the ongoing expansion of Alberta's oil sands industry is dependent on a sustainable supply of water through recycling and reusing of the process-affected water.

1.2 Treatment of SAGD produced water

Alberta's oil sands production has rapidly increased over the past decades, as the production of the molasses-like hydrocarbon, bitumen, has increased since 2000 from 0.7 to 3.1 million barrels per day [6,8]. The bitumen in Alberta's oil sands constitutes about 97% of Canada's oil reservoirs

which is considered as the third largest reservoirs in the world [9]. In 2019, the in-situ extraction technologies accounted for about 50% of the total crude bitumen production in Alberta [8,9].

Steam-assisted gravity drainage (SAGD) operation is one of the most common in-situ extraction techniques during which a pair of horizontal wells is drilled and steam is injected through the top well or injection well [9,10]. The surrounding heavy oil is heated by the injected steam and its viscosity is decreased, allowing the heavy oil to flow into the bottom well, known as the production well [10]. Afterward, the emulsion of oil and steam condensate is pumped up to the ground level for separation of bitumen and treatment of water (**Figure 1.1**) [10]. The emulsion first goes through a sequence of gravity separation vessels to eliminate the gases and separate the bitumen and water [11]. This water is then de-oiled and mixed with recycled boiler blow-down (BBD) and make-up water (fresh and/or brackish) and goes through a warm lime softener (WLS) to separate silica [12]. Finally, the produced water is passed through some filters and ion exchangers (IX) to separate Ca^{2+} and Mg^{2+} so that the treated water meets the quality requirements of boiler feed water (BFW), as the feed of steam generators [12]. SAGD plants employ once-through steam generators (OTSG's), which are able to tolerate high concentrations of dissolved solids (8000-12000 mg/L) and organic matters (300-1000 mg/L) [11,12]. The traditional WLS-IX water treatment process is not able to decrease the content of total dissolved solids (TDS) and dissolved organic matters (DOM) in the BFW [11]. Due to the relatively low quality of BFW, OTSG's commonly generates a low-quality steam (75-80% steam), leading to the production of a large volume of BBD water [11]. A part of the BBD is then recycled in the WLS and the rest is directed to deep disposal wells, zero liquid discharge facilities, or third-party waste disposal operators [12]. To decrease the volume of disposal BBD water, evaporators are employed as a downstream recovery process [12]. Evaporators can also be used for direct desalination of the produced water to provide high-quality BFW; however, the energy uptake is high [12]. The high concentrations of TDS and DOM in BFW can also contribute to operational problems, including clogging of injection well, heat-exchanger fouling, and fouling in the downstream pipelines and equipment [11,13,14]. The environmental and economic demands necessitate applying more efficient technologies for the treatment and reusing of SAGD produced water. Membrane separation technology is a single-step technique that has shown great promise for wastewater treatment, as it is able to remove almost all divalent ions and silica and separate more than 90% of TDS and DOM [15]. Employing membrane-based separation processes for treatment of SAGD

produced water reduces the operating costs and produces high-quality BFW, which is suitable for higher efficiency drum boilers that consume less energy than desalination evaporators [12].

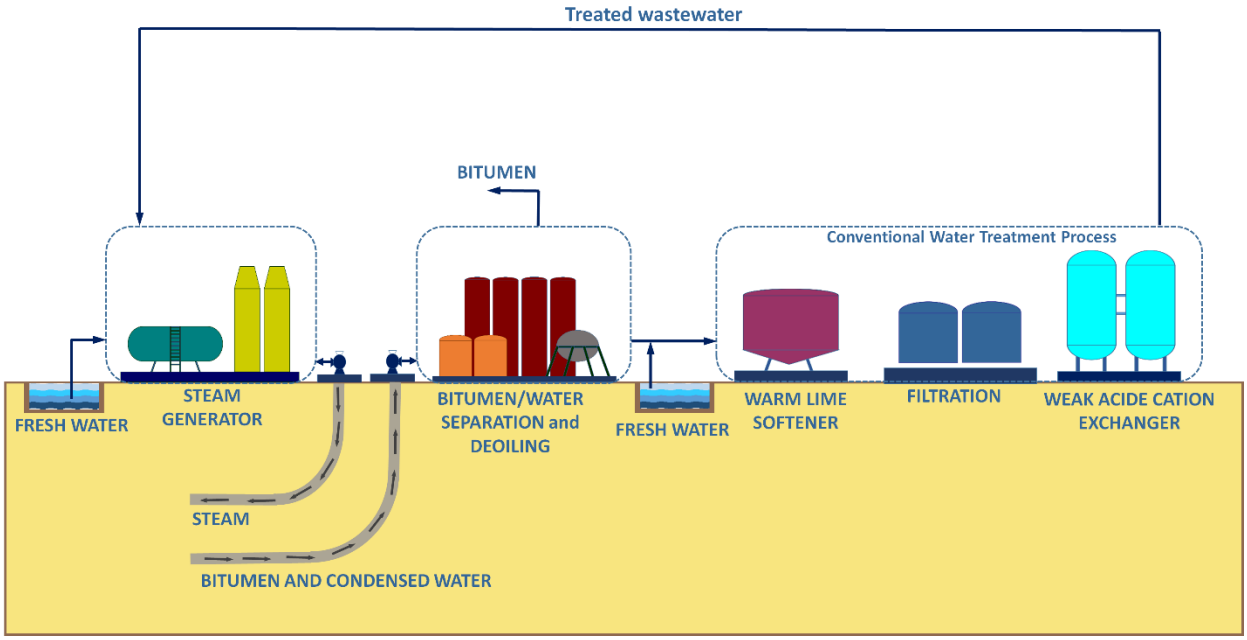

Figure 1-1: Schematic diagram of conventional SAGD produced water treatment

1.3 Membrane technology for wastewater treatment

Membrane technology has secured an important place in wastewater treatment due to its advantages, including negligible chemical footprint, compact modular structure, and high-quality end product [16]. A membrane is a thin interface between two phases that allows selective mass transport [17,18]. The selective separation is achieved due to the differences between physical and chemical properties of membrane and constituents of feed solution: solvent and solute(s) [19]. Under the applied driving force, the solvent and the solutes move toward the membrane, where the solvent passes across the membrane while the solutes are either retained in the feed side or transported across the membrane based on their size, activity, charge, or partial pressure [19].

Table 1.1 shows an overview of different membrane processes. Transport through a membrane can be driven by pressure, temperature, or concentration gradient across the membrane [17]. Pressure-driven membrane processes are the most common ones and can be categorized as microfiltration (MF), ultrafiltration (UF), nanofiltration (NF), and reverse osmosis (RO). MF membranes with the average pore diameter on the order of 10 µm to 0.1 µm are mostly used for

the separation of large colloidal and particulate organic matter [11,17]. The average pore diameter of UF membranes is in the 0.1 μm to 1 nm range and can filter out dissolved bio-macromolecules, such as proteins and viruses [17,20]. NF membranes can reject species in the range of 1 nm to 0.5 nm in size, which includes most viruses and organic molecules [20,21]. NF membranes can filter divalent ions as well; therefore, they are used to soften hard water [20]. The free-volume size of RO membranes is less than 0.5 nm to 0.3 nm, which is in the thermal motion range of the polymer chains of the membrane [20,21]. RO membranes can separate low-molecular-weight species, including aqueous inorganic solids (such as salt ions, metal ions, and minerals) and organic molecules (such as glucose and sucrose) [17,20].

Nevertheless, pressure-driven membrane processes need the use of electricity, an increasingly expensive form of energy, to produce the hydraulic pressure. This drawback has led to the emergence of osmotically driven membranes, such as forward osmosis (FO) [22]. The FO process is an engineered osmotic process in which the driving force is the concentration or osmotic pressure difference [23]. The semi-permeable FO membranes with the free-volume size of 1 nm to 0.4 nm allow tiny molecules such as water to pass through the membrane while blocks larger molecules, including salts, starches, sugars, viruses, proteins, bacteria, and parasite [23].

Table 1.1: Summary of the membrane separation technologies

Filtration process	Type of membrane	Materials passed	Materials retained	Driving force	Transport mechanism
Microfiltration	Porous with an average pore diameter of 10 μm - 0.1 μm	Water, Dissolved solutes	Colloidal and particulate organic matter, oil	Pressure difference	Sieving
Ultrafiltration	Porous with an average pore diameter of 0.1 μm - 1 nm	Water, Dissolved salts	Dissolve bio-macromolecules, such as proteins, Pyrogens, Viruses	Pressure difference	Sieving
Nanofiltration	Porous with an average pore diameter of 1 nm - 0.5 nm	Water, Dissolved salts	Most viruses and organic molecules, Divalent ions	Pressure difference	Sieving
Reverse osmosis	Dense with the free-volume size < 0.5 nm - 0.3 nm	Water	Aqueous inorganic solids and organic molecules	Pressure difference	Solution diffusion
Forward osmosis	Dense with the free-volume size < 1 nm - 0.4 nm	Water	Salts, Starches, Sugars	Concentration difference	Solution diffusion

Polymeric membranes can be classified based on morphology or bulk structure into symmetric (isotropic) and asymmetric (anisotropic) membranes. The symmetric membranes consist of a uniform structure throughout the entire membrane cross-section. The thickness of the symmetric membranes ranges approximately from 10 μm to 200 μm [17]. The mass transfer resistance of the symmetric membranes is defined by the total thickness of the membranes [17]. Asymmetric membranes have a very dense top layer, or skin layer, supported by a porous sublayer, where the selective layer performs the actual separation function and the porous sublayer provides the mechanical integrity [21]. The mass transfer resistance of asymmetric membranes is defined mainly by the thin top layer [17]. The asymmetric membranes provide the high selectivity of dense membranes and the high permeation of thin membranes [17]. The skin of the asymmetric membranes has a thickness of about 0.1 μm to 0.5 μm compared to the sublayer thickness of 50 μm to 150 μm [17]. The asymmetric membranes can be classified as integrally skinned and thin-film composite (TFC) membranes [24]. The integrally skinned membranes are formed in a single-step fabrication process, and the resulting membranes serve as both the porous support and the dense skin layer [25]. TFC membranes, developed in the late 1970s, are synthesized through a multiple-step operation by forming an ultrathin selective layer on a porous support layer, where the support and skin layer possess different structures and materials [24,25].

Polymeric membranes can be categorized in terms of internal free-volume into porous and dense membranes [11]. Porous membranes such as MF and UF have a rigid structure consisting of randomly spread, interconnected pores [21]. Dense membranes do not possess pores, but their chain segments have thermally stimulated motions that produce penetrant-scale transient voids (free volumes) in the membrane matrix [26]. These free volumes allow the penetrants to diffuse across the membrane [26]. Most pervaporation, gas separation, NF, FO, and RO processes use dense membranes to conduct the separation [21].

1.4 Synthesis techniques of porous and dense membranes

Figure 1.2 classifies membrane fabrication techniques by bulk morphology and internal free volume of membranes. Among these techniques, phase inversion, also called phase separation, is the most versatile fabrication technique that is widely used to synthesize both isotropic and anisotropic porous membranes [21]. Interfacial polymerization (IP) is the most accepted route for synthesizing TFC membranes [25].

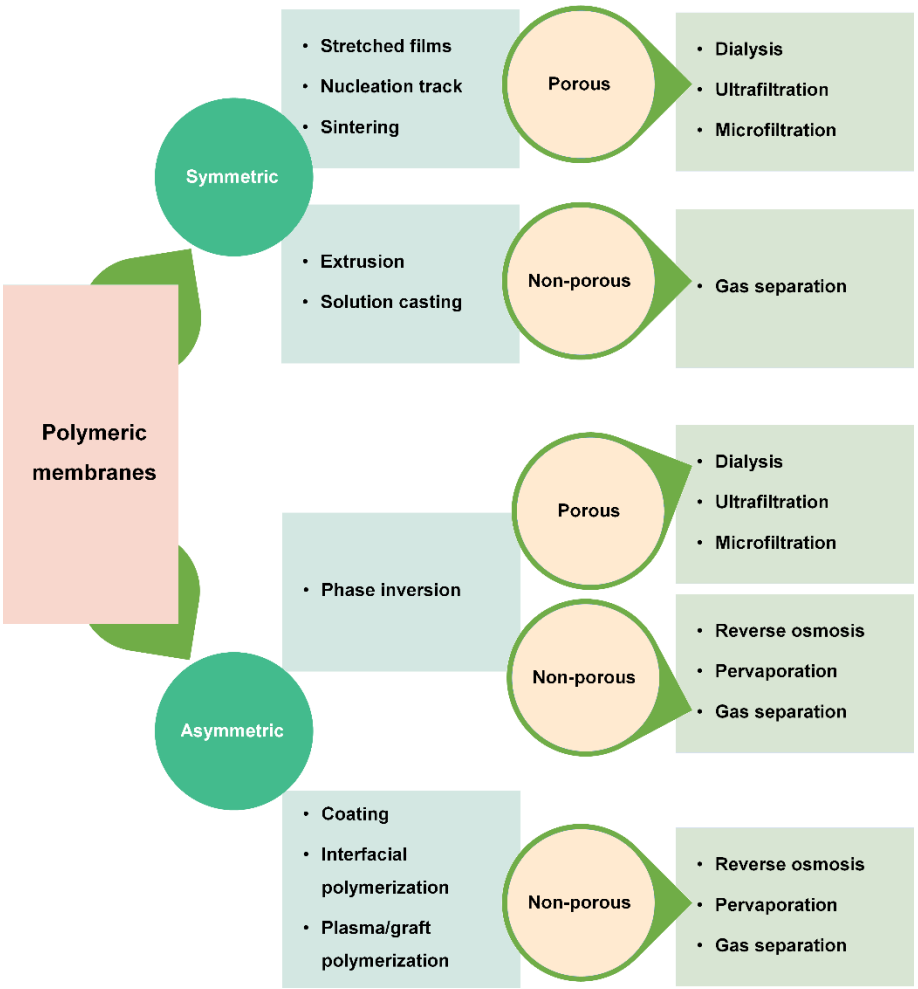

Figure 1-2: Classification of polymeric membranes according to the bulk morphology, fabrication techniques, internal free volume, and application [17,21].

The modern era of membrane technology started with the fabrication of the first integrally skinned asymmetric membrane by Loeb and Sourirajan in the late 1950s [24]. They employed the so-called phase separation method that became the foundation for a discipline that revolutionized the field of separation. As the term phase separation implies, during this fabrication technique, a one-phase casting liquid solution is precipitated into two separate phases: a solid, polymer-rich phase that forms the membrane matrix and a liquid, polymer-poor phase that creates the membrane pores [27]. Precipitation of the liquid polymer solution can be performed in several methods. Precipitation can be achieved by immersing the polymer solution into a bath of non-solvent (mainly water) or by penetration of water vapor from a moist atmosphere [21]. Precipitation can also be obtained by casting a film of high-temperature polymer solution and then reducing the temperature to initiate the precipitation [21]. Another precipitation method involves casting a

polymer solution (not necessarily in high temperature) containing a volatile solvent and a nonsolvent (typically water) [17]. As the volatile solvent evaporates, the cast film is enriched in nonsolvent and eventually precipitates [17]. The nonsolvent-induced phase separation technique is the most widely practiced method for fabricating asymmetric porous membranes [27]. During this technique, the film of thermodynamically stable polymer solution is immersed into a nonsolvent (usually water) bath [28]. When the homogeneous polymer solution comes in contact with the nonsolvent, solvent leaves the polymer solution, and solvent enters the film leading to the increase of the nonsolvent concentration at the film's surface, and consequently, phase separation occurs [27]. However, in the interior parts of the film, the polymer concentration is lower than the limiting concentration of phase separation [27,28]. Therefore, the phase separation first takes place at the surface of the film, which results in the formation of a very sharp gradient in the polymer chemical potential and net polymer movement perpendicular to the surface. Hence, the polymer concentration in the surface is enhanced, and the dense surface layer makes the skin of the membrane. This skin layer acts as a rate-limiting barrier for the transport of the nonsolvent into the polymer solution, leading to a less steep polymer concentration gradient, slower precipitation, and consequently formation of a structure of randomly distributed pores [27].

Interfacial polymerization is the most common technique for the synthesis of composite asymmetric membranes. In this technique, a microporous membrane is employed as the support for the formation of a dense, thin separating layer through interfacial polymerization technique. This technique is widely used for the fabrication of anisotropic NF, RO, and FO membranes [21]. The microporous support first is impregnated with an aqueous solution of a reactive monomer (such as diamine). Afterward, the amine-loaded support is immersed into a water-immiscible organic solution of a multivalent cross-linking component (such as polyacyl chloride) [21]. The amine and reactant react at the interface of the two immiscible solutions leading to the formation of an extremely thin (on the order of 0.1 μm) and densely cross-linked polymer film [21].

1.5 Separation and transport mechanisms

1.5.1 Porous membranes

The most important characteristic of a membrane process is the possibility of controlling the permeation of different constituents of feed solution. Separation in microporous membranes takes

place by molecular sieving mechanism, which is based on the shape and the size of the solutes relative to the membrane pores. In this mechanism, some of the permeants are excluded from the membrane pores while other permeants are able to pass through [21]. Surface pores in these membranes are smaller than some particles in the feed solution, leading to the capture and accumulation of these particles on the membranes' surface [21].

Pore-flow model is used to describe the permeation mechanism in a porous medium [21]. According to this model, the permeants are transferred through a membrane by pressure-driven convective flow across tiny pores [17]. Darcy's law (**Equation 1.1**) is the basic equation for describing transport in porous media:

$$J = -\frac{\kappa}{\mu}\frac{dP}{dx} \tag{1.1}$$

In this equation, J is the volume flux, κ is a coefficient that reflects the structural factors of the porous medium, μ is the fluid viscosity, and dP/dx is the pressure gradient across the porous medium [29]. Darcy's law is the best to explain the transport phenomena for the membranes in that the pores are relatively large, fixed and attached to one another [21]. For these membranes, the pores do not oscillate in volume or location on the permeant motion timescale [21].

1.5.2 Dense membranes

Separation in dense membranes takes place due to the solubility and diffuse rate differences of solute molecules within the membrane [20]. In dense membranes, the free-volumes are tiny voids between polymer chains resulted from the thermal motions of the polymer molecules. These voids appear and disappear on the timescale of the permeant motions [21]. Diffusion through these randomly distributed free-volumes is the dominant transport mechanism in dense membranes [20]. Solutes first are dissolved in the membrane surface [20]. Afterward, the dissolved solutes diffuse through the membrane due to the concentration gradient along the membrane's cross-section due to the applied osmotic pressure difference [20]. The dissolved solutes are then desorbed on the permeate side to complete the transport process [11].

The solution-diffusion model is used to explain the transport of flow in dense membranes [21]. According to this model, transport phenomena occur under a concentration gradient. In the absence of a concentration gradient, the molecules are in random molecular motions in the membrane

medium with no preferred direction [21]. However, if a concentration gradient of penetrants is exerted across the medium, a net transport takes place from the high concentration toward the low concentration region [21]. This phenomenon is formulated by Fick's law of diffusion as:

$$J_i = -D_i \frac{dC_i}{dx} \tag{1.2}$$

where J_i is the transfer rate of component i (g/cm^2.s), D_i is the diffusion coefficient (cm^2/s) which measures the mobility of each component, and dC_i/dx refers to the concentration gradient of component i across the membrane [21].

1.5.3 FO membranes

In FO process, there is a net flow of water through a selectively permeable membrane under the osmotic pressure difference ($\Delta\pi$) between a feed solution and a draw stream. The hydraulic pressures of the feed and draw sides are typically maintained at atmospheric pressure; therefore, the transmembrane pressure (ΔP) is zero [26]. The concentration of solute in feed stream is lower than that of the draw stream. The difference in the solute contents produces an osmotic pressure difference across the FO membrane, which forces the water molecules to move from the feed to draw solution to equalize the osmotic pressure of the streams without the passage of solute or ions. This selective passage is one of the outstanding features of the FO membranes [26]. A typical FO process involves two steps: the flow of water from the feed stream with low osmotic pressure to the draw stream with high osmotic pressure and the reconcentration of the diluted draw solution to produce freshwater [26]. The reconcentrated draw solution is usually reused as the draw solution to keep a constant osmotic driving force. The main advantages of FO over pressure-driven processes such as RO are the capacity of this technique to reject almost all solutes and ions and operating at atmospheric pressure [26]. Additionally, FO membranes have a lower fouling tendency. The attachment of foulants to the surface of FO membranes is loose and can be easily removed, which significantly reduces the need for membrane cleaning to keep the expected water flux [26].

A high-performance FO membrane is dense enough to separate solute molecules or ions of the draw and the feed solutions while allowing high water passage [26]. FO membranes are mainly asymmetric with a porous support layer and a dense selective layer, while the draw and the feed streams flow counter-currently or co-currently at both sides of the membrane. Thus, the FO process

can be conducted in two different membrane configurations, the active layer facing the draw solution (AL-DS) and the active layer facing the feed solution (AL-FS) [26].

When a liquid mixture with different permeation rates of individual components permeates through a semipermeable membrane, the less permeable components accumulate in the boundary layer next to the membrane surface, leading to a concentration gradient from the more concentrated boundary solution toward the less concentrated bulk solution [26]. This phenomenon is known as concentrative external concentration polarization (ECP) and occurs on the feed side of FO membranes in AL-FS configuration. The convective permeate flow in the draw side drags the solutes away from the membrane surface, leading to a phenomenon known as dilutive ECP, which dilutes the solute concentration at the membrane surface in AL-DS and causes increasing concentration gradients toward the bulk draw solution [30]. FO membranes are also accompanied by a more complex phenomenon, known as internal concentration polarization (ICP), due to their asymmetric structure [30]. In the AL-DS configuration, where feed flows against the porous sublayer, water enters this layer and diffuses through the active layer into the draw stream. The solute in the feed solution can freely enter the porous structure of the backing layer by convective water flow [31]. However, the solutes in the sublayer cannot easily penetrate through the dense active layer and accumulate within the porous sublayer. The accumulation of the feed salt and the salt penetrated from the draw solution results in increased solute concentration within the porous sublayer, leading to a phenomenon referred to as concentrative ICP [31]. In the AL-FS configuration, the draw solution is in contact with the sublayer, and the ICP phenomenon occurs on the permeate side. As water penetrates through the active layer from the feed side, it dilutes the draw solution within the porous substructure of the sublayer and results in dilutive ICP [30]. The influence of ECP can be significantly suppressed by increasing the turbulence and shear rate of stream, however; the effect of ICP cannot be effectively decreased by altering the hydrodynamic conditions since ICP takes place within the porous sublayer [32].

The support layer ensures the mechanical strength for the selective layer; therefore, it tends to be thick, porous, and tortuous [30]. The mass transfer of solutes and consequently the performance of the FO process closely depends on the membrane sublayer [24]. ICP has been coined to explain this phenomenon. Moreover, the structural properties of the sublayer profoundly impact the

diffusive transport of components and the severity of ICP [24]. The structural parameter, *S*, is commonly used as a general measure to describe the structure of the sublayer:

$$S = \frac{\delta\tau}{\varepsilon} \tag{1.3}$$

where δ is the thickness of the sublayer, τ is its tortuosity, and ε is its porosity [30]. A thinner support layer with higher porosity and lower tortuosity has a lower *S* value and can mitigate the severity of the ICP, and subsequently, it can maintain higher effective osmotic pressure difference across the selective layer [30].

The active layer, as the selective transport barrier, is another key element that its effect on the FO performance cannot be overlooked since the water flux and reverse solute flux strongly depend on the intrinsic properties of this layer [30]. The selectivity of FO membranes toward water molecules and the magnitude of the driving force significantly affect the diffusion of water molecules through FO membranes and consequently influence the water flux [30]. FO driving force is defined by the osmotic pressure difference, therefore; the water flux (J_w) depends on the osmotic pressure difference and the inherent water selectivity of the FO membrane, and can be described as [30]:

$$J_w = A\left[\left(\pi_{D,b} - \pi_{F,b}\right) - \Delta P\right] \tag{1.4}$$

where *A* is the water permeability coefficient of the FO membrane, $\pi_{D,b}$ and $\pi_{F,b}$ are the osmotic pressure of the draw and feed bulk solutions, respectively, and ΔP is the hydraulic pressure difference applied across the membrane [26,30]. Based on **Equation 1.4**, *A* quantifies the intrinsic selectivity of membrane toward water molecules and pure water permeation is directly proportional to *A* [30].

Likewise, the solute concentration difference between the draw and feed solutions and the solute selectivity of a FO membrane drive the solute diffusion through the membrane [30]. **Equation 1.5** describes the reverse solute flux of FO membranes (J_s) [26]:

$$J_s = B(C_{D,m} - C_{F,m}) \tag{1.5}$$

where *B* in this equation is the draw solute permeability coefficient, which is an indicator for quantifying the solute selectivity of FO membranes [30]. $C_{D,m}$ is the solute concentration at the

interface of the draw solution-membrane active layer and $C_{F,m}$ is the solute concentration at the interface of the membrane active layer-sublayer [26].

The experimental water flux under both AL-FS and AL-DS configurations considerably deviate from the theoretical fluxes calculated from **Equation 1.4** [26]. ICP and ECP have been known as the major causes of the low efficiency of the FO process. Concentration polarization reduces the effective osmotic pressure across the active layer, reducing the net driving force and water flux. Also, the solute diffuses reversely through the FO membrane and leaks to the feed solution, leading to a decrease in the effective driving force [26]. Therefore, **Equation 1.4** can be modified based on the effective osmotic pressure across the active layer as

$$J_w = A\left[\left(\pi_{D,m} - \pi_{F,m}\right) - \Delta P\right] \tag{1.6}$$

where $\pi_{D,m}$ and $\pi_{F,m}$ are the osmotic pressure of the draw and feed bulk solutions, respectively, at the interface of the active layer.

Under the AL-DS configuration (**Figure 1-3a**), dilutive ECP takes place and the concentration of the draw solution at the surface of the membrane ($C_{D,m}$) is much lower than the bulk concentration of draw solution ($C_{D,b}$). The mass transfer equation in this ECP boundary layer is as follows [33]:

$$J_s = D_s \frac{dC(x)}{dx} - J_w C(x) \tag{1.7}$$

At steady state condition, the salt flux, J_s, can be substituted from **equation 1.5** [33]:

$$B(C_{D,m} - C_{F,m}) = D_s \frac{dC(x)}{dx} - J_w C(x) \tag{1.8}$$

Following boundary conditions are applied to the **equation 1.8** [33].

$$C(x) = C_{D,m} \;\; at \; x = 0 \tag{1.9}$$
$$C(x) = C_{D,b} \;\; at \; x = t_b \tag{1.10}$$

where t_b is the thickness of the ECP boundary layer. Integrating **equation 1.8** across this boundary layer followed by applying the boundary conditions yields

$$C_{D,m} = C_{D,b} \exp(-\frac{J_w}{k}) - \frac{B}{J_w}(C_{D,m} - C_{F,m})\left[1 - \exp(-\frac{J_w}{k})\right] \tag{1.11}$$

where k is the mass transfer coefficient of the boundary layer [33]. The first term on the right-hand side of **equation 1.11** accounts for the bulk concentration of draw solution, $C_{D,b}$, modified by the effect of ECP, $exp(-J_w/k)$ [33]. The second term on the right-hand side of this equation applies the effect of decline in the solute concentration as a result of solute diffusion across the active layer [33].

Concentrative ICP also happens in AL-DS configuration (**Figure 1-3a**), resulting in a higher concentration of the feed solution at the interface of the active and support layers which traps the solute as a boundary layer. The mass transfer equation across the porous support layer is [33]:

$$J_s = \frac{D_s \varepsilon}{\tau} \frac{dC(y)}{dy} - J_w C(y) \tag{1.12}$$

At steady-state condition, the solute flux can be replaced from **equation 1.5** [33]:

$$B(C_{D,m} - C_{F,m}) = D_s \frac{dC(y)}{dy} - J_w C(y) \tag{1.13}$$

Assuming that the effect of ECP on the feed side is negligible due to the relatively large thickness of the support layer, the boundary layer conditions are as follows [33]:

$$C(x) = C_{F,b} \;\; at \; x = 0 \tag{1.14}$$
$$C(x) = C_{F,m} \;\; at \; x = \delta \tag{1.15}$$

Integrating **equation 1.13** across the sublayer results in

$$C_{F,m} = C_{F,b} \exp(\frac{J_w S}{D_s}) + \frac{B}{J_w}(C_{D,m} - C_{F,m}) \left[\exp\left(\frac{J_w S}{D_s}\right) - 1\right] \tag{1.16}$$

The first term on the right-hand side of this equation indicates the correction of the bulk feed solution concentration, $C_{F,b}$, by the concentrative ICP effect, $exp(J_w S/D)$ [33]. The second term on the right-hand side of **equation 1.15** presents the increase of solute concentration at the interface of the active layer and support layer due to the reverse solute passage from the draw side into the support layer [33]. Subtracting the **equation 1.16** from **1.11** and rearranging the resulted equations gives

$$C_{D,m} - C_{F,m} = \frac{C_{D,b} \exp(-\frac{J_w}{k}) - C_{F,b} \exp\left(\frac{J_w S}{D_s}\right)}{1 + \frac{B}{J_w}\left[\exp\left(\frac{J_w S}{D_s}\right) - \exp\left(-\frac{J_w}{k}\right)\right]} \tag{1.17}$$

The van't Hoff equation (**equation 1.18**) is used to correlate the osmotic pressure to the solute concentration:

$$\pi = nCRT \tag{1.17}$$

where n is the number of ionic species that each solute molecule can dissociate into, C is the solute concentration (mol/L), R is the universal gas constant (8.314 J/mol K), and T is the absolute temperature (K) [48].

Calculating the effective osmotic pressure difference ($\pi_{D,m}$-$\pi_{F,m}$) and substituting into **equation 1.6** yields:

$$J_w = A\left\{\frac{\pi_{D,b}\exp\left(-\frac{J_w}{k}\right) - \pi_{F,b}\exp\left(\frac{J_w S}{D_s}\right)}{1+\frac{B_s}{J_w}\left[\exp\left(\frac{J_w S}{D_s}\right) - \exp\left(-\frac{J_w}{k}\right)\right]} - \Delta P\right\} \tag{1.18}$$

which incorporates the performance-limiting phenomena of ECP and ICP, as well as the reverse solute permeation for the water flux in AL-DS configuration [33].

Under AL-FS operation mode (**Figure 1-3b**), the draw solution flows against the porous sublayer and leads to the formation of dilutive ICP at the draw side [26]. Consequently, the effective concentration of the draw solution at the interface of the sublayer and active layer is significantly lower than the bulk solution concentration. Concentrative ECP also happens in AL-FS mode at the feed side, which leads to the higher effective concentration of the feed solution at the surface of the membrane. Water flux in AL-FS can be derived following the same steps as was performed for AL-DS configuration. Following equation represents the water flux in AL-FS mode, incorporating the effect of ECP and ICP as well as the solute passage through the membrane [34] [24]:

$$J_w = A\left\{\frac{\pi_{D,b}\exp\left(-\frac{J_w S}{D_s}\right) - \pi_{F,b}\exp(\frac{J_w}{k})}{1+\frac{B_s}{J_w}\left[\exp\left(\frac{J_w}{k}\right) - \exp(-\frac{J_w S}{D_s})\right]}\right\} \tag{1.19}$$

It has been observed that the water flux under the AL-DS configuration is higher than that under the AL-FS configuration. This is because, under the AL-FS configuration, the diluted ICP

within the porous sublayer is more significant than the diluted ECP under the AL-DS configuration [26]. Moreover, the effect of concentrative ECP on the effective osmotic pressure difference in the AL-FS configuration is more than that in the AL-DS configuration. Consequently, the effective osmotic driving force is always higher under the AL-DS configuration [26].

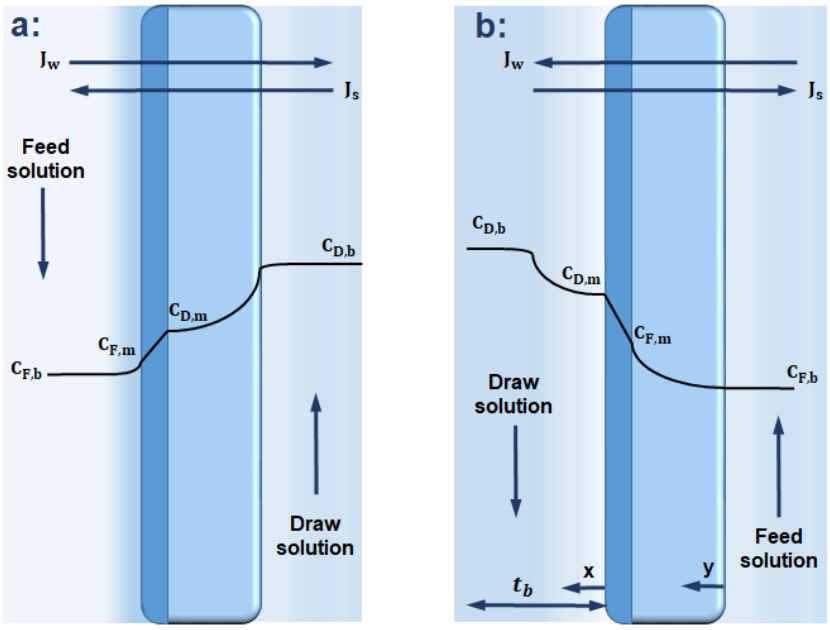

Figure 1-3: Schematic diagram of the solute concentration profiles across TFC membranes in (a) AL-FS concentration and (b) AL-DS configuration at steady-state condition [24].

1.6 Membrane Fouling

As an economical alternative to conventional water/wastewater treatment technologies, the membrane separation technique should not only provide a high-quality permeate with a fast rate but also need to be able to keep a high production rate for a long period. However, fouling is the main problem with membrane technology that seriously hampers the widespread application of this technique. The term fouling is used to explain the undesirable deposition of retained colloids, particles, and macromolecules at the surface of the membrane and/or inside the pores (**Figure 1-4**) [35,36]. As fouling progresses, the permeation flux declines, and higher operating pressure or more energy is required to gain the desired throughput. Depending on the membrane operation and the chemical nature of foulants, various types of fouling can happen in a membrane system. Fouling can be classified as particulate/colloidal fouling, inorganic fouling or scaling, organic fouling, and biofouling [36]. Colloidal fouling refers to the fouling of membrane surface with

suspended and colloidal particles with size from a few nanometers up to a few micrometers [37]. The formation of scale is caused by increasing the concentration of minerals and divalent ions above their solubility limits, leading to the ultimate precipitation of these materials on the membrane surface [35]. Organic fouling occurs by the deposition of organic compounds such as humic substances, proteins, and polysaccharides at the membrane surface [38]. Biologically active organisms cause biofouling that includes the colonization and growth of microbial organisms, leading to the formation of microbial biofilms at the membrane surface [35,37].

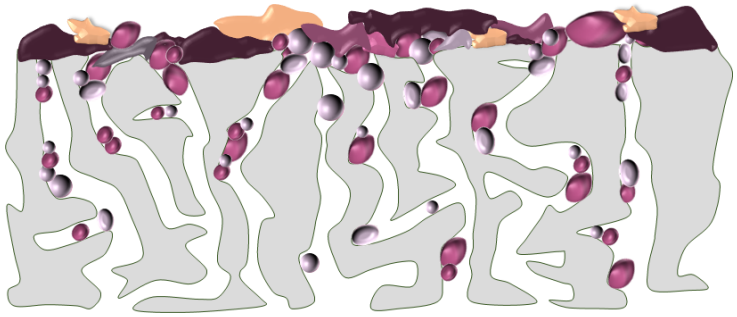

Figure 1-4: Schematic presentation of fouling on the surface of membranes

Various characteristics of the membrane surface, including hydrophilicity, roughness, and charge, are known to strongly affect the fouling tendency of membranes. Most of foulants are hydrophobic material, and can form strong hydrophobic interactions to unmodified membranes. There is a consensus in the literature that hydrophilic surfaces are less prone to fouling. The hydrogen bonding between water molecules and the membrane hydrophilic functional groups forms a thin layer of bounded water on the membrane surface. This layer prevents or decreases the undesirable adsorption/adhesion hydrophobic interactions of foulants to the membrane surface [39]. The surface roughness of membranes also strongly affects their fouling tendency. A higher surface roughness provides more surface area on membranes for the attachment of foulants [40]. Additionally, the ridge-and-valley structure of rough membranes favors the accumulation of foulants in the valley regions [39]. Therefore, it is likely that the membranes with rougher surfaces are more susceptible to fouling [40]. The surface charge of membranes plays an important role in their antifouling properties, as well. It is common to employ a membrane with the same surface electric charge as the foulants so that the electrostatic repulsion forces between the foulant and the membrane surface prevent the deposition of foulants on the membrane and thus mitigate the fouling [35].

Prevention of membrane fouling has been the goal of much research since the early 1960s [35]. There are three major areas of interest when it comes to reducing fouling and improving the membrane performance: modification of the filtration operating condition, modification of surface properties of membranes, and modification of bulk properties of membranes. To maximize the filtration efficiency, the operating conditions, such as properties of the feed solution**,** cleaning intervals, and operating pressure, must be optimized [39]. However, very often, such optimization is not adequate to cope with fouling, and further countermeasures must be employed to reduce the severity of fouling. Taking into consideration the profound influence of the surface characteristics of membranes on the fouling tendency, the main strategy to inhibit or decrease fouling is restraining the undesired adhesion/adsorption interactions between foulants and membrane through surface hydrophilization, surface smoothing, and introducing charged groups on the membrane surface [35].

1.6.1 Surface modification of membranes

Surface modification of membranes allows introducing desirable surface characteristics to the membrane while preserving the bulk polymer properties, such as chemical and mechanical stability [41]. Different surface modification techniques, e.g., plasma treatment, surface graft polymerization, physical coating/adsorption, and self-assembly, are summarized in **Table 1.2**.

Table 1.2: Summary of the previous works on various surface modification techniques employed for modification of membrane properties

References	Modifier	Support /resulting membrane	Surface modification technique	Target material to be removed /Foulant	Summary of results
Wavhal et al. [42]		PFS /(Ultrafiltration)	Carbon dioxide plasma treatment	BSA	• The water contact angle at the downstream side was reduced to zero for treatment times more than 1 min (P = 10 W). • Water fluxes of the modified membranes significantly increased compared to the control membrane. • Treated membranes had a nearly 100% flux recovery ratio after gentle cleaning in water.
Kim et al. [43]		Nanofiltration PA TFC membranes	Low-pressure NH_3 plasma treatment	NaCl solution BSA, Aldrich HA	After treatment, compared to the pristine: • The membrane surface hydrophilicity was enhanced. • Permeate flux increased with increasing plasma treatment time. • The protein adsorption decreased at higher plasma treatment time.

Kim et al. [44]		PSF	Oxygen plasma treatment	— Aqueous gelatin solution	The modified membranes had • Lower water contact angle at higher plasma treatment time. • Higher pure water flux and flow rate of gelatin solution. • 60% flux recovery ratio, while it was 50% for the untreated membranes.
Straub et al. [45]	[2-methacryloyloxy ethyl]-tri-methylammoniu and 3-sulphopropyl methacrylate	PVDF /(Ultrafiltration)	Redox-initiated graft polymerization	Soluble microbial products and extracellular polymeric substances extracted from municipal wastewater	For the modified membranes: • Contact angle reduced to 22.5° from 45.6° for the pristine membrane. • Water flux increased about 123% compared to the pristine membrane. • The averages of the TOC rejection increased to 66.9% from 55.4 % for the pristine. • Flux recovery after backwashing was 50%, while it was 37% for pristine membrane. • The flux at the end of the fouling test was 123% higher than that of the pristine membrane.
Ngo et al. [46]	Acrylic acid (initiators: $K_2S_2O_8$/ $Na_2S_2O_5$ solution)	PA TFC membranes	Redox-initiated graft polymerization	Reactive red dye RR261 Aqueous solutions of RR261 dye, BSA, and HA	After modification: • Water contact angle reduced to about 25° from 51° for the unmodified membrane. • Separation performance and water flux increased. • Total flux decline ratio and irreversible fouling factor decreased as compared to the unmodified one. • The maintained flux percentages during filtration of RR261, HA, and BSA solutions increased to 71%, 68%, and 57%, respectively. These values were only 50%, 47%, and 41% for the unmodified one.
Lu et al. [47]	Zwitterionic SPP ([3-(methacryloylamino) propyl] dimethyl (3-sulfopropyl) ammonium hydroxide),	PES/(Ultrafiltration)	Redox-initiated graft polymerization	Soluble microbial products from the biomass, sampled of an MBR in the Traverse City Wastewater Treatment Plant	• The water flux of the modified membrane reduced from 12.3 LMH to 7.6 LMH (38%) for SMP of 0.13 mg TOC/cm^2, and the water flux of the unmodified membrane decreased from 14.8 LMH to 9.1 LMH (39%). • The water permeability of the grafted membranes decreased about ~18% compared to the pristine one.
Gu et al. [48]	poly(vinyl alcohol)	PVDF /(Ultrafiltration)	γ-ray irradiation graft polymerization	soybean oil/water and chloroform/water emulsions	Modified membranes had • Oil rejection up to 99.5% and water flux up to 6.9 × 102 LMH/bar under low pressure (0.084 bar). • The flux recovery of 98% compared to 33% of the pristine membrane.
Liu et al. [49]	Poly(ethylene glycol) methyl ether methacrylate	PVDF	Electron beam irradiation graft polymerization	— BSA	After modification: • The contact angles decrease significantly. • The pure water flux improved from 180.4 LMH to 226.1 LMH. • The flux decline ratio decreased to 30% from 85% for the pristine membrane.
Shen et al. [50]	Hydroxyethyl acrylate	PVDF	γ ray radiation graft polymerization	— sodium alginate, BSA	After modification: • The pure water flux increased to 1096 LMH from 486 LMH for the pristine membrane. • The flux recovery ratio increased to 92.03% (69.68% for the unmodified membrane), and the irreversible fouling ratio decreased to 11.54% (32.76% for the unmodified membrane) for sodium alginate

					• The flux recovery ratio for the filtration of BSA reached 92.03%, which is higher than that of the pristine membrane (69.68%).
Park et al. [51]	Hyperbranched polyglycerols	PVDF /(Ultrafiltration /microfiltration)	Argon plasma-induced grafting + cross linking	BSA and lysozyme	• The surface hydrophilicity improved after modification. • The total flux decline ratio decreased 16%–33% after modification. • The membrane coated with negatively charged hyperbranched polyglycerols showed the highest fouling resistance.
Wavhal et al. [52]	Acrylamide	PES /(Ultrafiltration)	Argon plasma-induced graft polymerization	— BSA	After modification: • Flux recoveries increased. • The total flux decline ratio decreased about 18%. • Water flux increased from 100 LMH LMH to 300 LMH at 5 psi.
Chen et al. [53]	Poly(acrylic acid)	PVDF	Plasma induced (cold plasma-induced Ar, and O_2 gas) graft polymerization	commercial diesel oil-water emulsion	The modified membrane provided • A water flux of 832.52 L/m^2·min compared to 68.45 L/m^2·min of the pristine membrane. • COD rejection rate of more than 90%
Ju et al. [54]	Poly(ethylene glycol) diacrylate	PSF /(Ultrafiltration)	UV-initiated graft polymerization	Poly (ethylene glycol) Soybean and canola oil-water mixture	• Modified membrane possessed high organic rejection to oil/water mixtures. • Water permeability increased significantly from 10 LMH/bar to 150 LMH/bar. • During the fouling test, the water flux of the modified membranes was 400% higher than that of an uncoated membrane.
Igbinigun et al. [55]	Allylamine/ graphene oxide	PES /(Ultrafiltration)	UV-initiated graft polymerization	dextran A feed solution containing NaCl, $CaCl_2$, and HA	After modification: • The contact angle decreased to 55° compared to 76° for the pristine membrane. • The pure water flux decreased from 14074 LMH to 5577 LMH • 70% of the initial water flux was recovered. It was 28% for the pristine membrane.
Susanto et al. [56]	Poly(ethylene glycol) methacrylate	PES /(Ultrafiltration)	UV-initiated graft polymerization	Reconstituted sugarcane juice polysaccharides fraction or the protein BSA	All modified membranes exhibited: • Higher antifouling properties and rejection compared to the pristine. • Lower water permeability compared to the unmodified membranes.
Saraswathi et al. [57]	Polydopamine and silver nanoparticles	Poly (ether imide) /(Ultrafiltration)	Coating	BSA, HA and oil-water emulsion	The modified membranes possessed • Improved permeability (97.2 LMH), hydraulic resistance (13.8 kPaLMH), and contaminant rejection (>97%). • A higher flux recovery ratio (>95%). • High anti-biofouling property against gram negative as well as gram-positive bacteria.
Islam et al. [58]	Star-shaped block copolymers	PSF /(Ultrafiltration)	Coating by filtration	Dextran BSA	After modification: • The permeation flux increased almost 7 times during oil emulsion filtration due to 3 times improvement in the oleophobicity. • The flux recovery ratio increased to 100% compared to no flux recovery for the pristine membrane.
Wang et al. [51]	Dopamine and tetraethoxysilane	PVDF /(Microfiltration)	Coating	— Chloroform oil-water emulsion	• Water flux improved 34 times after modification. • Modified membranes had high oil-in-water emulsion separation efficiency at atmospheric pressure. • Excellent antifouling performance.

Li et al. [59]	Polyethyleneimine, poly(allylamine hydrochloride) and poly(sodium-4-styrene sulfonate), glutaraldehyde as a crosslinker and Pluronic F127	PSF /(Ultrafiltration)	Spray assisted LbL assembly	NaCl aqueous solution, boron BSA	After modification: • The salt rejection and permeate flux of the modified membrane were 92% and 11 LMH at 1.6 MPa, respectively. • After filtration of BSA solution, the water flux of the modified membrane decreased to 74% of the initial value (68% for the unmodified membrane) and was recovered to 87% (83% for the unmodified membrane)
Zhang et al. [60]	Hexadecyl trimethyl ammonium bromide (cross-linker: polyvinyl alcohol microspheres)	Terylene /(Micrfiltration)	Dynamic LbL assembly (filtration with a dead-ended filtration)	— Activated sludge (cultivated in submerged MBR with synthetic substrate)	By increasing the number of bilayers to 8 • The water contact angle decreased. • The water flux decreased to 3 ($m^3m^{-2}h^{-1}$) compared to 20 ($m^3m^{-2}h^{-1}$) for the unmodified one. • The flux decline ratio decreased to 47% from 93% for the pristine membrane. The flux recovery ratio also increased from 20% to 96%.
Liu et al. [61]	Poly (diallyl-dimethylammonium chloride), Poly (sodium 4-styrene sulfonate) with functionalized multiwall carbon nanotubes	PES	Spray-assisted LbL assembly	HA	By increasing the number of bilayers • Contact angle decreased to about 40° from 60° for the unmodified membrane. • Flux decline decreased. • The flux recovery ratio increased relative to the pristine (46%). • Rejection increased.
Diep et al. [62]	Core-shell star block copolymers	PSF /(Ultrafiltration)	LbL assembly by deposition	Congo Red dye	After modification: • The oil in water contact angle of the modified membrane decreased to 69° as compared to 103° of the unmodified membrane. • the modified membranes with 2.5-5 bilayers had high water flux (30 LMH -75 LMH) at 50 psi relative to other membranes for dye filtration (30 LMH -60 LMH under 70-150 psi)

(i) Plasma treatment:

Plasma is a highly reactive chemical environment, which consists of highly excited ionic, atomic, molecular, or radical species [41]. The ionized gas collides the reactants in the reactor and generates various kinds of radicals. By increasing the molecular weight of the products, they sediment on the surface of the membrane and form cross-linked polymer chains [17]. As presented in Table 1.2, various plasmas such as carbon dioxide, low-pressure NH3, and oxygen have been used in an attempt to increase the antifouling properties of membranes. However, the major drawback associated with this method is 'hydrophobic recovery', which refers to the alteration of the targeted properties of the modified surface with time. It is believed that in contact with a nonpolar media, the segments of the membrane surface chain gradually reorient [41]. This

reorientation can result in the time variation of the surface characteristics of the plasma-treated membrane [41].

(ii) Graft polymerization:

Surface graft polymerization is a chemical modification technique in which proper macromolecular chains are tethered on the surface of the membrane through covalent bonding [41]. This technique provides the advantage of tailoring the membrane surface to achieve distinctive properties through selecting various grafting monomers [41,63]. Despite the advantages of this technique, such as high chemical stability, it is an energy-intensive method. Therefore, the modification cost is high, which results in the difficulty to scale-up [64]. Based on the methods employed for the generation of reactive groups, surface grafting can be categorized as chemical-, radiation-, plasma- and UV-induced grafting.

In chemical-induced grafting, functional groups on the surface of membranes are activated and react with the monomers or macromolecules [65]. The initiators produce the active sites and transfer them to the substrate. The initiators then react with the monomers to form grafted copolymers [41]. Redox reaction, namely M^{n+}/H_2O_2, persulphates using various monomers such as acrylic acid, zwitterionic SPP ([3-(methacryloylamino) propyl] dimethyl (3-sulfopropyl) ammonium hydroxide), [2-(methacryloyloxy)ethyl]-tri-methylammonium and 3-sulphopropyl methacrylate can generate a typical free radical grafting (**Table 1.2**) [45–47].

In the grafting initiated by radiation technique, irradiation can result in hemolytic fission of membrane polymer chains and, therefore, can produce free radicals on the surface of the membrane for grafting polymerization [41]. As **Table 1.2** summarized some of the previous works, radiation-initiated grafting has been widely employed for the surface modification of polymeric membranes with various hydrophilic monomers, including poly(vinyl alcohol), poly(ethylene glycol) methyl ether methacrylate, and hydroxyethyl acrylate using γ ray radiation and electron beam irradiation [48–50]. However, high-energy radiation affects the outmost layer of the membrane and thus may change the chemical and physical properties of the substrate.

In plasma-grafting polymerization, exposing a polymeric membrane to plasma such as helium or argon for a short time produces many radicals at the membrane surface [41]. The membrane is then put in contact with a monomer vapor or solution at an elevated temperature [41]. Table 1.2

summarizes some of the previous works that employed plasma grafting to immobilize monomers, including poly(acrylic acid), acrylamide, and polyglycerols on the surface of membranes to improve the antifouling performance [51–53].

In UV-induced graft polymerization, surface groups of a polymeric membrane can turn into excited states by absorption of light. Consequently, they may dissociate into reactive radicals and increase the content of active species at the interface of the membrane surface and the monomer solution [65]. Therefore, the grafting process is initiated on the polymer chain [65]. However, UV irradiation may also cause the photodegradation of polymer membranes [41]. As presented in Table 1.2, different hydrophilic monomers, including allylamine monomer, graphene oxide, poly(ethylene glycol) methacrylate, poly(ethylene glycol) diacrylate, have been employed for the modification of polymeric membranes [54–56].

(iii) Coating:

Coating is a physical modification technique during which hydrophilic components are deposited on the surface of the membrane [41]. The deposition mechanism takes place through the adsorption/adhesion mechanism [41]. In this mechanism, the coating layer is physically attached to the base polymer, which leads to the major obstacle of this technique, instability of the coating layer [64]. As presented in Table 1.2, coating hydrophilic materials such as star-shaped block copolymers, silver nanoparticles, and polydopamine on the membrane surface can enhance the antifouling and permeation performance of membranes [57,58,66].

(iv) Layer-by-layer (LbL) assembly:

LBL-assembly is a new technique for the surface engineering of membranes. Film assembly in this technique is accomplished through alternated adsorption of polycations and polyanions [41]. The formation of the film is easy and can be used for almost any charged surface [41]. This method has many advantages, such as preparing an ultrathin multilayer with controllable thickness, surface potential, permeability, and structure at a molecular level [62,67,68]. The fabrication is based on spontaneous adsorption without a need for stoichiometric control to maintain the surface functionality [41]. LBL-assembly technique has been extensively used for immobilizing the hydrophobic material such as poly(styrenesulfonate)/ poly(diallyldimethylammonium chloride), chitosan/poly(acrylic acid), polymethacrylic acid sodium salt/ polyallylamine hydrochloride, and

poly(allylamine hydrochloride)/ poly(sodium-4-styrene sulfonate) on the surface of membranes (Table 1-2) [61,69,70].

1.6.2 Modification of membrane bulk properties

Modifying the bulk properties of membranes or blending technique is a process through which one or more hydrophilic components as additives are physically mixed into the primary polymer solution prior to the fabrication of membrane [64]. Unlike the surface modification techniques that require extra production steps and additional costs, blending requires minor adjustment to the composition of the polymer solution and is considered as the easiest method to manipulate the membrane properties [71]. Therefore, despite the emergence of many surface modification techniques, only facile blending-based methods are favored by industry [71]. Two categories of blending compounds have been studied: organic and inorganic materials. Various hydrophilic organic polymers, including polyvinyl pyrrolidone, polyethylene glycol, polyethylene oxide, Polyvinylalcohol, polycarbonate, and poly(amide-imide) have been employed for modification of membrane properties [72–74]. **Table 1.3** summarizes some of the studies that successfully employed organic modifiers for improving the fouling resistance of membranes.

Table 1.3: Summary of the previous studies, employed organic materials for the bulk modification of membranes

References	Additive	Base polymer /Resulted membrane	Target material to be removed /Foulant	Summary of Results
Zhang et al. [72]	Polyvinylalcohol	PVDF and Polyethersulfone /Ultrafiltration	— Wastewater of Quyang plant	The 0.3% polyvinylalcohol-blended membrane exhibited • Significantly higher hydrophilicity and permeability. • Significantly improved long-term antifouling properties. • Water contact angle of 58.8° (69.2° for the unmodified one)
Liu et al. [75]	poly(methylmethacrylate)-block-poly(ethyleneglycol)-block-poly (methylmethacrylate)	PVDF	BSA	The modified membranes showed • 150% higher water flux, 330% higher BSA solution flux, and 97% higher flux recovery ratio than those values for pristine membrane, Significant decrease in contact angle
Behboudi et al. [76]	Polycarbonate	PVDF	BSA	• Antifouling properties of membranes increased, and the water contact angle decreased (88.6° to 66.4°) with increasing the additive content. • The water flux increased from 403 kg/m^{2}h for the pristine to 1260 kg/m^{2}h for 70% polycarbonate membrane. • The pristine membrane had the least rejection while 50% polycarbonate membrane had 99% rejection.
Kakihana et al. [74]	A copolymer containing quaternary ammonium cations	PVDF	Polystyrene E. coli by bacterial	The modified membrane (blended with 0.9 wt.%) showed • Significantly high antibacterial activity against Escherichia coli (E. coli) as a model micro-organism foulant. • Oil in water contact angle of ~145°, much higher than the contact angle of ~110° for the pristine membrane • Almost 7 times higher water permeability, the rejection decreased to 80% (100% rejection of pristine).

Ahmad et al. [77]	Pluronic F127, bentonite nanoclay, inorganic salts (NaCl, KCl, NH_4Cl, $MgCl_2$ and $CaCl_2$)	polyvinyl chloride /Ultrafiltration	Polyethylene glycol and dextran Oil-field produced water	The KCl-blended membrane showed • Enhanced pure water flux (607.8 LMH), produced water permeate flux (265.7 LMH), and oil rejection (> 92.8%) compared to the other membranes. • Higher fouling resistance (flux recover ratio>71.65 %) compared to the other membranes. The KCl-bentonite nanoclay-blended membrane had • Super-hydrophilicity (water contact angle <10°). • Enhancement in the pure water flux and oil field produced water flux of 42.25 % and 37.61 %, respectively, while oil rejection >92.0 % compared to the other membranes.
Rahimpour et al. [73]	Poly(amide-imide)	PES /Ultrafiltration	Pasteurized and homogenized milk	After modification: • The flux recovery ratio increased to 82% compared to the flux recovery of 62% for the pristine. • The pure water flux increased from 150 kg/m^2h to 256 kg/m^2h and protein rejection slightly increased
Cheng et al. [78]	Amphiphilic terpolymer poly(styrene-acrylic acid–N-vinylpyrrolidone)	PES /Ultrafiltration	Polyethylene glycol BSA	After modification: • The water contact angle decreased to 74.6◦ compared to the pristine membrane, 84.2◦. • The water permeability increased from 22 ml/(m^2h mmHg) for the pristine to 154 ml/(m^2h mmHg) for the blended membrane and flux recovery ratio significantly improved.
Wu et al. [79]	Co-polymer Pluronic F127	PVDF /Ultrafiltration	BSA HA, Sodium alginate and BSA	The modified membrane had • Pure water flux of 82 LMH and the contact angle of 62° as compared to the pristine membrane with pure water flux of 14 LMH and the contact angle of 80°. • improved antifouling properties toward NOM models in the following order: BSA > SA > HA
Kaner et al. [80]	Copolymers of methyl methacrylate with two different zwitterionic copolymers, sulfobetaine methacrylate, and sulfobetaine-2-vinyl pyridine	PVDF /Ultrafiltration	BSA BSA, Soybean oil-in-water emulsion	The modified membranes had • Doubled water flux (up to 99 LMH/bar), similar BSA rejection (between 86% and 99%), lower contact angle, and complete fouling resistance against oil suspensions and protein solutions. • The water contact angle of 35° much lower than that for pristine membrane, 93°

Apart from organic polymers, inorganic nanoparticles (NPs) are other promising modifiers. To date, various types of inorganic NPs such as titanium dioxide, zinc oxide, and silica have been embedded as additives for enhancing the characteristics of membranes. **Table 1.4** presents a summary of the works on the NPS-incorporated membranes.

Table 1.4: Summary of the previous studies, employed inorganic materials for the bulk modification of membranes

References	Additive	Base polymer	Target material to be removed /Foulant	Summary of Results
Kumar et al. [81]	PSF and chitosan /Nanofiltration	Titanium dioxide nanotubes (TiO_2NT)	NaCl BSA	The TiO_2 modified membrane provided • A contact angle of 58°, whereas the unmodified membrane had a contact angle of 73°. • Higher water permeability than that of non-modified one. • Lower water permeability, higher salt rejection, and lower fouling flux decline.

Damodar et al. [82]	PVDF	TiO_2	— BSA	• The modified TiO_2 membranes had higher permeability. • 2% TiO_2 membrane showed lower fouling resistance compared to others. • 1% TiO_2 membrane had the lowest contact angle (82.2°), whereas 4% TiO_2 membrane had a contact angle of 87.6◦.
Yang et al. [83]	PSF /Ultrafiltration	TiO_2	BSA	• The modified membranes held excellent water permeability, hydrophilicity, and good anti-fouling properties with almost unchanged retentions. • Higher TiO_2 content (>2 wt.%) resulted in a decline in the performances of membranes.
Shen et al. [84]	PES /Ultrafiltration	SiO_2	BSA Raw water from Shangtang River	• All the membranes had 90% rejection of BSA. • The permeability of the membrane improved with an increase in the content of SiO_2 (0–2 wt.%). • The concentration of SiO_2>4wt.% caused a decrease in the membrane permeability. • The pristine membrane had a higher flux decline compared to the hydrophilic modified membrane.
Ahmad et al. [85]	PSF /Ultrafiltration	SiO_2 Palm oil-in-water emulsion		• The increase of SiO_2 content improved the water flux. • The best modified membrane had 16 times higher water. Permeability than that of the unmodified membrane. • By increasing SiO_2 content from 1.0 g to 3.0 g, the flux decline ratio decreased from 98.28% down to 86.55%, and the flux recovery ratio increased from 10.34% to 34.01%.
Liang et al. [86]	PVDF /Ultrafiltration	ZnO Sodium alginate, HA, BSA, $CaCl_2$/$MgCl_2$, $NaHCO_3$ NaCl		The modified membranes showed • 2 times higher water permeability compared to the pristine one. • Almost 100% flux recovery ratio whereas the pristine membrane only showed 78%.
Leo et al. [87]	PSF /Nanofiltration	ZnO	— Oleic acid	2 wt% ZnO membrane showed • A lower contact angle of 63° as compared to 85° for the pristine membrane. • Significantly higher flux decline than that of the pristine membrane. • The highest water permeability.
Akin et al. [88]	PSF and polyaniline /Ultrafiltration	Reduced graphene oxide	NaCl	The modified membranes exhibited • Higher permeability relative to the pristine membrane. • Maximum salt rejection of 82% for NaCl. • The water contact angles of 72° as compared to the pristine membrane, 82°.
Wang et al. [89]	PVDF /Ultrafiltration	Graphene oxide	BSA	After modification • The contact angle decreased from 79.2° for the modified membrane to 60.7°. • The permeability improved by 96.4%. • All membranes had a rejection of more than 90%. • The flux recovery ratio increased from 78% for the pristine membrane to 93% for the modified membrane.
Huang et al. [90]	PES /Ultrafiltration	Silver loaded sodium zirconium phosphate (nanoAgZ)	BSA BSA and suspension of E. coli or Pseudomonas sp.	The modified membranes exhibited • The contact angle of 52.6° compared to 71.5° for the pristine membrane. • Slightly lower rejection of 96% relative to 98.5% for the pristine membrane. • Enhanced BSA- and bio-fouling resistance.
Huang et al. [91]	PES /Ultrafiltration	Ag–SiO_2	BSA Suspension of E. coli or Pseudomonas sp.	The Ag–SiO_2-blended membranes showed • Higher pure water flux than that of the pristine membrane. • Lower contact angle of 52.6° compared to 67.7° for the pristine membrane. • Higher values of flux recovery ratio relative to the pristine membrane. • A clean surface free of bacteria growth.

Based on **Tables 1.3 and 1.4**, enhanced fouling resistance of membranes can be achieved by blending organic and/or inorganic materials with the polymer. Nevertheless, many complexities are involved in the membrane fabrication process with modifiers that must be considered. In the case of employing inorganic NPs, the interactions between host polymer and NPs are critical in fabricating defect-free membranes [92]. The weak compatibility of NPs with the host polymer and their aggregation and the subsequent non-uniform dispersion in the membrane matrix create non-selective voids that reduce the separation performance significantly [92]. In the case of organic/polymeric additives, the range of available additives that are suitable for membrane modification and are synthesized on a large scale is limited [93]. Most hydrophilic polymers, such as amphiphilic polymers, block-copolymers, and zwitterionic polymers, are expensive and costly for large-scale applications.

The need to develop cost-effective, sustainable and processable materials for membrane modification has shifted the attention of many industrial and academic researchers toward agro-industrial materials. The advantages of agro-industrial-based materials over synthetic or man-made materials are low cost, competitive properties, sustainability, recyclability, and biodegradability. Annually, about five billion metric tons of agro-industrial waste is produced via industrial processing of agricultural or animal products [94,95]. Accumulation of such an enormous amount of biomass not only increases waste management expenses but also results in adverse environmental impacts and waste of natural resources [96]. Therefore, as a result of the growing awareness about global environmental issues and the requirement of developing renewable materials, the principles of eco-efficiency, industrial ecology, green chemistry, and engineering have been combined to develop the next-generation materials for membrane modification. Various agro-industrial-derived materials have been successfully employed for surface or bulk modification of membranes. **Tables 1.5 and 1.6** summarize some previous studies that utilized agro-industrial waste for surface and bulk modification of membranes, respectively.

Table 1.5: Summary of the previous studies, employed agro-industrial wastes for the surface modification of membranes

Reference	Biopolymer	Base membrane /resulted membrane	Surface modification technique	Target material to be removed /Foulant	Summary of Results
Wang et al. [66]	Dopamine and tetraethoxysilane	PVDF /Microfiltration	Coating	Chloroform oil-in-water	The membrane, modified with optimized coating, had • high water flux which was 34 times greater than that of the pristine membrane. • Highly efficient oil separation ability at atmospheric pressure (flux of 140 LMH). • Excellent antifouling performance.
Mehta et al. [97]	Chitosan (cross-linker: glutaraldehyde)	TFC reverse osmosis	Coating	NaCl BSA	Modified membrane showed • 180% increase in water flux compared to the pristine membrane. • About 2.7% increase in divalent ion rejection compared to the pristine membrane. • The decline in contact angle from 46° to 29°. • The permeate flux decline of 42.30% as compared to 49.20% for pristine membrane.
Xu et al. [98]	Sericin	TFC reverse osmosis	Coating	NaCl, $MgCl_2$, Na_2SO_4 and $MgSO_4$ NaCl+BSA	Compared to the pristine membrane, the modified membrane exhibited • a degraded salt rejection higher than 94%. • Smoother surface. • More hydrophilic and negatively charged surface under neutral condition. • Enhanced fouling resistance. • 10% less flux decline ratio. • 15% more flux recovery ratio.
Song et al. [99]	Tannic acid (TA) and ferric ions	Polypropylene /Microfiltration	Coating	Petroleum ether, toluene, isooctane or hexadecane oil-water emulsions	The two-pot treated substrate had • The water contact angle of 0 compared to the water contact angle of 144.3° for the pristine membrane. • 4.5 times higher water permeability than that of the one-pot modified membrane. • Provided final oil contents of lower than 40 ppm.
Xu et al. [100]	Catechol and octaammonium polyhedral oligomeric silsesquioxane	Nanofiltration	Coating	Methyl Orange, Rose Bengal, Crystal Violet, Orange G, Acid Fuchsin, Methyl Blue and Solvent Blue II	The optimized nanocomposite membrane exhibited • The permeance of 1.26 LMH/bar with a rejection of 99% to Rose Bengal. • Remarkable separation performance for dye removal. • Stable performances along a two-day long-term test in DMF.

Table 1-6: Summary of the previous studies, employed agro-industrial wastes for the bulk modification of membranes

Reference	Biopolymer	Base polymer / resulted membrane	Target material to be removed /Foulant	Summary of Results
Qu et al. [101]	Cellulose fibrils	PES /ultrafiltration	BSA	Compared to the pristine membrane, • the contact angles of the modified membranes dropped gradually from 55.8 º to 45.8 º. • The pure water flux of the modified membrane reached a maximum of 813.3 LMH. • The water flux of the modified membranes increased by 1.36 times. • BSA rejections of composite membranes remained at a high level, 91% to 95%.
Manawi et al. [102]	Acacia gum	PES /nanofiltration	Lead nitrate SA	Compared to the pristine membrane, • The contact angle of the modified membranes decreased by 20%. • The permeate flux of the modified membranes increased by up to 130%. • Lead rejection with modified membranes was much higher. • Modified membranes had higher antifouling properties.
Kumar et al. [103]	Xanthan gum	PES /ultrafiltration	HA	After modification • The contact angle decreased from 72° to 64°. • Modified membranes had higher water permeability of 68.9 m/skPa. • Better rejection of HA for modified membranes was achieved.
Ibrahim et al. [104]	Tannic acid-functionalized halloysite nanotubes	PSF /nanofiltration	Salts (NaCl and Na_2SO_4) and dyes (reactive black 5 and reactive orange 16 BSA	The modified membranes exhibited • Increased hydrophilicity, antifouling performance. • Higher dye rejection (>90% of reactive orange 16 and > 99% for reactive black 5). • The highest pure water flux of 92 LMH compared to the pristine membrane of 18 LMH. • 16° less contact angle compared to the pristine membrane. • The flux recovery ratio of 74% compared to the pristine membrane of 27%.
Han et al. [105]	Heparin-like Polyurethanes PU	PES /ultrafiltration	BSA	After modification, the modified membrane showed • Higher hydrophilicity and lower water contact angles. • Higher permeability and antifouling properties. • Lower protein adsorption. • Suppressed platelet adhesion, prolonged clotting times, and reduced complement activation.
Jiang et al. [106]	Polydopaminena noparticles	PVDF /ultrafiltration	BSA	Compared to the pristine membrane, the modified membrane had • Enhanced permeate fluxes of pure water and protein solution. • Higher hydrophilicity. • Higher flux recovery ratio and lower flux decline ratio. • Higher protein rejection with the decreasing permeates flux.
Tafreshi and Fashandi [107]	Nanoparticles prepared from basil seed gum	PSF /ultrafiltration	Methylene blue and BSA	The low value of NPs yielded • 75.9% increase in the pure water permeability of the membrane. • The flux recovery ratio of 100%. • Long-term high antifouling properties.

Among various agro-industrial wastes, lignin is the most plentiful biopolymer after cellulose. Lignin serves as a continuous matrix component that strengthens the trunks and stems of plants [108,109]. The vast availability of lignin worldwide and its incredible potential as a raw material

have turned lignin into one of the most valuable bio-wastes and motivated numerous research on producing value-added lignin-derived products.

1.7 Lignin, an agro-industrial waste

In 1838, Anselme Payen observed that oxidizing wood with concentrated nitric acid followed by washing by an alkaline solution yielded losing a portion of its substance and leaving a major solid and fibrous residue that he called "cellulose" [110]. Later studies showed that the fibrous residue consisted of other polysaccharides besides cellulose [110]. The dissolved material contained higher carbon content than cellulose and was termed "lignin" by Schulze [111]. This term is derived from the Latin word 'lignum' meaning wood. Later, the technical development of pulping processes attracted more attention to lignin and its reactions [110]. The pioneering classical organic chemistry research of Klason, Nimz, Hibbert, Nakano, and others disclosed fundamental knowledge about the chemical nature of lignin [111]. After that, the advent of polymer concepts prepared a new framework that promoted the understanding of the physical and chemical behavior of lignin. Lignin is now known to have a complex structure consisting of various functional groups such as syringyl, p-hydroxyphenyl propane, and guaiacyl-type units [112]. The types and number of the inter-unit bonds and constitutive units vary depending on the extraction process, the wood species, and post-treatment methods [113].

In industrial applications, lignin is produced in large quantities as a by-product of paper processing, wood pulping, and similar industries [109,114]. Nowadays, kraft pulping, as the most common pulping process, produces about 50 million metric tons of kraft lignin annually in the form of black liquor [115–118]. The produced black liquor has long been considered as a low-value product and is mostly burned as an energy source for pulping boilers [116–119]. However, in most kraft mills, the produced energy is far greater than the internal energy demand [116,117]. Therefore, recently modern kraft mills are integrated with a kraft pulping plant to extract a part of kraft lignin from the black liquor [118,120]. As a result, 100 kilotons of kraft lignin is extracted per year that can be a raw material to produce value-added bio-products [116]. The inherent properties of lignin including sustainability, nontoxicity, biodegradability, cost-efficiency, and biocompatibility, led to the production of lignin-derived products as promising green composite materials [108,120–125].

Several works have studied the potential of lignin derivatives to control diseases including obesity, diabetes, and human immunodeficiency virus [126–128]. The studies of Hasegawa et al. [128] showed that lignosulfonic acid as a non-competitive inhibitor for α-glucosidase could hinder the activity of α-glucosidase and reduce the glucose uptake leading to control diabetes. Lignin-based components have also been employed in the production of supercapacitors and showed great potential to enhance cycling durability and gravimetric capacitance [129–131]. Mesoporous carbon fibers, produced from alkali lignin, were utilized by Ago et al. [130] to make supercapacitor electrodes. It was observed that the mesoporous structure of the lignin-based carbon fibers had a large pore distribution, which improved the electrochemical performance. Thus, the electrodes generated a high specific capacitance (205 Fg^{-1}) which was one of the highest among the biopolymer-derived electrodes. Studying the application of lignin-based products for generating high-performance batteries showed promising results as well [132,133]. Gnedenkov et al. [133] employed hydrolysis lignin for producing the cathodes of lithium batteries and reported that the lignin-modified battery possessed a significantly high discharge capacity of 450 $mAhg^{-1}$ at the discharge current density of 25 $\mu A/cm^2$. The potential of lignin-based products for wound dressing was examined in several works [134–136]. The findings of Spasojevic et al. [135] revealed that a model compound of lignin had antimicrobial influences on clinical bacterial strains, (e.g., L. monocytogenes and S. Typhimurium) with no toxic influences on the epithelial cells. The derivatives of lignin also have been employed by Wu et al. [137] as an adsorbent for the treatment of wastewater. It was reported that lignin could successfully be used as an adsorbent of Cr(III) for wastewater treatment. Zhang et al. [138,139] also employed a lignin derivative for stabilizing silty soils in the subgrade of the highway. They conducted a site test and compared the mechanical characteristics and bearing capacity of the lignin derivative with those of quicklime as the conventional soil stabilizer. They reported that the lignin-stabilized silt possessed higher mechanical characteristics relative to the quicklime-stabilized silt. In another work, Zhang et al. [140] systematically investigated the effect of influential factors such as the content of lignin, initial compaction, and curing time on the performance of the lignin-stabilized silty soil. It was observed that the content of lignin largely affects the mechanical parameters, particle size distribution, and pore volume of the stabilized silty soil.

The favorable properties of lignin such as hydrophilicity, film-forming ability, sufficient reactive functional groups, and compatibility with various industrial chemicals encouraged the

researchers to employ lignin for the modification of membrane characteristics, as well. Several works incorporated lignin into casting polymer solution and studied its effect on the performance and physicochemical characteristics of the modified membranes. Nevarez et al. [96] employed three types of lignin, namely, kraft, hydrolytic, and organosolv, to modify cellulose triacetate membranes. They used propionation reaction to improve the compatibility of the lignins with cellulose triacetate [96]. It was reported that among all the fabricated membranes, the propionated kraft lignin-modified membrane possessed the highest Young's modulus and tensile strength [96]. The results also showed that the elongation at break decreased for this membrane [96]. Moreover, higher propionation of lignin led to lower wettability and water flux for the modified membranes [96]. Alkali lignin was used by Vilakati et al. [141,142] as an additive for bulk modification of PSF membranes. They compared the performance of the lignin-blended membranes to that of the membranes, synthesized using PVP and PEG as additives. The lignin-incorporated membranes possessed higher permeation performance, thermal and mechanical stabilities relative to the PVP- and PEG-blended membranes. However, the incorporation of lignin increased the porosity of the membranes and consequently declined the tensile modulus, tensile strength, and rejection. Ding et al. [143] used cellulose nanofibrils and lignocellulose as additives to synthesize PSF UF membranes. It was reported that the membranes, modified with lignocellulose nanofibrils, possessed higher surface wettability, higher water flux, and thermomechanical stability relative to the cellulose-modified and pristine membranes. Ding et al. [144] also employed lignin-cellulose nanofibrils for modification of polyethersulfone (PES) membranes. Their findings revealed that the modified membranes exhibited enhanced surface wettability and mechanical performance compared to the unmodified membranes. Beck et al. [145] incorporated alkali lignin as a carbon nanofiber into polyacrylonitrile to fabricate electro-spun carbon nanofiber membranes with enhanced adsorption performance. The lignin-modified membranes exhibited significantly higher methylene blue adsorption capacity, permeability, and faster adsorption kinetics than traditional activated carbon sources. In an attempt to improve the antioxidant characteristics of membranes, Esmaeili et al. [146] incorporated lignin, extracted from birch wood, as an additive to fabricate PES membranes. The hydrophilicity, permeability, and antioxidant activity of the fabricated membranes improved by increasing the lignin content. They related the high antioxidant properties of the membranes to the presence of phenolic OH functional group in the structure of lignin. Zhang et al. [147] applied lignosulfonate to fabricate polysulfone membranes for electrolyte

transportation. They reported that the presence of lignin in the membrane structures facilitated the formation of larger pore and the prepared membranes showed high selectivity toward proton over methanol [147].

Although few studies have been performed on the application of lignin for the bulk modification of membranes, the surface modification of membranes by lignin received even less attention. In one study, Zhou et al. [148] investigated the potential of ammonium lignosulfonate to synthesize a TFC nanofiltration membrane using a poly(ether imide) substrate. The polyamide layer was formed by interfacial polymerization reaction between ammonium lignosulfonate and trimesoyl chloride as monomers. Despite the high organic solvent resistance, improved organic solvent permeability, as well as high rejection toward Brilliant Blue R-250, the fabricated membranes showed low NaCl and $MgCl_2$ rejection (~20%). Colburn et al. [149] also embedded lignin sulfonate on the surface of commercial nanofiltration membranes through an esterification reaction between lignin hydroxyl groups and carboxyl groups of the membrane surface. The lignin-embedded membranes showed a higher flux recovery ratio against BSA than the pristine membrane. However, the modified membranes possessed lower permeate flux without any improvement in rejection [149]. Colburn et al. [149] also studied the potential of lignin sulfonate as an additive for improving the fouling resistance, selectivity, and permeation performance of the cellulose membranes by employing ionic liquid cosolvents. The results showed that lignin-blended membranes possessed a considerably higher flux recovery ratio relative to the pristine membranes for the filtration of humic acid solution. This observation was related to the embedding of negative charges to the membrane surface. The lignin-blended membrane also exhibited a lower rejection and higher permeability relative to the pristine cellulose membrane. Yong et al. [122] employed lignin as a hydrophilic blending agent to improve the hydrophilicity and antifouling properties of polyvinyl chloride UF membrane. Their results revealed that the hydrophilicity of the lignin-blended membranes increased, which was attributed to the hydrophilic functional groups present in the lignin structure. It was also observed that the lignin-modified membranes had considerably higher antifouling properties against humic acid aqueous solution and oil-in-water emulsion. Zhang et al. [150] also studied the potential of alkali lignin for enhancing the performance of RO membranes. In their work, alkali lignin was deposited on the surface of polyamide membranes employing a cross-flow filtration setup [150]. They reported that the lignin-modified membrane possessed improved fouling resistance, water permeation, and salt rejection [150].

1.8 Research objectives

The main goal of the present research is to study the potential of sulfonated kraft lignin (SKL) as an industrial waste derivative for the fabrication of high-performance UF and FO membranes with enhanced antifouling characteristics for the treatment of SAGD produced water. To achieve this goal, the present research is according to the following two themes:

I. Development of robust and high-performance membranes by incorporation of SKL into the bulk polymer. Embedding hydrophilic additives into a polymer film to improve the antifouling and permeation performances does not necessarily induce the desired properties to the host polymer. It may possibly deteriorate the separation and permeation performances of the pristine membrane. The major challenges that require to be addressed are dissolving SKL into the employed solvent and the compatibility of SKL with the polymer linkage. The non-uniform dispersion of SKL within the host polymer leads to the synthesis of non-uniform and inconsistent film and the formation of non-selective voids in the film, which subsequently reduces the separation efficiency of the membranes. Moreover, accommodation of SKL into the bulk polymer can degrade the continuity of the polymer matrix and consequently reduce the separation performance of the membranes. Therefore, an effective fabrication protocol for the robust synthesis of membranes was developed to induce desired functionalities such as high antifouling and permeation performances to the pristine membrane.

II. Surface modification of the pre-fabricated membranes using SKL to synthesize high-performance membranes with enhanced antifouling propensities. It is well accepted that the final performance of membranes strongly depends on their surface characteristics. It is expected that embedding hydrophilic SKL on the surface of the membranes improves the antifouling performance; however, the stability of the SKL and its compatibility with the other employed materials need to be studied. Additionally, coating the surface of membranes may reduce their permeation performance. Therefore, the focus of this part was to investigate a proper modification protocol for the synthesis of membranes with enhanced antifouling properties and minimal loss of permeation performance compared to the pristine membranes.

1.9 Thesis structure

The current dissertation is organized in a paper-based format. Chapters 2, 3, and 4 each are written according to the published/submitted papers. An industrial waste derivative, SKL, as a hydrophilic additive is used for the modification of the membranes. The pristine membranes in the present research are PES UF and PA TFC FO membranes.

Chapter 2 provides the outcomes of the studies on the incorporation of SKL into the bulk polymer of the UF PES membranes using nonsolvent induced phase separation technique. The effect of SKL concentration on the permeation, separation, and antifouling properties of the fabricated membranes was studied. The antifouling propensities of the membranes were investigated through filtration of SAGD BFW.

Chapter 3 presents the findings of the physical coating of SKL on the surface of PES UF membranes using a layer-by-layer assembly technique to enhance the antifouling propensities of the membranes. In this work, SKL and (diallyldimethylammonium chloride) (pDAC) were used as the polyanion and the polycation, respectively. The effect of polyelectrolyte concentration and the number of polyelectrolyte bilayers on the antifouling, permeation, and separation performances of the membranes was discussed in this chapter.

Chapter 4 presents the results of developing TFC FO membranes with enhanced antifouling and permeation performances by embedding SKL into the skin layer. The effect of different SKL concentrations was investigated, and the permeation, separation, and antifouling performances of the lignin-embedded membranes were evaluated and compared with those of the pristine TFC membrane. The antifouling performance of the synthesized membranes was investigated using SAGD BFW.

Chapter 5 summarizes the main outcomes of this research and provides a concluding discussion. Furthermore, suggestions and recommendations for future research are provided.

Chapter 2

Development of Antifouling Membranes using Agro-industrial Waste Lignin for the Treatment of Canada's Oil Sands Produced Water*

* This chapter was prepared based on reference [16].

2.1 Introduction

Multiple approaches have been taken into account to minimize the membrane fouling, among which the improvement of surface hydrophilicity is found to be indispensable [121,122]. Hydrophilic functionalities can be immobilized on the surface of the membrane by modification of bulk properties. In the bulk modification method, the hydrophilic materials are blended as additive with the primary polymer prior to the membrane fabrication [151].

As summarized in **section 1.7**, recently, several studies have been conducted for the bulk modification of polymeric membranes using various lignin derivatives. These studies employed lignin mainly as an additive in the fabrication of membrane using the non-solvent induced phase separation (NIPS) method [143] and vapor-induced phase separation (VIPS) method [96]. Enhancement in several key properties such as hydrophilicity and antifouling properties [122], permeability and antioxidant activity [146], thermal stability [141], and adsorption capacity [145] has been reported for the lignin-modified membranes compared to the unmodified membranes. Although PES is one of the most common polymers for the fabrication of membranes due to its high chemical and thermal stability, there is no study on the application of SKL for improving the antifouling properties of PES for the treatment of SAGD produced water.

In the present work, SKL, as a derivative of agro-industrial waste, was employed to modify the bulk properties of PES UF membranes using the NIPS technique. The morphology, permeability, and physicochemical characteristics of the prepared membranes were evaluated by various surface and bulk characterization techniques. The antifouling propensity of the membranes was investigated by the filtration of BFW generated in the SAGD process. The separation efficiency and the antifouling propensity of the prepared membranes were rationalized by the permeability, surface morphology, surface charge, and surface wettability.

2.2 Materials and methods

2.2.1 Chemicals and reagents

PES (Ultrason E6020P, Mw. 58 kDa) was purchased from BASF (Florham Park, United States). Sulfonated kraft lignin (Mw. 5-8 kDa) was received from West Fraser Company (BC, Canada) and was used as the additive without further modification. Polyvinylpyrrolidone (PVP, Sigma-Aldrich, Mw. 360 kDa) was used as a polymeric additive. N-Methyl-2-Pyrrolidone (NMP,

anhydrous, 99.5%, Sigma-Aldrich) was applied as the solvent. Dextran was purchased from Fisher Scientific and used for conducting MWCO tests. SAGD produced water, provided from a bitumen extraction plant located in the Athabasca oil sands region of Alberta in Canada, was used as the industrial wastewater to perform the antifouling tests. The produced water was the inlet of the steam generator known as BFW. A summary of the specifications of the BFW is presented in **Table 2.1**. The concentration of the components in the BFW was evaluated using inductively coupled plasma-optical emission spectroscopy (ICP-OES, Agilent 735). N-hexadecane (99% Fisher Scientific, Canada) was used to measure the captive bubble contact angle.

Table 2-1: Properties of SAGD BFW at 25 °C. The BFW was employed as the feed solution for evaluating the antifouling propensities of the synthesized membranes

Parameter	Unit	Value
pH	-	8.9-10.1
Conductivity	mS	1.6-2.1
TOC	mg/L	560-670
TDS	mg/L	1800-2500
Sodium	mg/L	1500-1900
Silica (dissolved)	mg/L	5-10
Calcium	mg/L	0.3-0.6
Magnesium	mg/L	0.2-0.4

2.3 Characterization of kraft lignin

The chemical composition of the SKL powders was investigated by energy-dispersive X-ray (EDX) spectroscopy (Zeiss Sigma 300 VP), and Attenuated total reflectance-Fourier transform infrared (ATR-FTIR) spectroscopy (AVATAR 370). The ATR-FTIR spectra was obtained by recording 128 scans in the range of 4000-400 cm^{-1} and the resolution of 4 cm^{-1} in air. The surface charge of the SKL particles was measured using a Zetasizer Nano ZS (Malvern Instruments, UK) with a 633 nm red laser and a folded capillary cell (DTS1060). For Z-potential analysis, first, a mother dispersion (500 ml) was prepared by sonicating 0.06 wt.% SKL powders in deionized (DI) water for an hour. Prior to each measurement, a 20 ml sample was collected from the mother dispersion, its pH was adjusted and then was centrifuged at 10000 rpm. Finally, the supernatant was used for surface potential measurement. Surface morphology and size distribution of the SKL

particles were investigated with field emission scanning electron microscopy (FESEM, Zeiss Sigma 300 VP). The samples were sputter-coated with carbon before imaging.

2.3.1 Fabrication of PES membranes

Asymmetric membranes were fabricated via NIPS (immersion precipitation) technique using water and NMP as nonsolvent and solvent, respectively [27,152,153]. As presented in **Figure 2-1**, in the first step, the designed amount of SKL was dissolved in NMP by vigorous sonication for 30 min applying a high-performance probe sonicator (Q700 Qsonica). In the next step, the corresponding amounts of PES and PVP were added into the SKL-NMP suspension. PVP was used as pore former additive. The mixture was stirred at 125 rpm overnight to ensure homogenous mixing and then was allowed to settle for 5 h for the release of air bubbles. The prepared dope solution was poured over a glass plate, and an automatic film applicator (TQC Sheen, AB3120, The Netherlands) was applied to adjust the casting speed at 10 mm/s. A micrometer film applicator (Gardco, Pompano Beach, FL, USA) with the adjusted clearance gap of 300 μm was used to spread the dope solution over the glass plate with a constant casting speed provided by automatic film applicator. The glass plate was then immersed into a coagulation bath of distilled water at room temperature for 15 min. Finally, the membrane was peeled off and soaked into distilled water overnight to completely remove the residual solvent. In order to study the effect of SKL concentration on the membrane characteristics, three different membranes were fabricated with different SKL concentration of 1 wt.%, 2 wt.%, and 3 wt.% in addition to one pristine membrane containing no SKL modifier. The total solid concentration was fixed to 16 wt.% for all the membranes. **Table 2.2** presents the compositional details of the fabricated membranes.

Table 2-2: The concentration of the constituents employed for the synthesis of the membranes

Membrane	PES Conc. (wt.%)	PVP Conc. (wt.%)	SKL Conc. (wt.%)	NMP Conc. (wt.%)
M0	14	2	0	84
M1	13	2	1	84
M2	12	2	2	84
M3	11	2	3	84

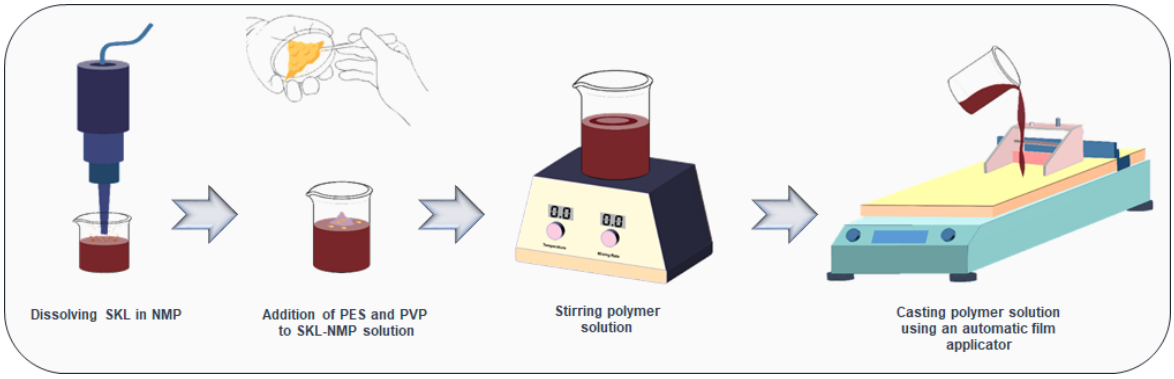

Figure 2-1: Schematic diagram of the blending procedure for the fabrication of SKL-modified PES membranes.

2.3.2 Evaluation of viscosity of the dope solution

The viscosity of the dope solution was evaluated using a rotational rheometer (Brookfield DV-III Ultra) at room temperature. The sample chamber was filled with the polymer solution and sufficient time was allowed for the chamber, spindle and solution to reach thermal equilibrium. Viscosities of polymer solutions were recorded in the shear rate range of 20-100 s^{-1}.

2.3.3 Evaluation of the surface topography of the membranes

The surface and cross-sectional morphology of the fabricated membranes were evaluated using a field emission scanning electron microscope (FESEM, Zeiss Sigma 300 VP) at the acceleration voltage of 10 kV. Prior to imaging, all the samples were sputter-coated with carbon. Atomic force microscopy (AFM, Bruker Dimension Edge, USA) was used to evaluate the surface topography of membranes. AFM tests were carried out in tapping mode at a scan rate of 1.0 Hz under ambient conditions of temperature and humidity. Nanoscope analysis software V.1.40 was used for the analysis of the AFM data, and the calculation of the surface roughness parameters.

2.3.4 Evaluation of surface wettability of membranes

To evaluate the underwater surface wettability of membranes, contact angle measurement was carried out by the captive bubble method at ambient temperature using a Krüss DSA 100 (Krüss GmbH, Germany) instrument. First, a strip of the membrane was attached to a sample holder and immersed into deionized water with the active surface facing down. A ‘J’ shaped needle was used to dispense a 5 µL drop of n-Hexadecane on the surface of the membrane. The contact angle was measured when the n-Hexadecane drop achieved the steady-state condition. To improve the

reliability of the results, contact angle measurements were repeated for 5 independent points of each sample.

2.3.5 Evaluation of the surface potential of the membranes

Surface zeta potentials of the membranes were evaluated using a Surpass^{TM} 3 Electrokinetic analyzer (Anton Paar, Graz, Austria). The zeta potential values were determined over the pH range of 4 to 9 and 25 °C using a 1mM KCl solution. The pH of the electrolyte solution was adjusted using HCl and NaOH solution.

2.3.6 Evaluation of hydraulic permeability of the membranes

Pure water flux tests were conducted using a dead-end filtration setup (Amicon, UFSC40001) applying compressed nitrogen gas. The effective membrane area was 41.8 cm^2. Each membrane was compacted at 10 psi until a steady flux was reached. The mass of permeate was recorded at regular time intervals with a weighing balance (ME4002, Mettler Toledo, USA) and the pure water flux (J_w) was calculated using [154]:

$$J_w = \frac{M}{\rho A_m \Delta t} \tag{2.1}$$

where M (kg) is the permeate mass, ρ (kg.m^{-3}) is water density, A_m (m) is the effective filtration area, and Δt (hr) is the measurement time. A series of filtration tests were conducted with distilled water at different transmembrane pressures (TMP). The hydraulic permeability (A) was calculated based on the slope of the flux-TMP plot. All the experiments were conducted at room temperature.

2.3.7 Evaluation of molecular weight cut-off (MWCO) of the membranes

MWCO of a membrane is the molecular weight of the solute molecules that is 90% rejected by the membrane. Dilute aqueous solutions (250 ppm) of dextran with different molecular weights (MW) of 75-500 kDa were used to evaluate the MWCO of the membranes. Before each experiment, the membranes were pre-compacted with pure water at 10 psi until the pure water flux reached a steady state. Starting from the lowest MW, dextran solutions were filtered at TMP of 6 psi in the dead-end filtration cell. The surface of membranes was washed by stirring distilled water for 20 min at 450 rpm before replacing the dextran solution. Permeate and feed samples were analyzed using a total organic carbon analyzer (TOC-L CPH, Shimadzu, Japan). The TOC rejection (R) was calculated using:

$$R\ (\%) = \left(1 - \frac{C_p}{C_f}\right) \times 100 \quad (2.2)$$

where C_p and C_f (mgL^{-1}) are the permeate and feed concentrations, respectively. MWCO of the membranes is considered as the minimum MW of the solutes with 90% retention. The retention versus molecular weight curve was extrapolated to the point of 90% retention for the calculation of the MWCO. The average pore size of the membranes was obtained based on the following correlation between the pore diameter (d_p in nm) and the molecular weight cut-off (MWCO in Da) of the membranes [155,156]:

$$d_p = 0.09(MWCO)^{0.44} \quad (2.3)$$

2.3.8 Evaluation of antifouling properties of the membranes

SAGD BFW was used as the foulant in this study. Prior to each fouling test, the membrane was pre-compacted using pure water at 10 psi until a steady flux was reached. Then, four consecutive steps were followed to investigate the fouling characteristics of the membranes [11]. First, in order to omit the flux decline resulted from the permeation drag, the initial pure water flux (J_{wi}) was maintained constant at 400 LMH (L m^{-2} hr^{-1}) by adjusting the TMP. Next, the pure water was replaced with the SAGD BFW and the permeation flux (J_f) was recorded after it stayed steady for at least 30 minutes. After that, the surface of the fouled membrane was washed for 20 min by stirring distilled water at 450 rpm. Finally, the recovered pure water flux (J_{wf}) was recorded after 30 min. The concentration of foulant in the permeate and feed solutions was measured using a TOC analyzer. The rejection percentage was calculated using **Equation (2.2)**. Total flux decline ratio (DR_t) and flux recovery ratio (FRR) were calculated by using the following equations to quantitatively evaluate the fouling propensity of the membranes [154]:

$$DR_t = 1 - \frac{J_f}{J_{wi}} \quad (2.4)$$

$$FRR = \frac{J_{wf}}{J_{wi}} \quad (2.5)$$

where DR_t is the summation of reversible fouling ratio (DR_r) and irreversible fouling ratio (DR_{ir}) which can be calculated using the following equations:

$$DR_r = \frac{J_{wf} - J_f}{J_{wi}} \quad (2.6)$$

$$DR_{ir} = 1 - \frac{J_{wf}}{J_{wi}} \quad (2.7)$$

2.4 Results and discussion

2.4.1 Chemical characterization of the kraft lignin

Lignin is a polyphenolic and amorphous material that emerges from dehydrogenative polymerization of phenylpropanoid monomers leading to the formation of guaiacyl, p-hydroxyphenyl propane, and syringyl-type units [109,157]. These structures are formed through the inter-unit bonds, such as ether and carbon-carbon linkages [158,159]. The extraction process of lignin followed by various post-treatments substantially may alter the chemical and physical properties of the mother lignin, for example, by fragmentation of crosslinked units, installation of new functional groups, and switching between solubility patterns. These inherent complexities of the structure and diversity of production processes bring challenges to indisputably identify chemical structures and physical properties of the lignin [96,109,159,160]. Encouragingly, the advent of the modern characterization facilities provides opportunities to explore the information of a material that is necessary for targeted applications. Consequently, FESEM, EDX and ATR-FTIR spectroscopic techniques were utilized to identify the morphology, the elemental composition and the corresponding functional groups in the lignin, used in this study, to justify its rationale for application as an anti-fouling coating material. The surface images of the raw SKL powders were presented in panels a and b of **Figure 2.2**. The as-received dry lignin powder has irregular shapes and forms aggregated islands of various sizes over FESEM stub. The **insets of Figure 2.2** panels a and b present the EDX spectrum of the kraft lignin. Based on the quantitative analysis, the kraft lignin contains carbon (66.0%), oxygen (29.1%), sodium (3.8%), and sulfur (0.9%). The elements carbon and oxygen are originating from the aromatic cross-linked structure as well as the constituent functional groups, while sodium and sulfur can be associated with the ionic functional groups, such as sodium carboxylate and sodium sulfonate. It is worth noting that the elemental composition determined by EDX here may not represent the absolute composition of kraft lignin since the carbon signal may also originate from carbon tape used for sampling. Nevertheless, it provides a useful estimate of the elements present in kraft lignin. This estimation

of the type of elements along with the FTIR analysis allows determining chemical nature and functional groups of lignin, which are essential for LbL coating and corresponding anti-fouling properties.

Panel c of **Figure 2.2** presents the ATR-FTIR absorption spectra of kraft lignin powder. The evolution of characteristic absorption peaks at 3361 cm^{-1} (O-H stretching of phenols and aliphatic alcohols), 1735 cm^{-1} (C=O stretching of carbonyl groups), 1580 cm^{-1} (C=C stretching of aromatic rings and C=O stretching of carboxylate groups), 1124 cm^{-1} (S=O stretching of sulfonate groups), 1026 cm^{-1} (C-O stretching of ether linkage), and 621 cm^{-1} (S-O stretching of sulfonate groups) along with the EDX elemental composition analysis indicate that the lignin used in this study is a sulfonated kraft lignin [161–163]. The accurate structure of lignin is not well-established due to its diverse and complex structure. Panel d of **Figure 2.2** shows that SKL possesses negative surface potential across over the pH range of 4 to 9. The negative surface charge of SKL can be related to the anionic functional groups, including sulfonates, carboxylates, and phenoxides [26]. The negative surface potential of the SKL increases with pH, likely due to the higher ionization of the SKL functional groups at basic pH.

Figure 2.3 illustrates the anticipated inter-unit linkages and chemical structures of the kraft lignin, based on the EDX and ATR-FTIR results, showing its segments essential for LbL coating and resulting anti-fouling properties. The presence of phenols, aliphatic alcohols, carboxylates, and sulfonate functional groups are pivotal for the hydrophilicity of lignin. These functional groups improve the anti-fouling properties of the lignin-coated membranes toward organic and microorganism contaminants. Moreover, the anionic phenoxide, carboxylates, and sulfonates functional groups result in the polyanionic characteristic of the lignin, which is advantageous for LbL coating in conjunction with a suitable polycation.

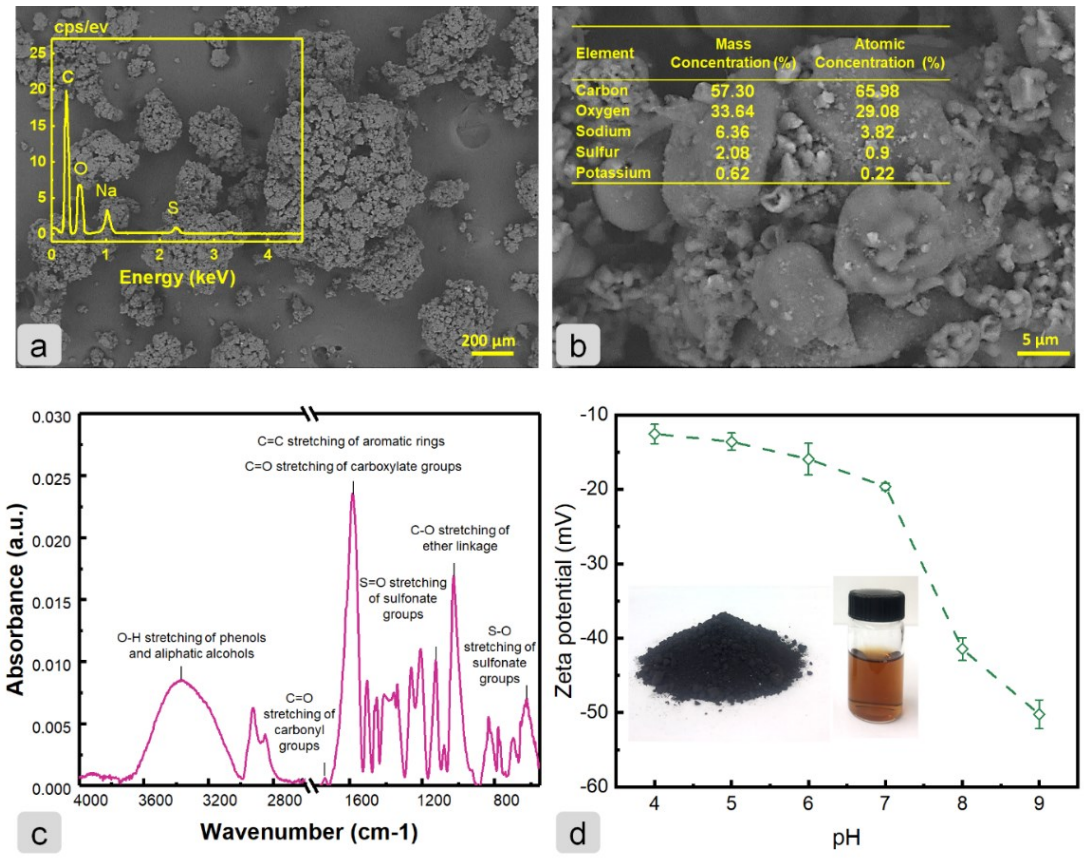

Figure 2-2: (a) and (b) FESEM surface images and EDX compositional analysis of the as-received dry SKL powders; (c) ATR-FTIR spectrum of the SKL powders, revealing the presence of absorption bands corresponding to hydrophilic functionalities including aliphatic carboxylates, alcohols, phenols, and sulfonates in SKL; (d) Surface zeta potential of the SKL powders. Negative surface potential with no isoelectric point was observed over the pH range of 4 to 9.

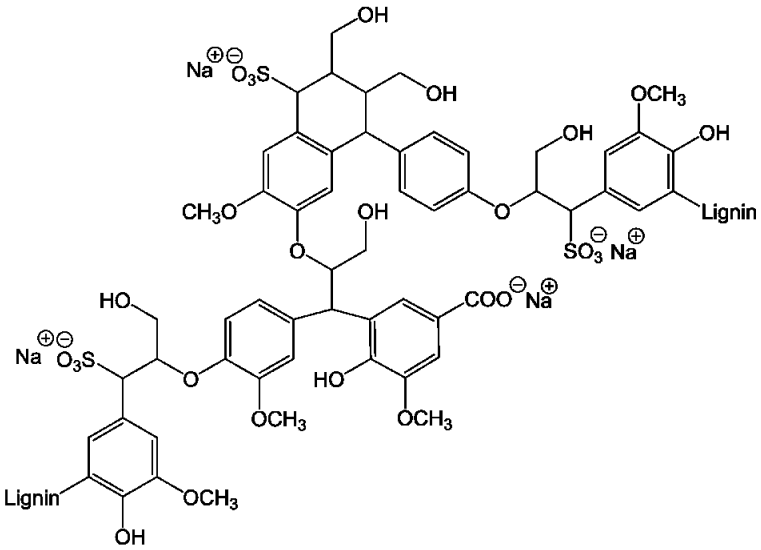

Figure 2-3: Schematic representation of the predicted substructure of sulfonated kraft lignin

2.5 Evaluation of the morphology of the membranes

Figure 2.4 shows cross-sectional FESEM images of the membranes fabricated with different SKL concentrations (0-3 wt.%). The membranes possessed asymmetric morphology with a top thin skin layer over a thick sub-layer containing "finger" type macrovoids. Such change of morphology from the dense skin layer to larger porosity toward the sub-layer is typical for the membranes fabricated using immersion precipitation technique [164]. A qualitative comparison of the size of the macrovoids within the internal structure suggests that the porosity of the membranes slightly increased with the increase in SKL concentration.

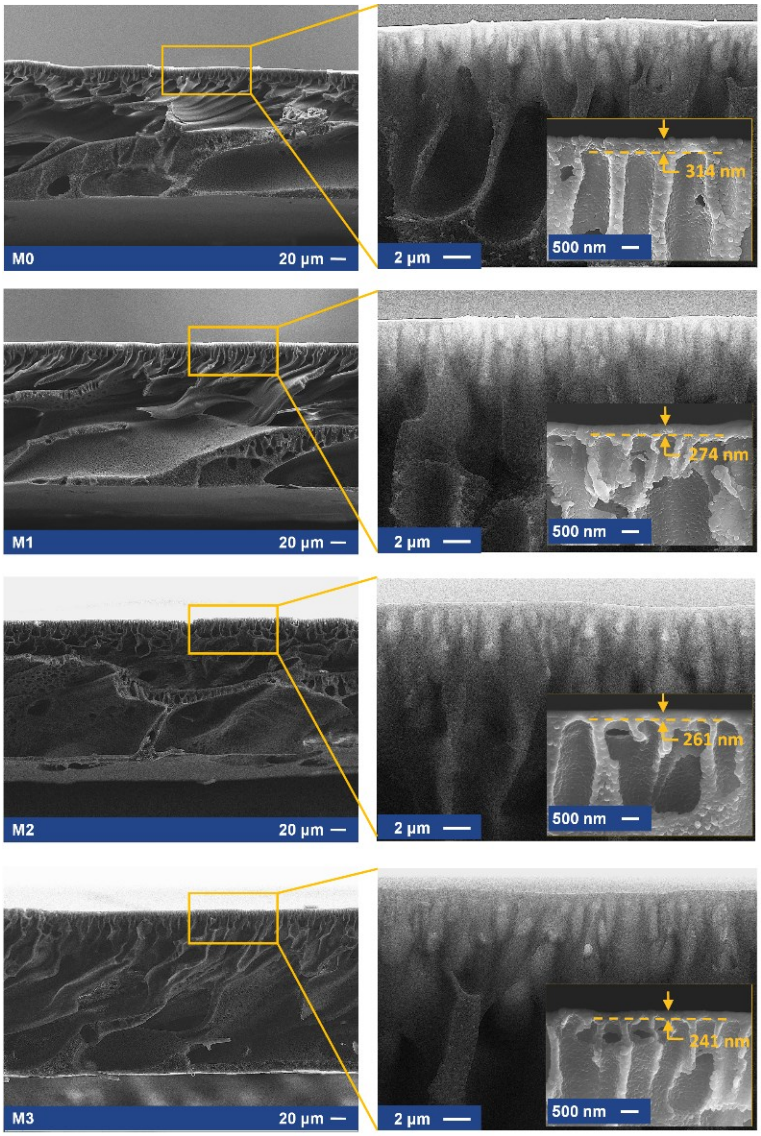

Figure 2-4: Cross-sectional FESEM images of pristine (M0), and the modified M1, M2, M3 membranes prepared with 1, 2, and 3 wt.% of SKL.

The phase inversion process of the SKL-blended casting solution is influenced by the trade-off between thermodynamic enhancement and kinetic hindrance. These two parameters manifest the influence of an additive on the structural properties of the resulting membrane [165]. The unfavorable interactions of hydrophilic SKL additives with the hydrophobic PES decrease the thermodynamic stability of the casting solution and thus accelerate the precipitation process [155,165,166]. Hence, the introduction of more SKL into the casting solution favors the thermodynamics for the precipitation of polymer resulting in the formation of membranes with enhanced porous structures consisting of finger-like pores [73,155]. The other parameter that influences the final structure of porous membranes is the kinetics of solvent and nonsolvent (water) demixing in the coagulation bath. In general, a greater hindrance to the demixing kinetics leads to the formation of denser structures [167].

Figure 2.5 shows the rheological behavior of the casting solutions containing various SKL concentrations. It can be observed that the viscosities of the polymer solutions decreased with the increase in the SKL concentration. The lower the viscosity of the polymer solutions, the higher the leaching rate of the solvent and additive into the coagulation bath [167]. In addition to the viscosity of the casting solution, the hydrophilicity of SKL can also enhance the water/additive demixing rate [146]. Therefore, the cumulative effect of thermodynamic and kinetic enhancements of polymer precipitation resulted in the formation of more porous structures at higher SKL concentrations.

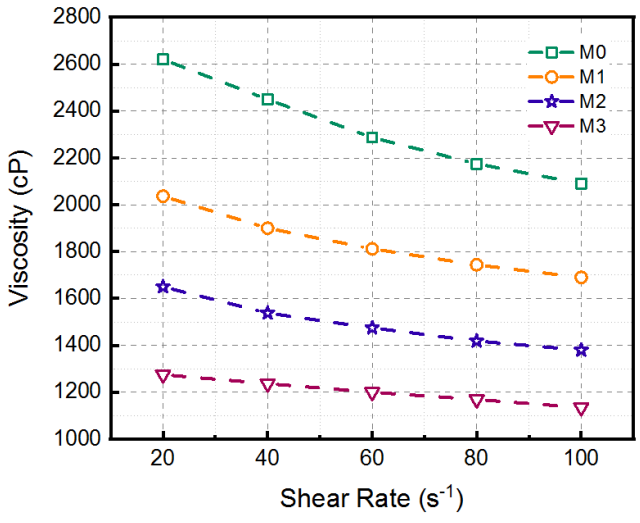

Figure 2-5: Variation of polymer solution viscosities versus shear rate for pristine (M0), and the modified M1, M2, M3 membranes prepared with 1, 2, and 3 wt.% of SKL additive.

The **Insets in Figure 2.4** present the top layer of the fabricated membranes. It can be observed that the size of fingers enlarged as the SKL concentration increased in the casting solutions. At a higher solvent/nonsolvent demixing rate, due to the presence of SKL, the creep relaxation of the polymer could not release the shrinkage stress of solidified film [155]. Therefore, the skin layer ruptured, and water intruded inside the cast film, leading to the formation of larger macrovoids [155]. The thickness of the skin layers decreased from 314 nm for the pristine PES membrane (M0) to 241 nm for the membrane with 3 wt.% loading of SKL (M3). This observation can also be attributed to the faster exchange of solvent and nonsolvent by the addition of SKL [168]. Moreover, lower viscosity of the casting solution results in a higher leaching rate of solvent and SKL additives into the water bath, which reduces the entrapment of SKL at the top of the cast film, leading to the formation of thinner skin layers [169]. The total thickness of the fabricated membranes, however, slightly increased by increasing the SKL concertation. The thickness of the pristine membrane (M0) was 165 μm, which increased to 194 μm, 199 μm, and 218 μm for the M1, M2, and M3 membranes, respectively. More penetration of water into the cast film, due to the higher thermodynamic instability of casting solution, as well as lower viscosity of this solution (kinetics promotion), at higher SKL concentrations, accelerated the polymer coagulation rate and, as a consequence, thicker membranes are formed [170,171].

The surface roughness of the fabricated membranes was evaluated by using FESEM surface morphology and AFM surface topography images. The top view of the surface in the FESEM images provides a visual illustration of a trend of lower surface roughness from M0 to M3 with the increase of SKL concentration from 0 wt% to 3 wt%. The arithmetic average surface roughness (R_a) and the root mean square average surface roughness (R_q) of the fabricated membranes were estimated from the AFM topography images, which are presented in the **insets of Figure 2.6**. The average surface roughness of the membranes slightly decreased with the increase of SKL concentration in the polymer solutions. The AFM 3D surface topographies in **Figure 2.6** exhibit a more illustrative comparison of surface roughness between the membranes. The ridges and valleys at the surface of the pristine membrane (M0) were sharp, which gradually flattened out as the SKL concentration increased from M1 to M3. The slightly lower surface roughness of the SKL-based membranes can be attributed to the instantaneous demixing of the solvent and nonsolvent.

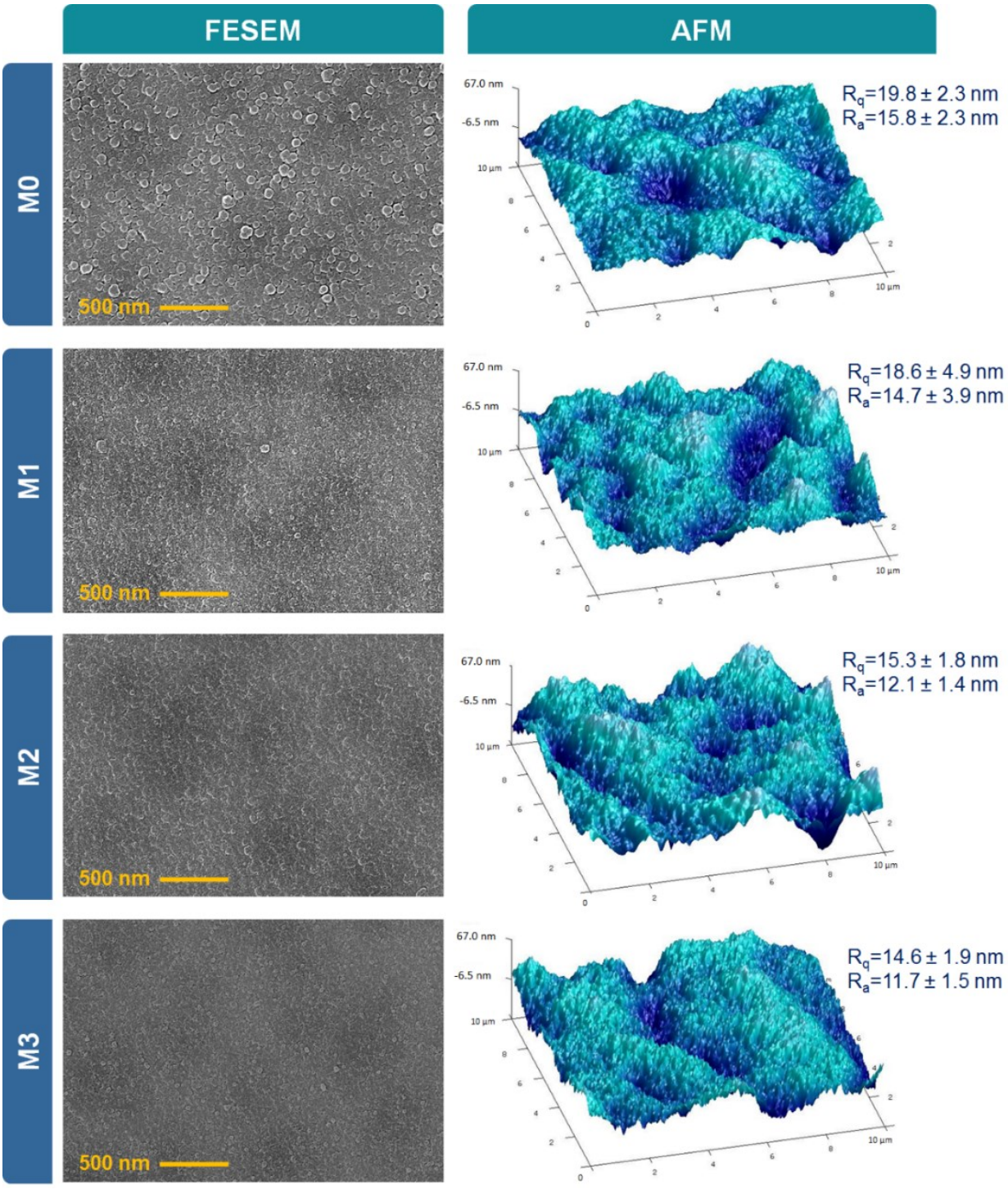

Figure 2-6: FESEM surface morphology, AFM surface topography images, and surface roughness data of the pristine (M0), and the modified M1, M2, M3 membranes prepared with 1, 2, and 3 wt.% of SKL concentration

2.5.1 Evaluation of the surface wettability of the membranes

The surface wettability of the membrane was evaluated by measuring the under-water n-Hexadecane contact angle (**Figure 2.7**). In general, the under-water oil contact angle is more relevant to measure the wettability of water filtration membranes since it simulates the real filtration condition more closely than under-air water contact angle measurement. The SAGD BFW contains a high concentration of suspended and dissolved solids and natural organic matter as the foulants. Natural organic matters such as humic substances and aliphatic and aromatic hydrocarbons consist of hydrophobic and/or negatively charged constituents in their structure and are feebly dispersed in water. These NOMs can cause irreversible attachment to the membrane surface via hydrophobic interaction if the membrane surface is not hydrophilic and/or negatively charged. Oil (e.g., n-hexadecane) is a hydrophobic material, and it has strong hydrophobic interactions to the unmodified membrane. Therefore, a modification that can suppress the oil affinity to the membrane surface is expected to prevent the fouling by NOMs. The drop contact angle was measured by dispensing a Hexadecane droplet on the surface of the membranes underwater. The addition of SKL additives improved the hydrophilicity (i.e., underwater oleophobicity) of the membranes, which is manifested by the increase of the drop contact angle from 132.8°±1.0° for M0 to 146.8°±1.0° for M3. The pictures in **Figure 2.7** show a darker brown color of the membranes containing a higher SKL concentration. This observation is consistent with the enhanced oleophobicity of the membranes prepared by higher SKL concentration.

2.5.2 Evaluation of the surface charge of the membrane

The surface electrical charge properties of the pristine PES and the modified membranes were studied by measuring the surface ζ-potential over the pH range of 4 to 9. **Figure 2.8** illustrates that all the membranes had negative zeta potential over the tested pH range. The negative ζ-potential for the bare PES membrane has previously been related to the adsorption of negative ions form the electrolyte solution on the membrane surface [172]. SKL consists of anionic functional groups, including carboxylates, phenoxides, and sulfonates [121]. The surface zeta potential of the modified membranes slightly enhanced from M1 to M3. The marked increase in the absolute value of the surface zeta potential of the modified membranes compared to the pristine PES membrane can be attributed to the presence of anionic functional groups of SKL on the surface of the membranes. The more negatively charged membranes are anticipated to be less prone to fouling

by organic matter, which mostly consist of net negative charge.

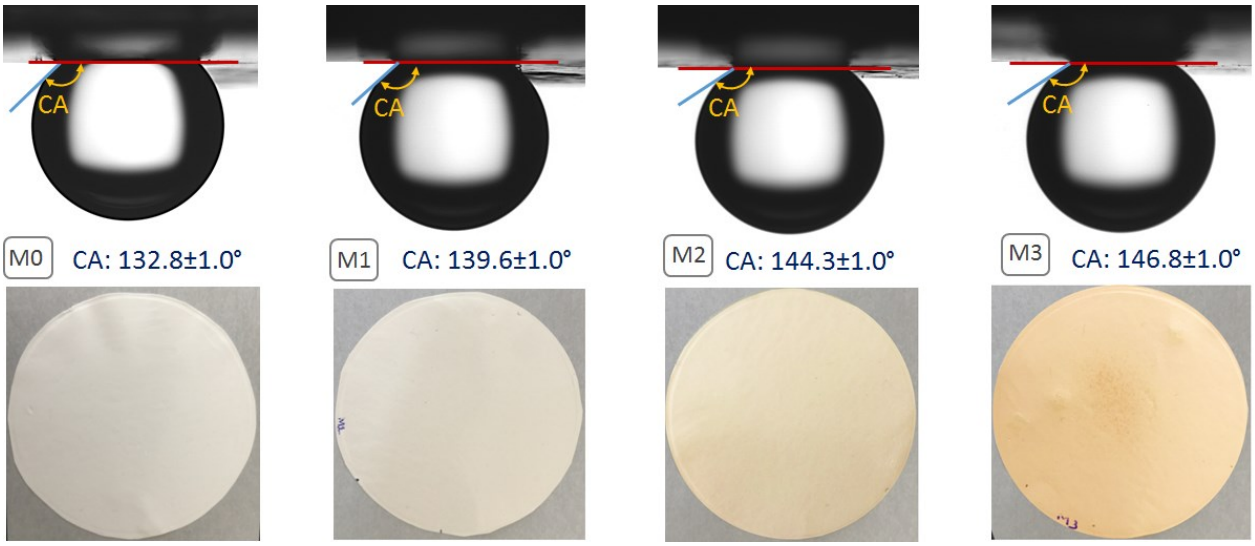

Figure 2-7: Underwater surface oleophobicity of pristine PES support (M0) and the modified membranes with 1 to 3 wt.% (M1-M3). The wettability analysis was performed applying the underwater captive n-hexane bubble. The higher oil contact angle represents the higher oleophobicity of the membranes. Photographs of the fabricated membranes acquired 24 hr after fabrication are also presented in this figure.

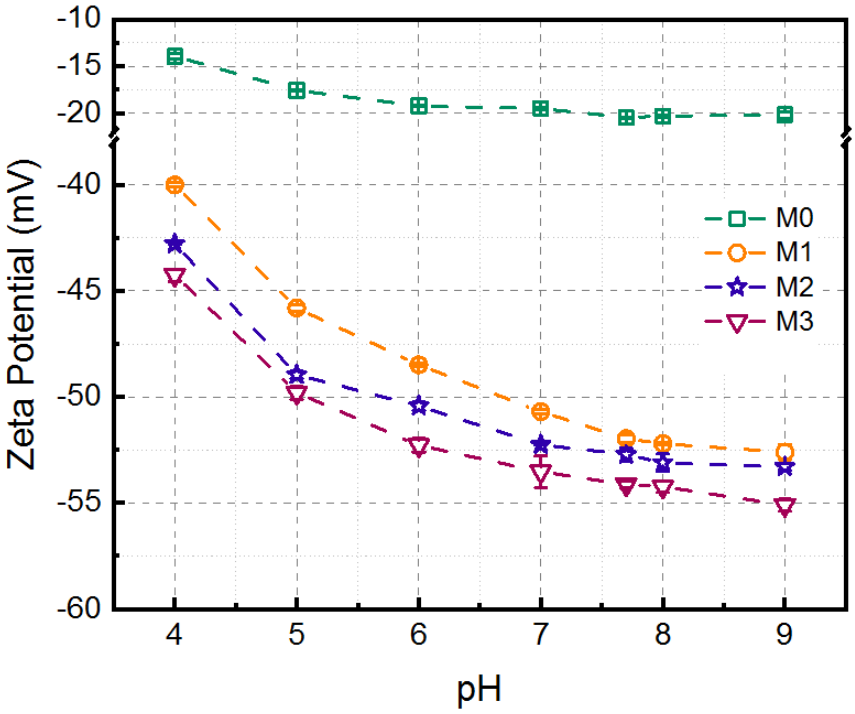

Figure 2-8: Surface zeta potential of the pristine PES and the modified M1, M2, M3 membranes prepared with 1, 2, and 3 wt.% of SKL concentration.

2.5.3 Evaluation of permeation performance and MWCO of the membranes

The permeation performance of the membranes was evaluated using a dead-end filtration setup. **Figure 2-9** presents the pure water flux versus TMP for the fabricated membranes. The table inside the figure presents the hydraulic permeability (A) of the membranes. By the increase of SKL concentration, hydraulic permeability of the resulting membranes improved from 25.3 LMH/psi for M0 to 47.3 LMH/psi, 67.8 LMH/psi, and 68.6 LMH/psi for M1, M2, and M3, respectively. This increase in the hydraulic permeability can be explained by the higher surface hydrophilicity and porosity of the modified membranes. The MWCO of the fabricated membranes is presented in **Figure 2-10**. The MWCO increased from 623.6 kDa for M0 to 686.3 kDa for M1, 702.8 kDa for M2, and 767.7 kDa for M3. The corresponding average pore size of the synthesized membranes was 31.9 nm for M0, 33.3 nm for M1, 33.6 nm for M2, and 34.9 nm for M3. This increase in the MWCO of the membranes with a higher SKL concentration is due to the larger porosity of the membranes caused by faster coagulation, as discussed in the earlier section.

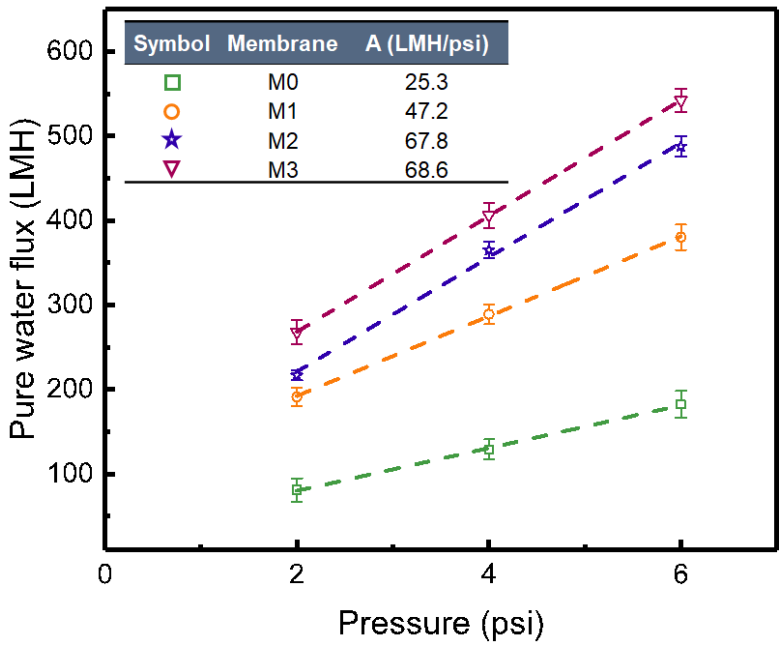

Figure 2-9: Pure water flux vs. TMP and hydraulic permeability of the prepared membranes. The modified membranes M1, M2, and M3 were synthesized, applying different SKL concentrations of 1, 2, and 3 wt.%, respectively.

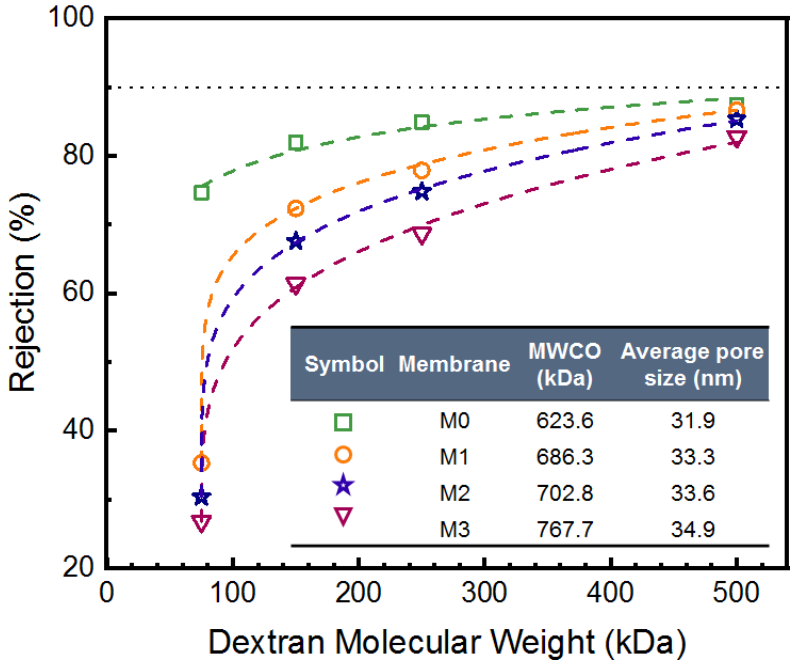

Figure 2-10: MWCO and average pore size of the pristine (M0), and modified membranes (M1 to M3) synthesized with various SKL concentrations of 1, 2, and 3 wt.%. Dextran solutions were filtered using a dead-end filtration setup to determine the MWCO of the membranes.

2.5.4 Separation performance and antifouling characteristics of the membranes

The separation performance and antifouling properties of the membranes were evaluated through the filtration of SAGD BFW using a dead-end filtration setup under constant initial permeate flux mode. **Figure 2.11** illustrates the fouling characteristics of the fabricated membranes. For all membranes, the permeation flux declined sharply at the beginning of the filtration of BFW following by a gradual decline that ended up to a steady permeate flux **(Figure 2.11a**). The sharp initial decline in the permeate flux can be attributed to the partial blockage of the membrane pores with the foulant particles [173,174]. The following gradual flux decline can be due to the formation of a cake layer on the membrane surface resulting from the accumulation of contaminants on the surface of the membrane [174,175]. The total flux decline ratio (DR_t) and the flux recovery ratio (*FRR*) of the fabricated membranes are presented in **Figure 2.11b**. All membranes exhibited high flux decline, which slightly improved for modified membranes. The high flux decline is due to the high concentrations of suspended and dissolved solids and organic materials in SAGD BFW, which contributes to the concentration polarization phenomenon and fouling through different mechanisms, including cake layer formation, pore blocking and adsorption of foulant on the membrane surface [176]. The pristine PES membrane exhibited the

largest DR_t of 86.4% and the lowest *FRR* of 52.2%. The flux recovery of the fabricated membranes improved by increasing the SKL concentration in the casting solutions. Among the fabricated membranes, M3 which was prepared from 3 wt.% of SKL, showed the lowest total flux decline of 77.8% and the highest flux recovery of 98.2%. It is important to note that the flux decline alone cannot determine the antifouling property of a membrane, particularly when the concentration polarization and deposition of foulants plays a dominant role in the flux decline. Therefore, *FRR* is more relevant for the evaluation of antifouling property in such situation. The remarkably higher *FRR* of the modified membranes compared to that for base PES membrane offers the possibility of long-term operation of these modified membranes with simple routine washing.

It is worth elucidating the reason behind the higher antifouling propensity of the SKL-modified membranes compared to the pristine PES membranes. Parameters, including surface hydrophilicity, surface charge, and surface roughness of membranes, play a determinant role in the antifouling properties [156,177,178]. It is well known that the membranes with higher surface hydrophilic functionalities are less susceptible to fouling since the hydrogen bonding and polar interactions between the surface functionalities and the surrounding water molecules construct a layer of water on the membrane surface. This hydration layer cuts off the direct contact of hydrophobic foulants with the surface of the membrane. The presence of more hydrophilic functional groups on the surface of the SKL-modified membranes, originating from SKL, improves their antifouling performance. The results of surface wettability also exhibit the increasing trend of the surface hydrophilicity of the modified membranes, which is consistent with the increasing trend of antifouling properties. It is also important to mention that the hydrophilic functional groups of SKL are anionic in nature, which can significantly increase the negative charge on the surface of the modified membrane (**Figure 2.8**). By forming an electric double layer (EDL), the negative surface charges of the membranes can repel the negatively charged foulants and prevent the adhesion of hydrophobic foulants. Most of the organic foulants in SAGD BFW are hydrophobic and/or anionic. Therefore, the increasing trend in the antifouling property of the modified membranes towards organic matter in BFW can also be related to the increasing trend in the negative surface charges. It is worth mentioning that due to the high salinity of SAGD BFW, the Debye screening can significantly lower the thickness of the EDL within the pores and over the surface of the membrane, and thus weaken the repulsion felt by the negatively charged foulants. Hence, the prepared membranes would possibly exhibit lower irreversible flux decline with higher

removal of organic matter if the ionic concentration of the BFW was lower (<<1000 ppm).

Lastly, fouling is strongly related to the surface roughness of the membranes. Membrane with a rougher surface is more prone to fouling since the ridge and valley structure of rough surface favors the entrapment of foulants at the valley regions (eddy zones occurring behind the peaks) [40,179,180]. According to the AFM analysis presented in **Figure 2.6**, the surface roughness of the fabricated membranes slightly decreased by increasing the SKL concentration in the polymer solutions leading to less drastic flux decline and improved flux recovery ratio during filtration of SAGD BFW. **Figure 2.11b** presents the separation efficiency of the organic matter from SAGD BFW by the fabricated membranes. It can be observed that the removal efficiency of the membranes slightly reduced by increasing SKL concentration. Although the MWCO of the membrane modified with 3 wt% SKL additive (M3) increased by about 144 kDa from that of pristine PES membrane (M0), the rejection of organic pollutants decreased by only 9%. The combined effect of hydrophilicity and the negative charges on the modified membrane repelled the organic pollutants comprising hydrophobic and/or anionic properties. Such a repulsion of organic matter maintained the rejection at an almost similar level to the pristine PES membrane. It is worth noting that reaching a solid conclusion about the order of contribution of the surface hydrophilicity vs. surface charge to the antifouling performance requires detailed surface analysis at a microscale using, for example, a quartz crystal microbalance (QCM) sensor [181]. The remarkably high antifouling property of the modified membranes outweighs the impact of the negligible decrease in their separation efficiency.

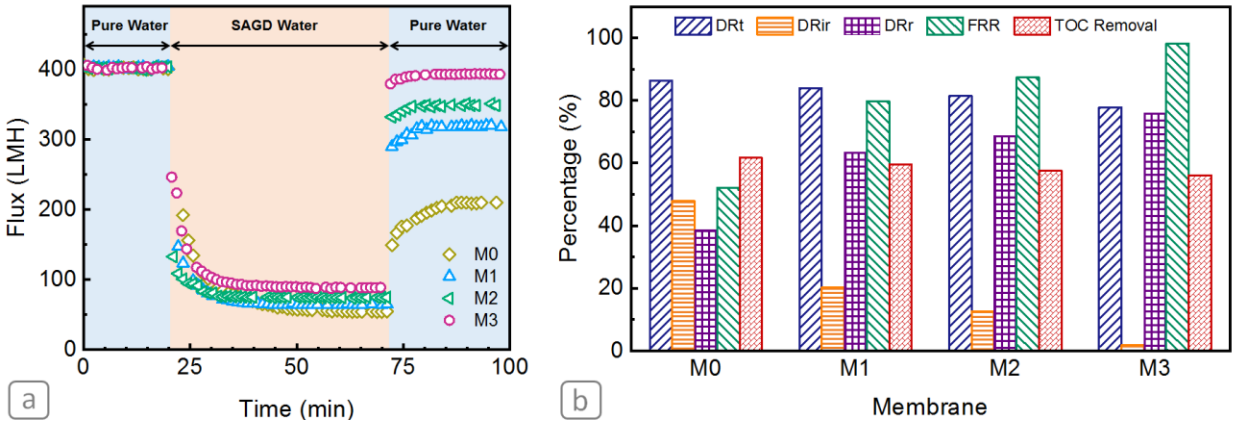

Figure 2-11: (a) Permeation flux of pristine (M0) and modified membranes M1, M2, and M3, during filtration of SAGD BFW, (b) the respective fouling parameters of the synthesized membrane. The TMP for each modified membrane was adjusted to yield the same initial flux as M0 membrane. The modified membranes M1, M2, and M3 were synthesized, applying different SKL concentrations of 1, 2, and 3 wt.%, respectively.

2.6 Conclusion

In this study, the SKL was applied to fabricate the modified membranes with enhanced antifouling performance using the phase inversion technique. The fabricated membranes were applied for the treatment of SAGD BFW. By increasing the SKL content in the casting solution, the permeability, MWCO, and underwater oleophobicity of the fabricated membranes increased. The increase in the loading of SKL additive resulted in the remarkable improvement of their antifouling properties. Although the total flux decline ratio decreased marginally from 86.4% to 77.8%, the flux recovery ratio improved substantially from 52.2% to 98.2%, with an increase in the SKL concentration to 3 wt.%. The high flux recovery ratio (98.2%) of the modified membranes represents negligible irreversible fouling, implying that the SKL incorporation would allow the continuous operation of the membranes with routine back flushing to remove the loosely adsorbed foulants instead of frequent shut-down and cleaning cycles. The improvement in the anti-fouling property of the modified membranes is attributed to the enhanced hydrophilicity, more negative surface charge, and the smoother surface as compared to the pristine membrane. The high separation efficiency of the modified membranes, in spite of their larger pore sizes than the virgin PES, was governed by the repulsion of the hydrophilic and/or negatively charged membrane with organic pollutants. This observation revealed that a high permeability membrane could be fabricated using SKL as an additive without sacrificing the separation efficiency significantly. Overall, this study provided an economical process for the treatment of produced wastewater (e.g., SAGD BFW) using SKL, which is plentiful as industrial waste. The fabricated SKL-blended membranes can be used as the pretreatment unit to filter the SAGD produced water before accommodating it into nanofiltration or reverse osmosis post-treatment. The pretreatment of the feed solution can effectively enhance the overall performance of the water treatment process. Additionally, the current water treatment scheme for the treatment of SAGD produced water, comprising warm lime softening and ion exchange resins, is only able to remove ~90% of silica and divalent ions. Nevertheless, the current processes do not provide any treatment for the dissolved organic matter. Hence, even 50-60% removal of organic matter would significantly reduce the risk of boiler failures due to the deposition of organic matter on the boiler tube walls and clogging of injection wells.

Chapter 3

Industrial Waste Lignin as an Antifouling Coating for the Treatment of Oily Wastewater[†]

[†] This chapter was prepared based on reference [121].

3.1 Introduction

Surface hydrophilization, particularly by coating hydrophilic material on the surface, is an effective technique to enhance the fouling resistance of polymeric membranes [182]. The rationale behind surface hydrophilization is that the adsorbed layer of water molecules on the hydrophilic surface of the membrane can repel the hydrophobic foulants [183]. Surface modification techniques such as LbL assembly offer the flexibility of using a variety of lab-prepared or commercial membranes with predetermined permeability and mechanical stability [67,184]. These techniques create a thin hydrophilic coating layer on the pristine membrane to provide enhanced fouling resistance with minimal loss of their original permeation performance.

The inherent properties of lignin, such as hydrophilicity, polyanionic structure, and nontoxicity, make it a potent candidate for the surface modification of membranes. As summarized before, a few works have been conducted for studying the surface modification of polymeric membranes using lignin derivatives. Zhou et al. [148] applied ammonium lignosulfonate as a monomer to fabricate a TFCnanofiltration membrane. The synthesized membrane exhibited an enhanced organic solvent resistance with a reduced permeation rate. In an attempt to improve the permeability of reverse osmosis membranes, Zhang et al. [150] deposited alkali lignin on polyamide membranes. The coated membranes showed enhanced water permeation, salt rejection, and anti-fouling performance. Colburn et al. [149] functionalized the lignin sulfonate on the surface of nanofiltration membranes through the esterification of hydroxyl groups of lignin and the carboxyl groups of membranes. They reported that the flux recovery ratio of the modified membranes improved significantly compared to that of the unmodified membrane during the filtration of the BSA solution.

Compared to the bulk modification, the surface modification of membranes using lignin-based materials has received less interest. Additionally, there is no study on the potential of SKL for the surface hydrophilization of PES membranes. Therefore, in this work, hydrophilic sulfonated kraft lignin, containing several anionic functional groups, was coated on the surface of PES UF membrane via the LbL-assembly technique using poly pDAC as polycation. The basic idea of LbL assembly technique is the alternate deposition of anionic and cationic polyelectrolytes (PEs) on the surface of the membrane [185–187]. The effects of concentration of PEs and the number of the PE alternative bilayers were examined to attain desirable permeation and anti-fouling properties

for the modified membranes. The anti-fouling properties of the membranes were evaluated by filtration of synthetic oil (n-hexadecane)-in-water emulsion as a model oily wastewater. The anti-oil fouling properties of the membranes were rationalized by the study of their permeability, surface wettability, and surface morphology.

3.2 Materials and methods

3.2.1 Materials

Flat sheet PES UF membranes with the MWCO of 10 kDa was purchased from Sterlitech Co. (WA, USA) and used as a substrate for the LbL coating. Poly (diallyldimethylammonium chloride) (pDAC, M_W of 200-350 kDa, 20 wt. % in water solution) was purchased from Sigma Aldrich and used as polycation. Kraft lignin (M_w of 5-8 kDa) was obtained from West Fraser Company (British Columbia, Canada) and used as polyanion. All aqueous solutions were prepared using deionized (DI) water (18.2 MΩ cm^{-1}, Milli-Q, Millipore). Isopropyl alcohol was purchased from Sigma Aldrich and used for the cleaning of PES membrane before coating. Hexadecane (n-Hexadecane, 99% Fisher Scientific, Canada) and Tween80 (Bio-Rad) were used as oil and emulsifier, respectively, to prepare the oil/water emulsion.

3.2.2 Preparation of LbL-assembled membranes

Figure 3.1 illustrates the LbL-assembly of the pDAC and lignin over the PES substrate. The cationic and anionic polyelectrolyte solutions were prepared by dissolving pDAC and lignin with the desired concentrations in DI water at neutral pH. The substrate was first washed thoroughly with isopropyl alcohol and water and then placed between acrylic frames and rubber gasket. Afterward, the pDAC solution was poured over the substrate and allowed to stay for 1 hr. The excess pDAC solution was poured out, and the substrate was immersed in DI water for 20 min to detach the loosely bonded polyelectrolytes. In the next step, the anionic lignin solution was poured on pDAC-coated substrate and left for 1 hr to form the first bilayer (BL) over the PES support. The second and third BLs were created by following similar steps. Fresh solution was prepared for each BL to prevent cross-contamination between the polyelectrolytes during the LbL process.

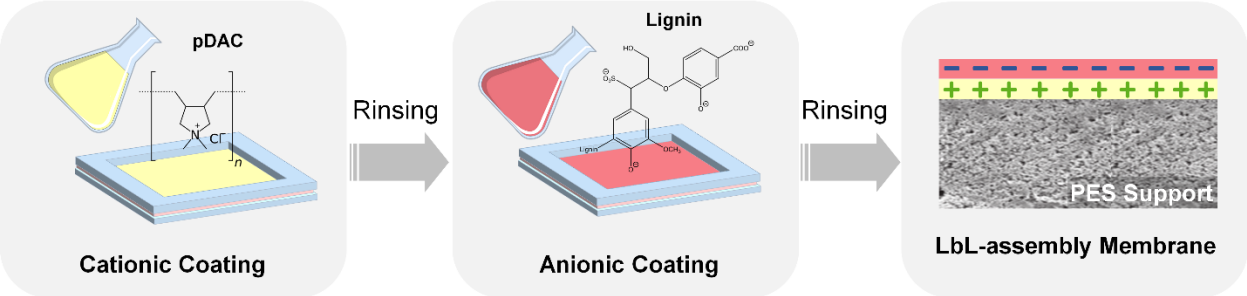

Figure 3-1: Schematic diagram of LbL-assembly of pDAC and lignin over the PES substrate. The LbL technique relies on the alternative deposition of cationic (pDAC) and anionic (sulfonated kraft lignin) polyelectrolytes on the surface of the membrane.

In order to study the impact of polyelectrolyte concentration and the number of BLs on the permeation and anti-fouling performance, different membranes were prepared by changing one variable at a time. **Table 3.1** presents the details of the PE concentrations and the number of PE BLs employed for LbL assembly. To investigate the effect of polyelectrolyte concentration, 4 membranes were coated by applying 2 BLs of PE solution with concentrations of 0.1, 0.5, 1, and 2 wt.% (M6, M5, M4, and M2, respectively). The concentration ratio of lignin to pDAC was set to one during the LbL-assembly for all the membranes. The effect of the number of BLs was studied by coating the pristine PES membrane with 1, 2 and 3 BLs using 2 wt.% pDAC and lignin solutions (M1, M2, M3, respectively). All the prepared membranes were kept in a water bath overnight and tested the next day. The coated membranes were designated based on the applied polyelectrolyte concentration and the number of BLs as $[pDAC(conc.)/Lignin(conc.)]_{(\#of\ BLs)}$ in **Table 3.1**.

Table 3.1: PE concentrations and number of PE BLs employed for the preparation of LbL-assembled membranes

Membrane	pDAC Conc. (wt.%)	Lignin Conc. (wt.%)	Number of BLs	Compositional Label [pDAC(conc.) / Lignin(conc.)] (#of BLs)
M0	0	0	0	Pristine
M1	2.0	2.0	1	$[pDAC(2.0)/Lignin(2.0)]_{(1)}$
M2	2.0	2.0	2	$[pDAC(2.0)/Lignin(2.0)]_{(2)}$
M3	2.0	2.0	3	$[pDAC(2.0)/Lignin(2.0)]_{(3)}$
M4	1.0	1.0	2	$[pDAC(1.0)/Lignin(1.0)]_{(2)}$
M5	0.5	0.5	2	$[pDAC(0.5)/Lignin(0.5)]_{(2)}$
M6	0.1	0.1	2	$[pDAC(0.1)/Lignin(0.1)]_{(2)}$

3.2.3 Probing the presence of lignin on coated membranes

X-ray photoelectron spectroscopy (XPS, Kratos AXIS ULTRA, UK) was used to analyze the surface elemental composition of some representative membranes. Survey spectra were obtained at a scan step size of 0.4 eV and sweep time of 100 s in the range of 0–1100 eV.

3.2.4 Evaluation of pure water flux and hydraulic permeability of membranes

Pure water flux of the membranes was evaluated using a dead-end filtration cell (Amicon, UFSC40001). Nitrogen gas was used to pressurized water through the membranes. The mass of permeate water was recorded over time using a weighing balance (ME4002, Mettler Toledo, USA). Prior to the permeation tests, the membranes were compacted at 70 psi until a steady-state flux was achieved. Pure water flux of the membranes was calculated using [176]:

$$J_w = \frac{M}{\rho A_m \Delta t} \tag{3.1}$$

where J_w is pure water flux, M (kg) is the mass of the permeate water, ρ (kg.m^{-3}) is water density, A_m (m) is the effective area of membrane (45.4 cm^2), and Δt (hr) is the time of permeation. The hydraulic permeability (A) of the membranes was obtained by calculating the slope of the linear fit of pure water flux versus the TMP.

3.2.5 Evaluation of anti-fouling properties of the membranes

A 1000 ppm emulsion of n-Hexadecane/Tween80 surfactant was used as a model foulant in this study. A synthetic oil emulsion was prepared by blending 0.5 g of n-Hexadecane with 0.75 mg of Tween80 in 500 mL of DI water as used as model foulant. The mixture was then blended in a homogenizer (Homogenizer 150, Fisher, Canada) at the highest speed for 4 min to prepare a stable emulsion. The fouling propensity of the membranes was investigated in four consecutive steps. First, the membrane was compacted using pure water at 70 psi until a steady flux was achieved. Afterward, the pure water flux J_{wi} of the membranes was measured. Next, the permeate flux (J_f) was measured using oil emulsion as a feed solution for 2 hrs. Finally, the surface of the membranes was simply washed by stirring with distilled water for 20 min, and then the pure water flux (J_{wf}) was evaluated once again.

In order to eliminate the effect of permeation drag on the flux decline of the membranes, the initial flux of all membranes was maintained the same by adjusting TMP. The fouling propensity

of the membranes was evaluated using the total flux decline ratio (DR_t) and flux recovery ratio (FRR) as follows [188]:

$$DR_t = 1 - \frac{J_f}{J_{wi}} \tag{3.2}$$

$$FRR = \frac{J_{wf}}{J_{wi}} \tag{3.3}$$

where DR_t is the sum of irreversible flux decline ratio (DR_{ir}) and reversible flux decline ratio (DR_r), which can be calculated using:

$$DR_r = \frac{J_{wf} - J_f}{J_{wi}} \tag{3.4}$$

$$DR_{ir} = 1 - \frac{J_{wf}}{J_{wi}} \tag{3.5}$$

3.2.6 Evaluation of surface wettability of membranes

The surface wettability of the membranes was studied by measuring the captive n-decane bubble contact angle in water using Krüss DSA 100 instrument (Krüss GmbH, Germany). A membrane sample was first cut to 2 cm×4 cm, mounted on a sample holder and immersed in DI water in a transparent container. A 5 μL drop of n-decane was placed on the active surface of the membrane with a rate of 2.6 μL/s using an inverted needle. The contact angle was recorded after the n-decane drop reached the steady-state condition. Measurements were repeated on five different locations of each sample and the average value of water contact angle, regarded as the complementary angle to oil contact angle, was reported.

3.2.7 Evaluation of MWCO of membranes

The MWCO of membranes was evaluated using PEG with molecular weight (MW) ranging from 400 to 20000 Da. Starting from the lowest MW, 250 ppm of PEG solutions were filtered through the membranes at a pressure of 30 psi. To minimize the gel layer formation and concentration polarization, the solution was stirred at 450 ppm during the experiments. The surface of the membrane was washed for 20 min at a stirring speed of 450 rpm before changing the PEG solution with a higher MW solution. The solute rejection (R) was evaluated by:

$$R\ (\%) = \left(1 - \frac{C_p}{C_f}\right) \times 100 \quad (3.6)$$

where C_p and C_f are the solute concentrations in the permeate and feed solution, respectively. The solute concentrations were measured by a TOC analyzer (TOC-L CPH, Shimadzu, Japan).

3.2.8 Analysis of the surface topography of membranes

The surface morphology of membranes was studied using a FESEM (Zeiss Sigma 300 VP). The microscope was equipped with EDX (Bruker) detector for elemental mapping. All membranes were sputter-coated with an approximately 10 nm thick layer of carbon prior to imaging. AFM (Bruker Dimension Edge, USA) was used to evaluate the surface topography of the membranes. AFM tests were carried out in tapping mode at a scan rate of 1.0 Hz at ambient conditions. Nanoscope analysis software V.1.40 was used for processing the AFM data, calculating the average roughness (R_a) and the root mean square roughness (R_q) values.

3.3 Results and discussion

3.3.1 Probing the presence of lignin on the coated membranes

The presence of lignin coating on the surface of the PES membrane was evaluated by comparing the XPS elemental composition of the pristine PES with some of the representative lignin coated counterparts. **Figure 3.2** presents the XPS survey spectra and elemental composition of the pristine PES support and the LbL-modified membranes, which were prepared with 1 BL (M1) and 3 BLs (M3) of the pDAC and lignin. The pristine PES substrate contains carbon, oxygen, sulfur, and nitrogen. The change in elemental composition for the M1 membrane was not significant, providing the fact that the XPS penetration depth is about 1-10 nm, and the detection limit is about 0.1% of the total elemental concentration. Therefore, it is difficult to measure an accurate composition difference of a very thin mono- or bilayer coating with respect to the composition of a thick background PES membrane. However, the variation in elemental compositions became evident after coating of 3 BLs of pDAC and lignin in M3. For this membrane, the ratio of carbon over nitrogen, and sulfur increased considerably compared to the pristine PES membrane due to the higher content of carbon in the coating polyelectrolytes. Moreover, the ratio of carbon over oxygen decreased since the lignin contains many oxygen-containing functional groups, including phenolic, carbonyl, and sulfonates. To obtain a direct

evidence of the presence of lignin on the coated layers, the presence of sodium (a signature element of sulfonated lignin as determined by the EDX elemental analysis) on the survey spectra was monitored and its compositional variation was compared between the membranes with 1 BL (M1) and 3 BLs (M3) of pDAC and lignin. A low-intensity peak for sodium was observed in the survey spectrum of M1, whereas the atomic percentage of this element was about 0.6% in M3. The presence of sodium (a counterion of sulfonate functional groups) in M1 and M3 clearly demonstrates the presence of sulfonated lignin coating on the PES membrane.

3.3.2 Permeation performance and fouling properties of LbL-assembled membranes

Impact of polyelectrolyte concentrations

The concentration of polyelectrolyte is an influential parameter on the thickness and thus hydraulic resistance of the LbL-coated membranes. **Figure 3.3** presents the pure water flux as a function of TMP for the pristine and LbL-modified membranes. The hydraulic permeability (A) of the membranes is presented in the **inset of Figure 3.3**. By increasing the polyelectrolyte concentration, the hydraulic permeability of the LbL-modified membranes decreased, suggesting the formation of a thicker LbL coating with larger mass transfer resistance at the surface of PES substrate.

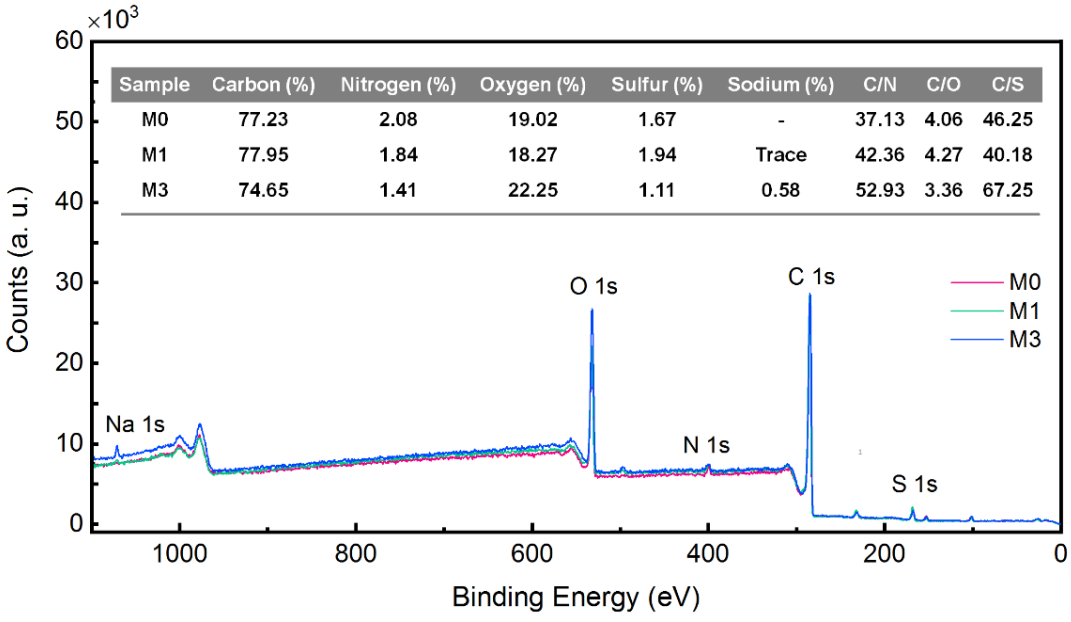

Figure 3-2: XPS survey spectra and elemental composition of pristine PES support and the LbL-modified membranes with 1 BL (M1) and 3 BLs (M3) of the pDAC and lignin.

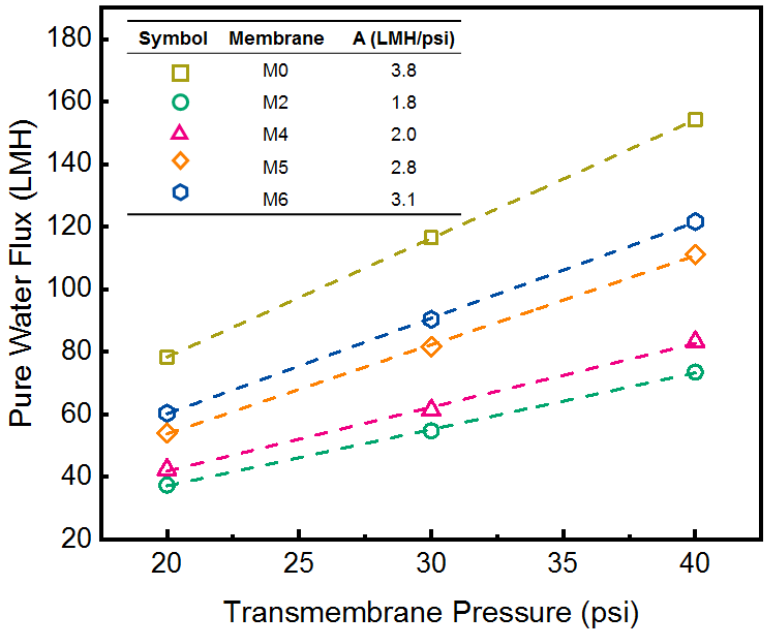

Figure 3-3: Pure water flux vs. TMP and hydraulic permeability of the prepared membranes. The modified membranes M2, M4, M5, and M6 were prepared with different polyelectrolyte concentrations of 2.0, 1.0, 0.5, and 0.1 wt.%, respectively.

To evaluate the anti-fouling propensities of the prepared membranes, cyclic filtration tests of oil/water emulsion was performed under constant initial permeate flux mode. **Figure 3.4** illustrates the fouling characteristics of the pristine and LbL-modified PES membranes. The permeate flux for all membranes declined sharply at the onset of the filtration test with oil emulsion, which was followed by a gradual decline leading to a steady-state flux at the end. The initial sharp flux decline can be due to the partial blockage of the membrane pores with the finely dispersed oil droplets. Further gradual flux decline can be attributed to the growth of the cake layer over the surface of the membrane due to the continuous accumulation of oil droplets at the membrane surface [174,175]. **Figure 3.4b** presents the flux recovery ratio and the flux decline parameters of the membranes that are evaluated after one cycle of filtration. The pristine PES membrane showed the largest flux decline (DR_t=44.2 %) and the lowest flux recovery ratio (FRR=76.0 %). The extent of flux decline was reduced and the flux recovery was enhanced for the membranes coated with a higher concentration of the polyelectrolyte solution. Among the coated membranes, M2 prepared from 2 wt.% of polyelectrolytes showed the lowest total flux decline of 28.3 % and the highest flux recovery of 92.4 %. Therefore, to study the effect of the number of polyelectrolyte BLs, the polyelectrolyte concentration was maintained constant at 2 wt.% to remove the impact of polyelectrolyte concentration.

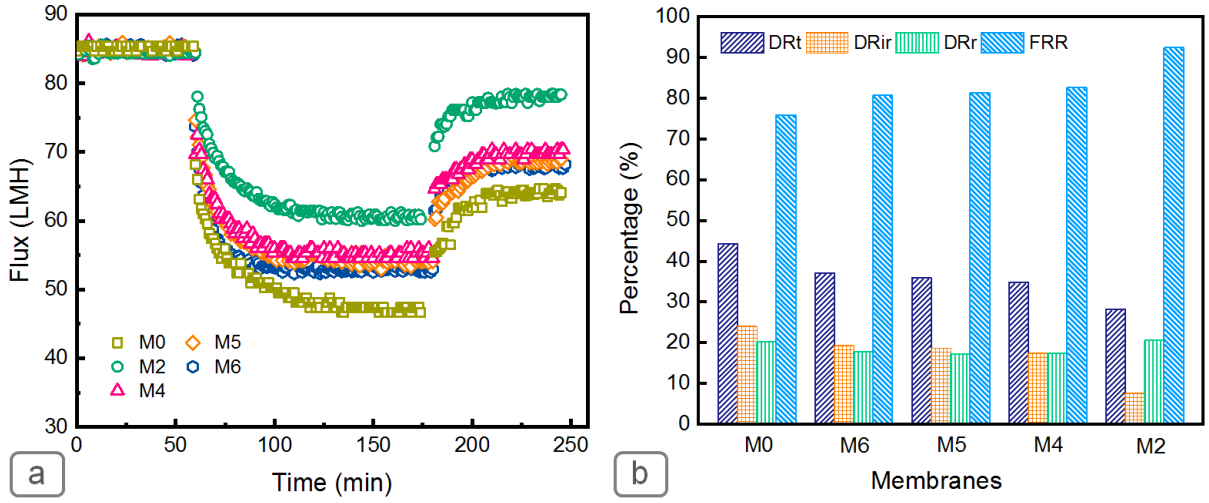

Figure 3-4: (a) Permeation flux and (b) anti-fouling characteristics of pristine PES membrane and the LbL-modified membranes. The LbL-coated membranes, denoted as M2, M4, M5, and M6, were prepared with 2 BLs of pDAC/lignin using polyelectrolyte concentrations of 2.0, 1.0, 0.5, and 0.1 wt.%, respectively. TMP for each LbL-coated membrane was adjusted to yield the same initial flux as the pristine PES membrane (M0).

Impact of the number of coated BLs

The number of coated BLs is another influential parameter on the permeability and anti-fouling property of the LbL-assembled membranes. **Figure 3.5** presents the pure water flux and hydraulic permeability of the LbL-modified membranes. The permeability of the coated membrane decreased from 2.13 LMH/psi (M1) to 1.6 LMH/psi (M3) with an increase in the number of coating BLs. The reduction of permeability was significant after the formation of 1 BL in M1 membrane compared to the pristine M0 membrane. However, the decline in permeability was less drastic beyond 2 BLs, which implies that the growth in mass transfer resistance of the coated film does not change linearly with the number of BLs. The close permeability of the modified membranes beyond 2 BL coatings enables the flexibility of using a higher number of BLs to improve anti-fouling property and selectivity with minimal effect on the permeate flux.

The influence of the number of BLs on the anti-fouling properties of the coated membranes and their potential for recyclability was examined by three consecutive oil emulsion filtration and water washing cycles. **Figure 3.6** illustrates the fouling characteristics of the pristine PES membrane and the LbL-assembled membranes. The unmodified M0 membrane showed the largest flux decline of 44.2% and the lowest flux recovery of 75.9 % compared to LbL-coated membranes. The increase in the number of BLs lowered the flux decline and improved flux recovery. The M3

membrane exhibited the highest anti-fouling propensity among all membranes by a flux decline of 23.1 % and a flux recovery ratio of 93.8%. The low flux decline and high flux recovery ratio over 3 cycles indicate that the foulants were loosely adsorbed to the membrane surface, and could potentially be removed during the cleaning operation.

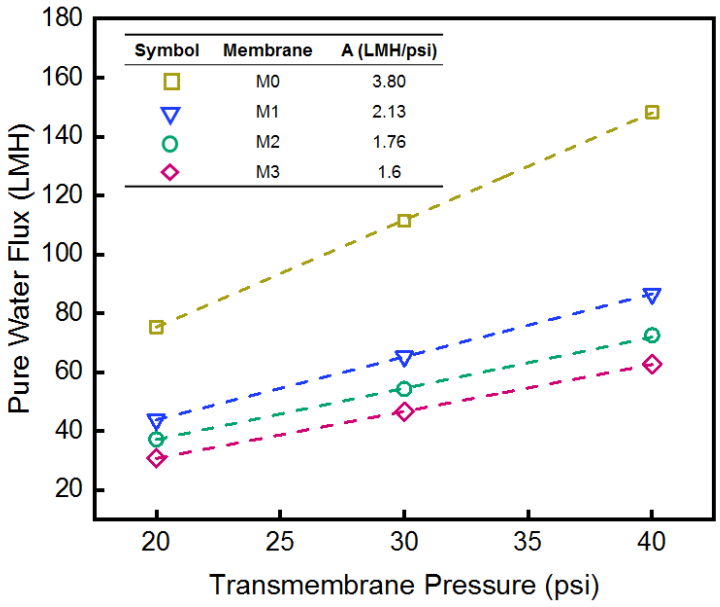

Figure 3-5: Pure water flux at different TMP on the membranes. The hydraulic permeability of the membranes was measured from the slope of the flux versus TMP plot. The modified membranes M1, M2, and M3 were fabricated by LbL-assembly of 1, 2, and 3 BLs of pDAC/lignin, respectively. The polyelectrolyte concentration was kept constant at 2 wt.%.

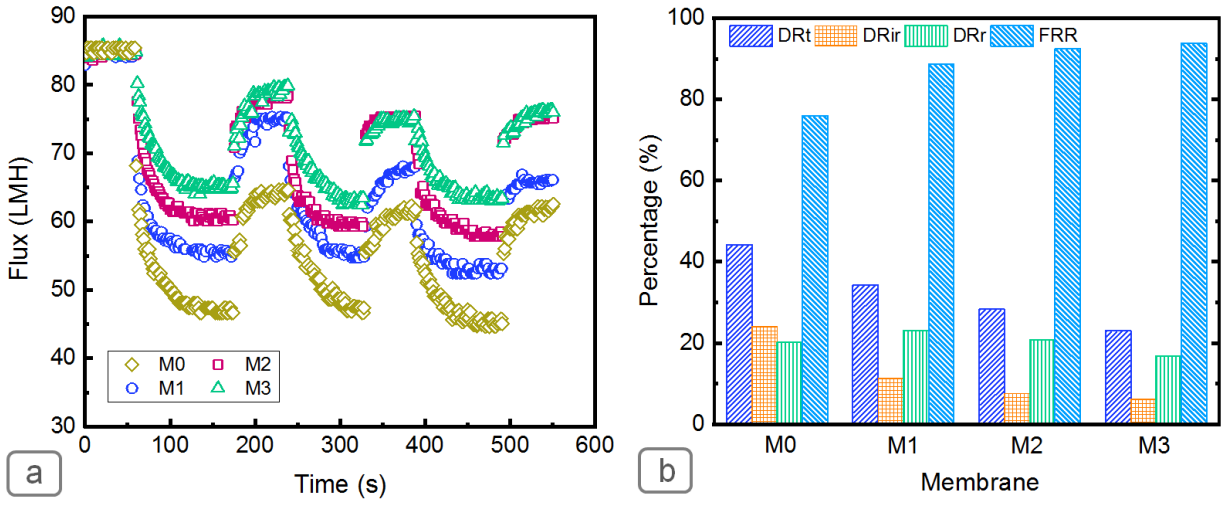

Figure 3-6: (a) Cyclic permeation flux of pristine (M0) and LbL-coated membranes M1, M2, and M3, during oil emulsion filtration, and (b) the respective fouling parameters of the membrane. The TMP for each LbL-membrane was adjusted to yield the same initial flux as M0 membrane.

The surface hydrophilicity, molecular weight cut off, and surface roughness can play a dominant role behind the anti-fouling propensity of the membranes [189]. **Figure 3.7** illustrates the water contact angle of the M0 to M3 membranes. For the pristine membrane, the n-decane droplet spread over a large area of the substrate with a water contact angle of 71.1° ± 0.7°. The water contact angle for the LbL-modified membranes decreased with the increase in the number of BLs, from 42.4° ± 0.2° to 33.1° ± 0.4° and then 22.6° ± 0.5° for M1, M2, and M3, respectively. This observation demonstrates the higher hydrophilicity of the LbL-modified membranes compared to pristine PES support. As described in section 3.1, the coated lignin layer contains multiple hydrophilic functional groups such as phenols, carboxylates, sulfonate, and aliphatic alcohols in its structure, which renders the hydrophilicity of the coated membranes. Accordingly, the higher anti-fouling propensity of the LbL-modified membranes compared to the pristine membrane can be attributed, in the first place, to the higher hydrophilicity of their topmost lignin layer which offers lower adhesion of hydrophobic foulants to their surface.

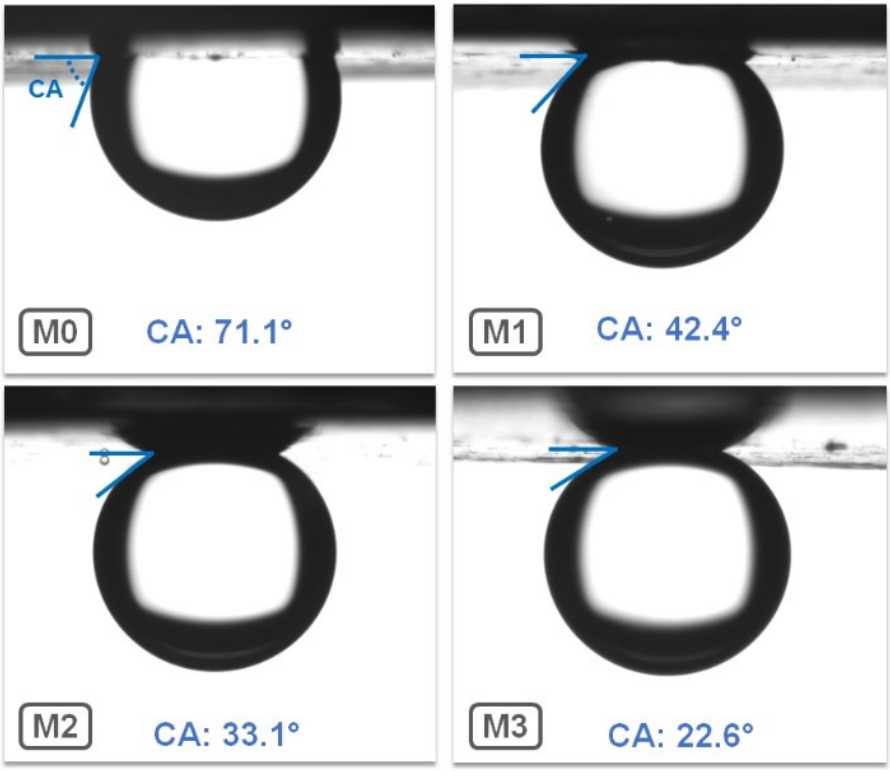

Figure 3-7: Underwater surface wettability of pristine PES support (M0) and the LbL-modified membranes with 1 to 3 BLs (M1-M3). The wettability analysis was conducted using the captive n-decane bubble under water. The reported values in the figure are the water contact angle (CA), which is the complementary angle of the n-decane contact angle with the surface of the membrane

In addition to surface hydrophilicity, the formation of a tighter structure for LbL-modified membranes compared to the pristine PES support can be another contributor to the lower irreversible fouling due to pore blockage. **Figure 3.8** presents the MWCO of the membranes. Compared to the pristine M0 membrane, the formation of the first BL significantly reduced the MWCO from 19 kDa to 4.8 kDa. The deposition of the second and third BLs resulted in a slightly tighter structure with the MWCO of 3 kDa and 2 kDa for M2 and M3 membranes, respectively. The lower MWCO of the LbL-assembled membranes may justify their lower flux decline and higher flux recovery ratio compared to the pristine membrane. The tighter structure of the LbL-assembled membranes prevents the foulants from penetrating into the pores and lowers the possibility of permanent blocking of the membrane pores.

Lastly, the surface morphology and roughness of the membranes can also affect their fouling tendency. In general, a membrane with a smooth surface is less prone to fouling compared to a rough membrane as it provides less contact area for the deposition of the foulants [40]. The FESEM surface images of the pristine and modified membranes in **Figure 3.9** illustrate that all the membranes have a smooth and featureless surface. Based on the AFM analysis, the surface roughness (**insets in Figure 3.9**) of the pristine membrane slightly decreased by the formation of pDAC/lignin BLs, suggesting that the roughness of the membrane surface can be smoothed by increasing the number of BLs [190,191]. The smoother features of the LbL-modified membranes may have contributed to their lower flux decline and higher flux recovery during the oil filtration.

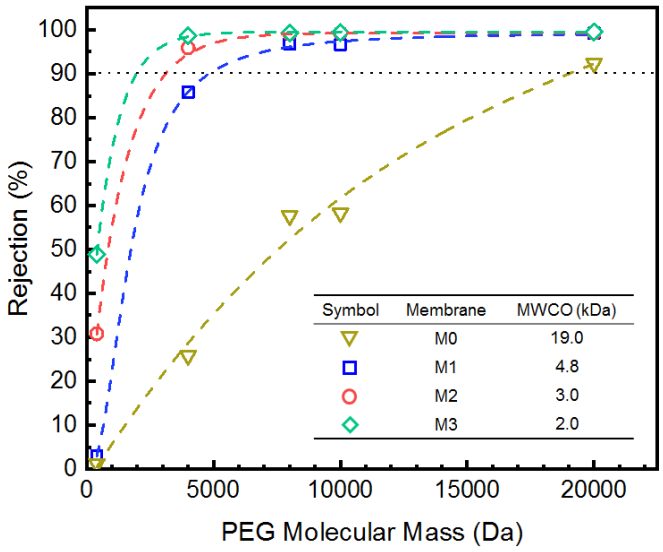

Figure 3-8: MWCO of the pristine (M0), and LbL-modified membranes (M1 to M3) prepared with 1 to 3 BLs. PEG was used to determine the MWCO of the membranes.

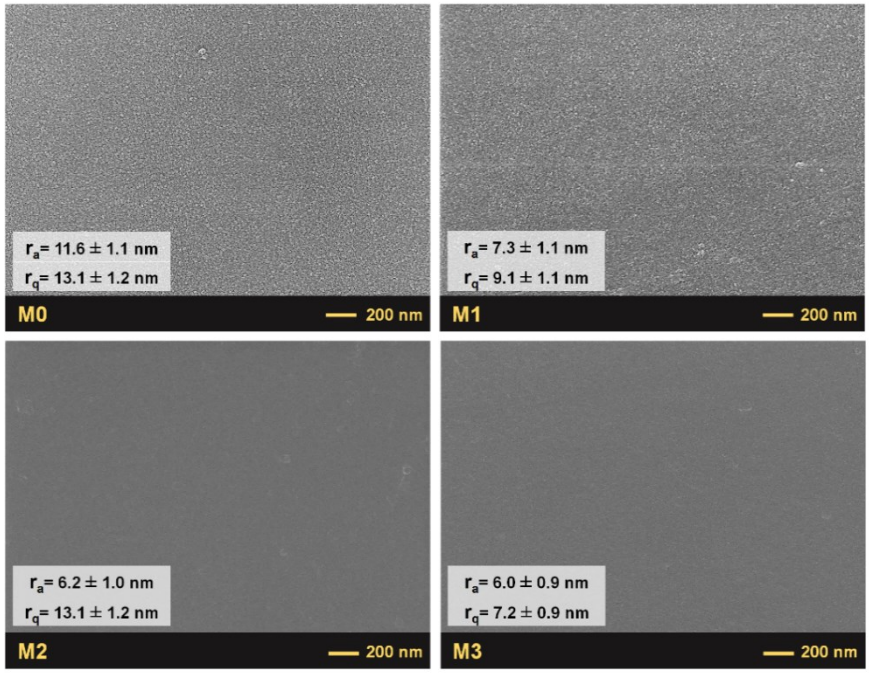

Figure 3-9: FESEM surface images of pristine (M0), and the LbL-modified M1, M2, M3 membranes prepared with 1, 2, and 3 BLs of pDAC/lignin. The parameters r_a and r_q are the average roughness and root mean square roughness, respectively.

3.4 Conclusion

In the present work, we utilized an industrial waste, sulfonated kraft lignin, for surface modification of the PES membrane. LbL assembly technique was used to coat alternative layers of lignin and pDAC on the PES surface. The influence of the concentration of polyelectrolytes and the number of coating BLs on the permeation and anti-fouling properties of the membranes was studied. The modified membrane, prepared with 3 BLs of pDAC/lignin from a 2 wt.% concentration of the respective solutions, demonstrated the highest surface hydrophilicity (22.6° ± 0.5° water contact angle), as well as, the highest fouling resistance (23% flux decline and 93.8 % FRR). In contrast, the pristine PES membrane provided the lowest resistance against fouling (flux decline of 44.2 %, FRR of 75.9 %, and contact angle of 71.1° ± 0.7°) under similar test conditions. Various chemical modification methods can be utilized to increase the versatility of the coating method on different types of membranes. For instance, quaternary ammonium groups can be introduced on lignin structure or silver nanoparticles can be deposited on the lignin coated membranes to attain anti-bacterial properties. The abundance of lignin as an agro-industrial waste and its inherent hydrophilicity make it as an effective coating material for the development of anti-fouling membranes.

Chapter 4

Novel Lignin-modified Thin Film Composite Polyamide Osmosis Membranes: Waste Material for Wastewater Treatment[‡]

[‡] This chapter was prepared based on a manuscript entitled as "Novel Lignin-modified Thin Film Composite Forward Osmosis Membranes: Waste Material for Wastewater Treatment", submitted to the journal of Membrane Science.

4.1 Introduction

Thin-film composite (TFC) membranes, which are widely used in forward osmosis (FO) operation, include a microporous support layer (~ 50-150 μm) with an ultrathin (~100-200 nm) polyamide (PA) active layer on top [26,27]. The PA active layer acts as a selective transport barrier, while the sublayer ensures mechanical support for the TFC structure [26]. The PA selective layer is made through interfacial polymerization (IP) over the support surface between an aqueous diamine and an organic acyl chloride solutions [28]. Due to high reactivity of monomers and immiscibility of the organic and aqueous solutions, the IP reaction results in an ultrathin PA layer at the interface [28]. The multilayer design of the TFC membranes offers the possibility of independent modification of the different layers of the membranes [29].

Despite the promising characteristics of lignin derivatives, the reported efforts have been mostly restricted to modifying the support layer to improve the permeation performance, contaminant removal, thermomechanical stability, and antifouling property of pressure-driven membranes [30–32]. Despite the many advantages of lignin, only one report by Zhou et al. [33] has studied the application of a lignin derivative for modifying the surface TFC membranes. They used ammonium lignosulfonate as a monomer to fabricate organic solvent nanofiltration TFC membrane using a crosslinked poly(ether imide) sublayer. Although the synthesized membranes exhibited strong organic solvent resistance, enhanced organic solvent permeability, and high rejection for Brilliant Blue R-250, their salt rejection performance was relatively low (~20% for NaCl and $MgCl_2$). In addition to the poor salt rejecting properties, the proposed synthesis route was also more complicated than the typical IP reaction to synthesize PA membranes, raising more concerns regarding the robustness of the synthesized membranes and their manufacturing scale-up.

In this study, we used SKL, a derivative of agro-industrial wastes, to modify the permeation performance and fouling resistance of TFC PA membranes. Different concentrations of SKL were added into the aqueous monomer solution, and the PA layer was synthesized via IP reaction over a PES microporous support. Three TFC membranes were synthesized by employing different concentrations of SKL. FESEM, transmission electron microscopy (TEM), AFM, ATR-FTIR spectroscopy, and drop shape analysis were utilized to investigate the surface morphological and physicochemical characteristics of the synthesized membranes. The water flux, solute rejection,

and antifouling performance of the TFC membranes were investigated in a FO operation. Sodium alginate was used as a model organic foulant, and SAGD BFW was used as an industrial wastewater in the fouling experiments.

4.2 Materials and methods

4.2.1 Chemicals and reagents

Flat sheet PES MF membranes (average pore size: 0.2 μm) were purchased from Sterlitech Co. (WA, USA) and used as the support layer of TFC membranes. M-phenylenediamine (MPD, ≥ 99%, Sigma-Aldrich) and trimesoyl chloride (TMC, 98%, Sigma-Aldrich) were used as reacting monomers in IP to form the PA film. Sulfonated kraft lignin (SKL, Mw.: 5–8 kDa, West Fraser Company, BC, Canada), triethylamine (TEA, Fisher Scientific, Canada), sodium dodecyl sulfate (SDS, Fisher Scientific, Canada) were used as additives in aqueous solution. Heptane (≥ 99%, Fisher Scientific, Canada) was used as a solvent in the TMC solution. Sodium chloride (NaCl, ≥ 99%, Fisher Scientific, Canada) was used to evaluate the salt rejection of the membranes. Sodium alginate (Mw. 12-80 kDa, Sigma-Aldrich, St. Louis, MO) was selected as a model organic foulant in fouling tests. Calcium chloride ($CaCl_2$, Fisher Scientific, Canada) was added to the filtration solution to cross-link the sodium alginate chains. BFW was obtained from a SAGD water treatment plant located in the Athabasca oil sands region, Alberta, Canada.

4.2.2 Synthesis of TFC PA membranes

The fabrication of TFC membranes is illustrated in Figure 1. The MPD-SKL dispersion was prepared by dispersing 1, 3, and 6 wt.% SKL in DI water and sonicating for 10 minutes using an ultrasonic bath (FS30H, Fisher Scientific, Canada). Afterwards, the samples were centrifuged at 12,000 rpm for 20 minutes to remove the suspended solids. The mass of precipitated SKL powders was almost negligible, about 0.01%, 0.75%, and 0.82% of the initial mass used to prepare 1, 3, and 6 wt.% SKL in DI water, respectively. The supernatant was then used to make the amine solution with the composition of 2 wt.% MPD, 1 wt.% TEA, and 0.2 wt.% SDS. Fabrication of TFC membrane started by impregnating the PES support with MPD-SKL dispersion for 9 min. Then, the MPD-SKL dispersion was discarded, and the residual amine was taken out by rolling the surface of the support. Next, a 0.2 wt.% TMC solution was poured over the PES support and left for 30 seconds. Then, the membranes were heated at 60 °C for 4 minutes. At the end, the

membranes were carefully rinsed with DI water to remove the residual compounds. Four membranes were fabricated using 0, 1, (~)3, and (~)6 wt.% SKL in MPD solution and labeled as M0, M1, M2, and M3, respectively.

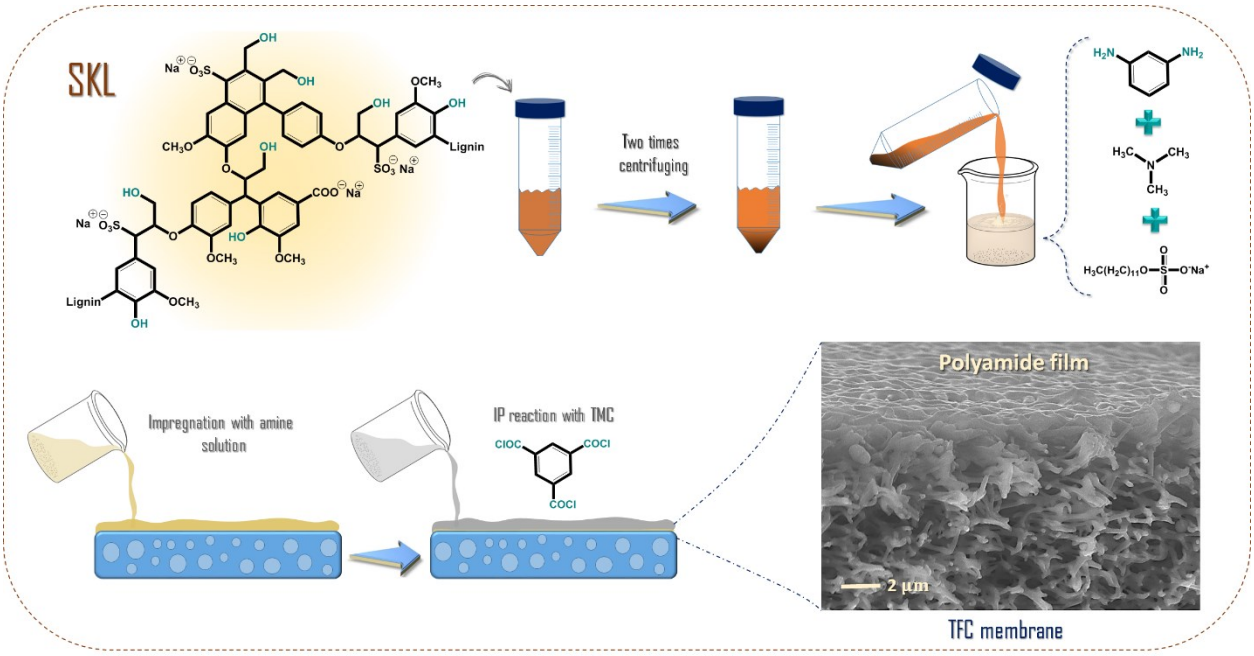

Figure 4-1: Schematic diagram of the fabrication of the TFC membranes via IP between MPD and TMC using SKL as an additive over the PES substrate.

4.2.3 Characterization of physicochemical properties of membranes

FESEM (Zeiss Sigma 300 VP) was employed to observe the surface morphology of the fabricated membranes. A thin film of carbon was sputter-coated on the surface of membranes before imaging. TEM (Philips/FEI Morgagni 268, The Netherlands) was used to observe the cross-sectional images of the TFC membranes. TEM samples were prepared by staining the TFC membranes in uranyl acetate and lead citrate. The samples then were embedded in Spurr's resin, and sectioned by ultramicrotome (Reichert-Jung Ultracut E, USA). AFM (Bruker Dimension Icon, USA) was employed to evaluate the surface topography of the PA layer. AFM analysis was performed in tapping mode under ambient conditions. ATR-FTIR was employed to investigate the chemical composition of the membranes. The spectra were recorded in air and at room temperature using an Agilent Technologies, Cary 600 series FTIR spectrometer. The surface wettability of the

membranes was evaluated by measuring the contact angle of water over the membrane surface at ambient conditions by sessile drop technique using a Krüss DSA 100 instrument (Krüss GmbH, Germany) instrument. A 5 µl droplet of DI water was placed on the membrane surface and the dynamic contact angle was recorded at a shooting frequency of 25 frames per second. The equilibrium contact angle was reported after 30 sec. The wettability measurement was repeated at five different positions on each sample.

4.2.4 Evaluation of membrane performance in FO

The performance of the synthesized TFC membranes were measured in two configurations, namely FO mode in which the poalyamide active layer faced toward the feed solution (AL-FS), and pressure retarded osmosis (PRO) mode where the active layer was in the draw solution (AL-DS) [27]. The specifications of the FO membrane cell is provided elsewhere [27]. The flow rates of the draw and feed streams were set to 1 L/min (LPM). FO filtration tests with the AL-DS configuration were conducted to evaluate the water permeability coefficient (*A)* and salt permeability coefficient (*B*). For these experiments, NaCl solution of different concentrations (0.5-2 M with 0.5 M interval) was utilized as the draw solution. To diminish the impact of concentrative internal concentration polarization (ICP), DI water was selected as the feed solution. In concentrative ICP, solutes are accumulated inside the porous sublayer due to the combined effect of water passage from the feed to draw solution, as well as reverse salt passage from draw to feed solution [36]. By using DI water as a feed solution, ICP occurs only due to the reverse draw salt passage to the feed solution [36]. The feed conductivities, measured in different time intervals, were used to obtain reverse salt flux (J_s). The water flux (J_w) was obtained through measurement of draw solution mass as follows [37]:

$$J_{\mathrm{w}} = \frac{\Delta m}{\rho A_{em} \Delta t} \tag{4.1}$$

Δm in **Equation 4.1** is the collected draw solution mass over time, Δt, A_{em} is the active area of the membrane surface, and ρ is water density. The permeation flux through the membranes was modeled by considering the dilutive external concentration polarization (ECP) as follows:

$$J_{\mathrm{w}} = A \Delta \pi_e \tag{4.2}$$

In this equation, A is defined as water permeability coefficient and $\Delta\pi_e$ is effective osmotic pressure gradient across the PA layer. Dilutive ECP occurs when the convective permeate flow drags draw solutes away from the top selective layer [38]. This phenomenon reduces the concentration of the draw solution at the surface of membrane, thereby decreasing the effective driving force [37]. Therefore, it is essential to find the overall effective osmotic driving force across the membrane. For this purpose, the solute concentration in the draw side over the membrane active layer, $C_{D,m}$, needs to be determined. The first step is to calculate Sherwood number using the following correlations for a rectangular channel [38]:

$$Sh = 1.85\left(ReSc\frac{d_h}{L_c}\right)^{0.33} \quad \text{(laminar flow)} \tag{4.3}$$

$$Sh = 0.04Re^{0.75}Sc^{0.33} \quad \text{(turbulent flow)} \tag{4.4}$$

$$Re = \frac{\rho d_h v}{\mu} \tag{4.5}$$

$$Sc = \frac{\mu}{\rho D_s} \tag{4.6}$$

where Re, Sc, d_h, L_c refer to the Reynolds number, Schmidt number, hydraulic diameter, and the channel length, respectively. Furthermroe, D_s is the solute diffusivity coefficient, μ is viscosity, v is velocity, and ρ is water density [38]. **Table 4-1** presents the values of μ, ρ, and D_s, employed in this work at 22 °C [39–41]. The solute mass transfer coefficient in draw side, k, is related to Sh number using **Equation 4.7** [36]:

$$Sh = \frac{kd_h}{D_s} \tag{4.7}$$

Table 4-1: the values of μ, ρ, and D_S at 22 °C, employed for the calculation of the membrane's intrinsic properties [39–41]

Draw solution Conc. (mol.Lit^{-1})	Viscosity (mPa.s)	Density (kg.m^{-3})	D_S ($\times 10^{-9}$m^2/s)
0.5	1.04	1017	1.47
1	1.09	1036	1.48
1.5	1.14	1054	1.50
2	1.20	1072	1.51

Afterward, the dilutive ECP modulus at each permeate flux, $J_{w,i}$, is calculated from **equation 1.17** by canceling the terms, related to the feed solution and solute leakage [36]:

$$\frac{C_{\mathrm{D,m}}}{C_{\mathrm{D,b}}} = \exp\left(-\frac{J_{\mathrm{w}}}{k}\right) \tag{4.8}$$

where $C_{D,b}$ is the draw solute concentration in the bulk, $C_{D,m}$ is the effective draw solute concentration in the draw solution at the surface of membrane resulted from the dilutive ECP, and J_w is the permeate flux at each step [42]. Once the draw solution concentration at the membrane surface was determined, van't Hoff equation (**Equation 4.9**) was used to calculate the effective osmotic pressure, $\pi_{D,e}$ (bar), as below [43]:

$$\pi_{D,e} = nC_{D,m}RT \tag{4.9}$$

where n is the number of ionic species that each solute molecule can dissociate into, $C_{D,m}$ is the solute concentration (mol/L), R is the universal gas constant (8.314 J/mol K), and T is the absolute temperature (K) [43].

To find A, the water flux was plotted against the effective osmotic pressure difference, and the value of A was determined as the plot slop based on **Equation 4.2** [42].

The selectivity of the membranes was modeled as follows:

$$J_s = B\left(C_{D,m} - C_{F,m}\right) \tag{4.10}$$

This equation provides the correlation of the reverse salt flux (J_s), measured through the experiments, with the effective salt concentration difference. B is the solute permeability coefficient, and $C_{D,m}$ and $C_{F,m}$ are the effective solute concentrations in the draw and feed solutions at the selective layer interface, respectively [44]. The bulk concentrations of the feed and draw solution were evaluated based on the conductivity of solutions measured using a conductivity meter (Accumet research AR50, Fisher Scientific, Canada).

The solute permeability, B, is obtained by dividing the reverse salt flux, J_s, by the effective concentration of the draw solution at the surface of the membranes, as follows [42]:

$$B = \frac{J_{\mathrm{s},i}}{C_{\mathrm{D,bi}}\exp\left(-\frac{J_{\mathrm{w,i}}}{k}\right)} \tag{4.11}$$

where k is the solute mass transfer coefficient, calculated for a rectangular cell [42]. The bulk solute concentration of the feed and draw solutions were evaluated based on the conductivity of the solutions measured using a conductometer (AR50 Accumet research, Fisher Scientific).

4.2.5 Evaluation of fouling performance of the membranes

Fouling experiments were performed in the AL-FS configuration with 0.5 mM of $CaCl_2$ and 1 g/L sodium alginate in water as the model foulants and SAGD BFW as the industrial wastewater. In all fouling tests, NaCl was used as the draw solute. During the fouling tests, the permeation of water through the membranes, the reverse solute passage, ICP, ECP, and fouling result in a gradual decline in the effective osmotic pressure and consequently a simultaneous decline in the permeation flux. To exclusively investigate the effect of fouling on the flux decline, a baseline experiment was performed for each fouling test with a feed solution containing only salt. $CaCl_2$ and NaCl were utilized as the salt for the baseline tests corresponding to sodium alginate and SAGD BFW, respectively. Given that the goal was to evaluate the fouling propensities of the membranes, the water flux results of the fouling experiments were corrected with the results of the baseline experiments to eliminate the effect of draw solution dilution. The following equation was used to calculate the total flux decline ratio (DR_t).

$$DR_t = 1 - \frac{J_{cw,f}}{J_{w,i}} \tag{4.12}$$

$J_{w,i}$ and $J_{cw,f}$ are the initial and final corrected water flux in the fouling experiments, respectively. Relative fouling degree (RFD) of the membranes was determined as the percentage of the flux drop due to the fouling contribution and was calculated as follows.

$$RFD = \frac{J_{w,b} - J_{w,f}}{J_{w,b}} \tag{4.13}$$

where the subscripts b and f stand for the *baseline* and the fouling experiments, respectively. $J_{w,b}$ is the water flux of the baseline experiment, and $J_{w,f}$ is the final water flux of the corresponding fouling experiment [42]. All tests were conducted for 4 hr, and the average of the last three data points was reported as the final flux value in each step.

4.3 Results and discussion

4.3.1 Chemical composition of the synthesized PA layer

Figure 4.2 presents the ATR-FTIR spectra of the TFC membranes. The evolution of characteristic peaks at 1410 cm^{-1}, 1481 cm^{-1}, and 1580 cm^{-1} correspond to the benzene ring vibration of the PES support. The PA characteristic absorption peaks at 1541 cm^{-1} (C=O stretching of the amide I bond), 1611 cm^{-1} (aromatic amide ring stretching), and 1667 cm^{-1} (N–H bending of amide II in the –amide group) arise for the TFC membranes (M0, M1, M2, and M3) that endorses the formation of the PA active layer on the support [45,46].

4.3.2 Surface morphology and wettability of the TFC membranes

FESEM and TEM characterization techniques were used to examine the top surface and the cross-sectional morphologies of the synthesized membranes. All the synthesized TFC membranes, presented in **Figure 4.3a-d**, were covered by a PA layer having a ridge-and-valley structure. The TEM cross-sectional images in **Figure 4.3e-h** illustrate that the addition of SKL additives to MPD-aqueous solution generated more free volumes with different size and spatial distribution within the PA layer. Furthermore, it can be observed that compared to the pristine membranes the PA layer of the SKL-modified membranes had larger ridges and valleys. **Figure 4.3i-l** presents the average contact angles of the synthesized membranes. Embedding the SKL to the PA layer has reduced the water contact angle from 88.7° ± 2.7° for M0 to 70.6° ± 1.3° for SKL-modified membranes. This observation shows the enhancement of the wettability of the SKL-incorporated membranes relative to unmodified membrane due to the presence of hydrophilic functionalities such as aliphatic alcohols, phenols, carboxylates, and sulfonates in SKL [2].

AFM was used to evaluate the surface topography and roughness of the membranes. The average (R_a) and root-mean-square (R_q) surface roughness of the TFC membranes are presented in **Figure 4.4**. The 2D and 3D images confirm the formation of the ridge-and-valley structure over the surface of the TFC membranes. Moreover, the results showed that the addition of the SKL additives improved the surface roughness of the modified membranes relative to the pristine M0 membrane.

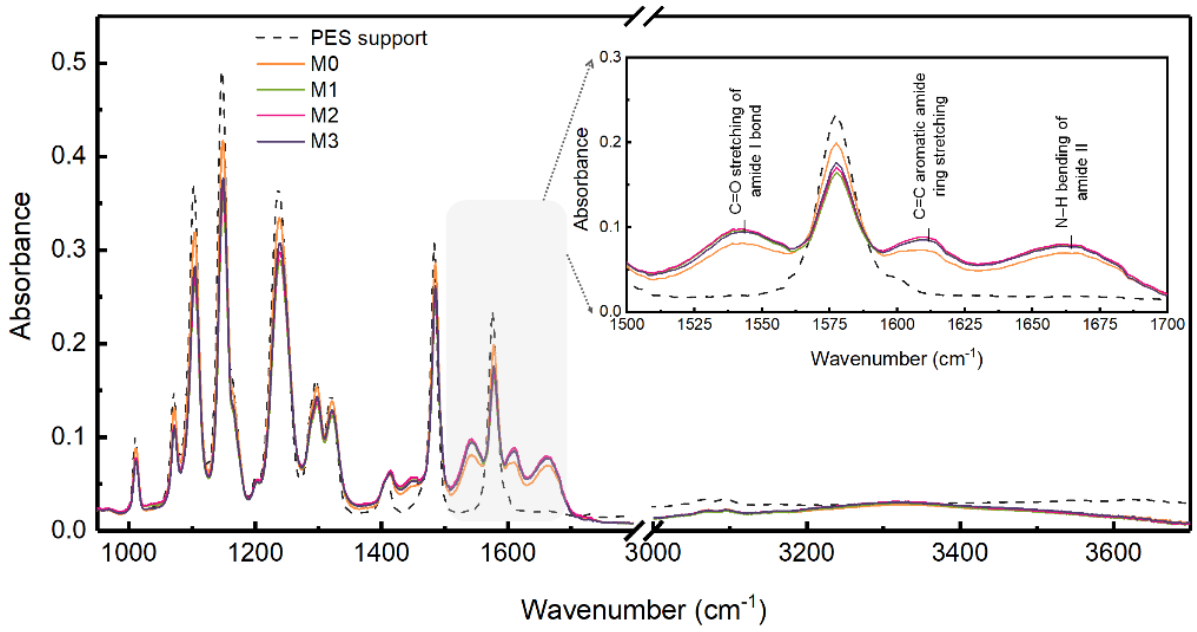

Figure 4-2: ATR-FTIR spectra of the PES support and the synthesized TFC membranes (M0, M1, M2, and M3).

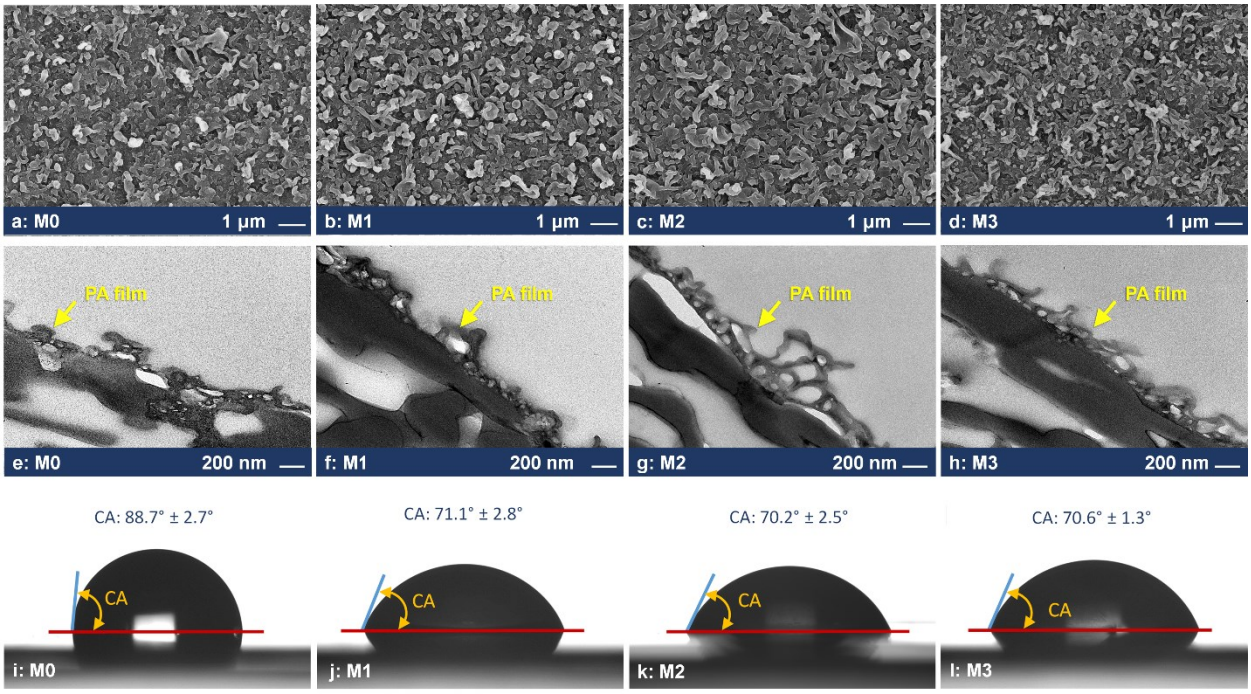

Figure 4-3: Top surface FESEM photos of the (a) M0 (pristine TFC), and SKL-incorporated TFC membranes (b) M1, (c) M2, and (d) M3. TEM cross-section images of the (e) M0, (f) M1, (g) M2, and (h) M3. Surface wettability of (i-l) the pristine (M0) and the SKL-modified (M1-M3) membranes.

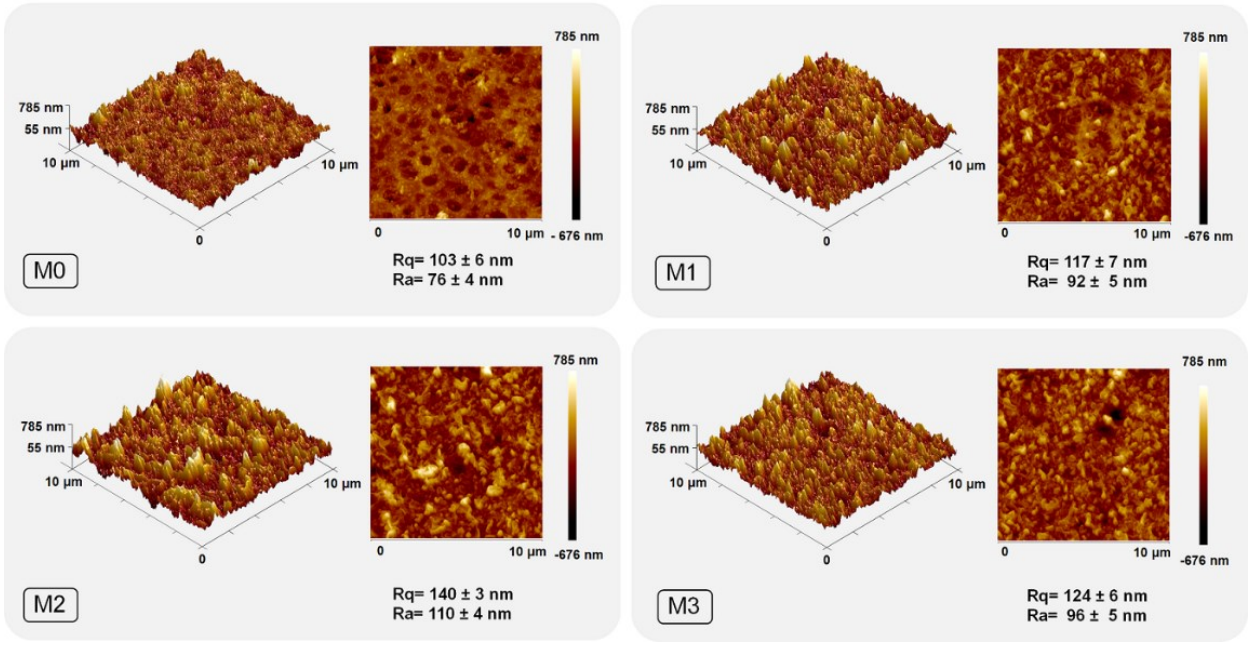

Figure 4-4: AFM 3D and 2D images and the surface roughness results of the unmodified membrane (M0) and SKL-embedded TFC samples (M1, M2, and M3).

4.3.3 Characterization of the membrane transport properties

Figure 4.5a illustrates the water flux versus the effective osmotic pressure difference across the membrane by considering the effect of dilutive ECP in the draw side. The water permeability coefficient of the membranes was improved from 0.2 LMH/bar for M0 (0 wt.% SKL content) to 0.3 LMH/bar for M3 (6 wt.% SKL content) at the expense of an increase in the salt permeability from 0.05 LMH for M0 to 0.1 LMH for M3 (**Figure 4.5b**). The improved water permeability of the SKL-modified membranes can be ascribed to (i) enhanced wettability of these membranes due to the presence of hydrophilic SKL additives and (ii) decrease of crosslinking density and formation of larger nanovoids within their PA structure [47]. The latter seems to be more significant as wettability analysis provided almost similar contact angle values for SKL-modified membranes, and salt permeability increased by increasing SKL loading.

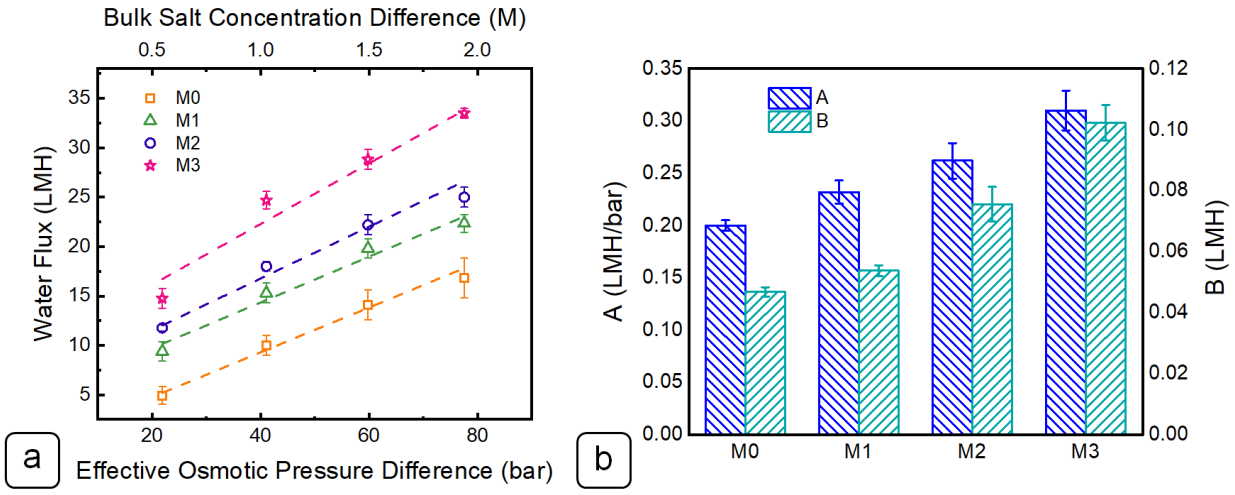

Figure 4-5: (a) Water fluxes versus effective osmotic pressure gradient in AL-DS mode; (b) Water permeability coefficient (A), and salt permeability coefficient (B). NaCl concentrations of 0.5, 1, 1.5, and 2 M were applied as the draw solutions. DI water was used as the feed solution and the cross-flow velocities of the feed and the draw sides were adjusted at 1 LPM.

Figures 4.6a and 4.6c present the FO water flux of the TFC membranes over a range of bulk osmotic pressure difference in AL-DS and AL-FS configurations, respectively. In general, the water flux in the AL-DS configuration is higher than the AL-FS configuration due to milder effect of ICP in the support layer. With DI water as the feed solution, the diluted ICP within the porous sublayer is more significant in the AL-FS configuration than the diluted ECP under the AL-DS mode [48]. Consequently, the effective osmotic driving force is always greater in AL-DS configuration. In both operational modes water flux improved by increasing the osmotic pressure gradient across the membranes. The water flux increased at a lower rate when the osmotic pressure was large (1.5 and 2 M), mainly due to higher impact of ICP inside the porous support layer in AL-FS configuration, as well as larger ECP at the PA layer-draw solution in AL-DS configuration. The addition of SKL additive from 1 wt.% (M1) to 6 wt.% (M3) could increase the water flux about two to three times.

Figures 4.6b and 4.6d illustrate the reverse salt flux (J_s) of the membranes for 2 M draw solution concentration in AL-DS and AL-FD configurations. All the synthesized membranes showed the reverse salt flux of less than 8 gMH in both operation modes, indicating that the modification procedure did not result in destructive effects on the selectivity of the PA layer. The reverse salt flux was approximately the same for M0 and M1 and increased slightly for M2 to M3

in both configurations. The higher values of J_s for M2 and M3 is likely due to the lower crosslinking density of their PA layers, leading to lower salt rejection than that of M1 and M0 membranes. The specific salt flux (J_s/J_w) is another important parameter in FO that indicates the amount of salt transported across the membrane per unit volume of the transported water [27]. Lower values of reverse salt flux and specific salt flux are desirable for a high-performance FO membrane [49]. The results of both configurations suggest that, while M0 provided the lowest reverse salt passage, its specific solute flux was higher than all SKL-modified membranes. For the case of M1 membrane, the positive contribution of SKL additives on the enhancement of the water flux outweighed its adverse effect on salt permeability, and thus provided the lowest specific solute flux among all the TFC membranes.

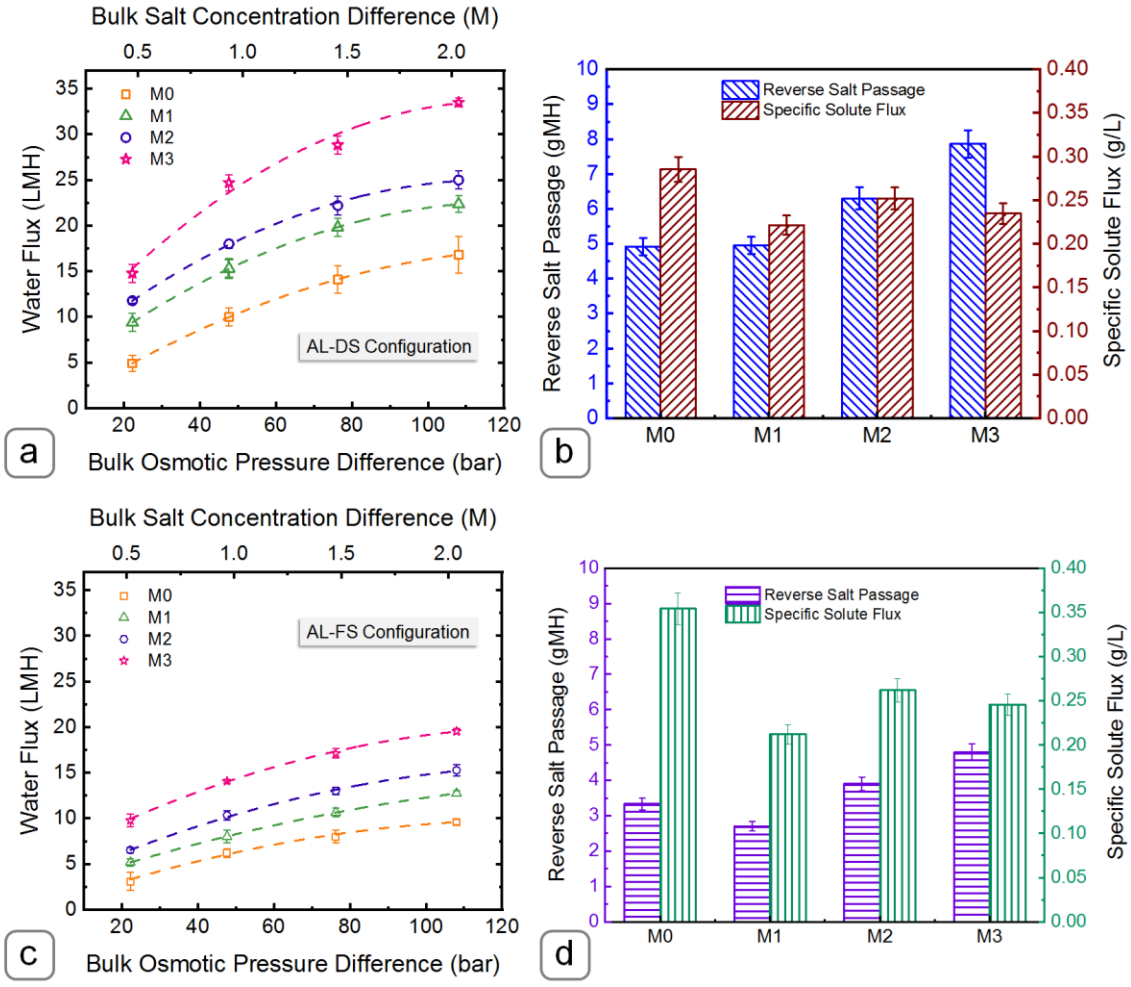

Figure 4-6: (a) Permeation performance in AL-DS configuration, (b) reverse salt passage and specific solute flux in AL-DS configuration for 2 M draw solution; (c) Water flux in AL-FS operation mode; (d) Reverse salt flux and specific salt flux in AL-FS configuration for 2 M draw solution

4.3.4 Evaluation of the fouling resistance of the membranes

Figure 4.7a presents the fouling behavior of the synthesized membranes for filtration of sodium alginate solution. All membranes exhibited a fast flux reduction during the initial 30 min of the fouling tests. Afterward, the membranes showed a gradual decline, whereas the rate of the flux decline decreased by increasing the SKL loading. Among the membranes, M3 possessed the minimum DR_t of 11.5% compared to the 18.9% DR_t of the pristine M0. Moreover, the M3 membrane exhibited an RFD of 10.2%, much lower than 27.7% RFD of the M0 membrane. The initial sharp flux drop is likely due to formation of a gel layer at the membranes' surface. In the presence of Ca^{2+}, carboxylate groups of alginate molecules attach together and form a gel network on the surface [50]. The deposited alginate film caused additional resistance to water passage and resulted in a sharp initial flux decline [51]. Once a gel layer was formed, further bridging could be developed between the alginate molecules in feed solution and alginate film at the surface, which contributed to the continuous growth of the gel layer at the membrane surface and consequently gradual flux decline [51]. Moreover, the ions that diffused through the active layer due to reverse salt flux could be piled up within the gel layer and decrease the effective osmotic pressure gradient [52]. This phenomenon, cake-enhanced osmotic pressure, could also contribute to the gradual flux reduction in the later stages of the fouling tests [52].

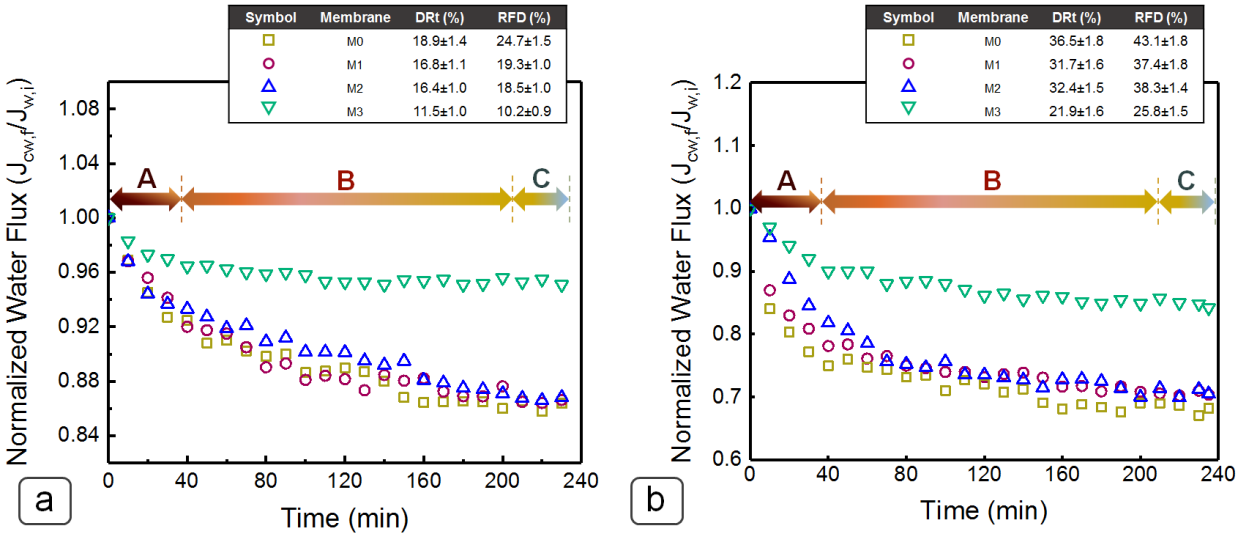

Figure 4-7: Permeation flux and fouling parameters of the membranes during the filtration of (a) 1000 ppm of sodium alginate and (b) SAGD BFW in AL-FS configuration. The normalized water flux was calculated by dividing the corrected water flux by the initial water flux ($J_{cw,f}/J_{w,i}$). A, B, and C correspond to the initial sharp flux decline region, gradual flux decline region, and steady-state region, respectively.

A similar trend of initial fast decline followed by a gradual decrease was observed for the membranes during the filtration of SAGD BFW. **Figure 4.7b** illustrates that the SKL-modified membranes provided superior antifouling performance in comparison with the pristine TFC. Although water permeability was almost comparable for M0, M1, and M2 membranes, M3 showed a better performance than that of the other membranes. The DR_t of M3 membrane decreased to 21.9% compared to 36.5% for the pristine M0. Moreover, M3 showed 17.3% less *RFD* relative to the pristine M0 (**Figure 4.7b**). During the first stage of fouling, the organic matter present in the SAGD BFW could possibly plug the hot spots of polyamide surface owing to the van der Waals and hydrophobic attractions, which led to the fast decline of permeate flux [51,53]. Hot spots refer to the valley regions on the surface of membrane, where the PA thickness is minimum, and thus the local permeate flux is maximum. The subsequent gradual flux reduction can be attributed to the accumulation of more organic matter as a result of foulant-foulant attraction as well as cake enhanced osmotic pressure. For both sodium alginate and SAGD BFW, the higher antifouling properties of M3 than M0 can be ascribed to its enhanced hydrophilicity due to the existence of the SKL additives in its structure. The abundance of the hydrophilic functional groups in SKL structure could act as hydrogen bond acceptors to generate a hydration film at the membrane-feed interface. Therefore, it could promote the water permeation and reduce the foulant deposition at the membrane's surface [25].

4.4 Conclusion

In this study, SKL particles were used as a hydrophilic modifier of the PA selective layer of TFC membranes to enhance the permeation and antifouling performances. It was found that by increasing the SKL content to 6 wt.%, the water permeation through the resulting membrane increased by up to two folds compared to pristine membrane at the expense of a slight increase in the reverse salt passage. Moreover, the SKL-embedded membranes showed higher antifouling properties than the pristine TFC membrane when tested with sodium alginate and SAGD BFW solutions. During filtration of sodium alginate, the total flux decline ratio decreased (DR_t) from 18.9% for the unmodified membrane to 11.5% for M3, modified with the maximum concentration of SKL 6 wt%. Moreover, relative fouling degree (*RFD*) reached 10.2% for M3 compared to RFD of 27.7% for the pristine membrane. The DR_t of M3 membrane also decreased to 21.9% compared to 36.5% of the pristine M0 when tested with SAGD BFW solution. M3 membrane exhibited

17.3% less *RFD* compared to the pristine M0 under the same conditions. This improvement was primarily ascribed to their enhanced hydrophilicity by adding the SKL into the PA structure. To further enhance the TFC membrane performance, the polymerization reaction conditions, such as monomer concentrations, can be optimized to include higher loadings of the SKL additive. This study presents a novel route to reuse a waste byproduct, lignin, to fabricate FO TFC membranes with enhanced permeation performance and antifouling properties.

Chapter 5

Conclusion and future work

5.1 Conclusion

Lignin, as one of the most plentiful biopolymers, has exhibited great potential for the modification of membrane properties and opened up a new paradigm in the fabrication of high-performance membranes. Nevertheless, employing lignin for membrane modification encounters some challenges, such as low solubility of lignin in organic solvents and its weak compatibility with host polymer or other employed materials. Due to these drawbacks, non-selective voids can be formed at the surface of the membrane, which adversely influences the separation performance of the modified membranes. In this work, we investigated the potential of sulfonated kraft lignin, an industrial waste derivative, for the modification of UF and FO membranes. We performed comprehensive studies to overcome the drawbacks of incorporating SKL into the polymer films.

Initially, the potential of SKL as a hydrophilic additive for bulk modification of PES UF membranes was studied. To investigate the influence of SKL content on the membrane performance, three membranes with different SKL contents of 1 wt%, 2 wt%, and 3 wt% were synthesized through nonsolvent-induced phase separation technique. The performance of the SKL-blended membranes was compared to the performance of a pristine membrane, fabricated without the addition of SKL. The total concentration of solid was fixed to 16 wt% for all the fabricated membranes. It was observed that the porosity of the SKL-embedded membranes slightly increased compared to the pristine membrane. Studying the surface topography of the fabricated membranes revealed that the surface roughness slightly decreased with increasing the SKL concentration in the polymer solution. The surface wettability of the synthesized membranes was investigated by evaluating the under-water oil contact angle. It was found that the oil drop contact angle increased from 132.8°±1.0° for the pristine membrane to 146.8°±1.0° for the 3 wt% SKL-embedded membrane, indicating that embedding SKL additive enhanced the surface hydrophilicity (i.e., underwater oleophobicity) of the synthesized membranes. The surface electrical charge of the SKL-modified membranes significantly increased relative to the pristine membrane. The results of studying the permeation performance of the synthesized membranes indicated that the hydrodynamic permeability increased from 25.3 LMH/psi for the pristine membrane (MWCO of 623.6 kDa) to 68.6 LMH/psi for the membrane modified with the maximum SKL concentration, 3 wt% (MWCO of 767.7 kDa). The antifouling performance of the synthesized membranes was studied via filtration of SAGD BFW. It was found that the flux decline ratio slightly decreased by

increasing the SKL concentration, while the flux recovery ratio significantly increased from 52.2% for the pristine membrane (DRt of 86.4%) to 98.2% for the 3 wt% SKL-modified membrane (DRt of 77.8%). The improved antifouling characteristics of the SKL-embedded membranes were related primarily to the enhanced hydrophilicity of these membranes due to the presence of hydrophilic functional groups of SKL on the surface of these membranes. Moreover, due to the anionic nature of the organic foulants in SAGD BFW, the higher negative surface charge of the SKL-modified membranes could also contribute to the improved antifouling properties of these membranes against the organic matters in BFW. The surface roughness of membranes strongly affects the antifouling characteristics of membranes. The smoother surface of the SKL-embedded membranes, confirmed by the AFM results, could enhance the fouling resistance of the modified membranes. Interestingly, it was observed that despite the increase of the MWCO of the SKL-embedded membranes compared to the pristine membrane by 144 kDa, the rejection of the organic matter decreased by just 9%, which can be related to the combined effect of the enhanced hydrophilicity and negative surface charge of the SKL-embedded membranes. The findings of this study open up an economical process for using the abundant industrial waste, SKL, for the treatment of process-affected water (e.g., SAGD BFW). The fabricated SKL-modified can be employed as a pretreatment step for the filtration of SAGD produced water prior to delivering it to NF or RO post-treatment. The pretreatment of the wastewater as the feed solution can significantly improve the overall performance of the membrane-based water treatment processes. Moreover, the current traditional water treatment processes employed in the SAGD produced water treatment only separate ~90% of divalent ions and silica and do not provide any separation for the dissolved organic matter. Therefore, employing the SKL-blended membrane to remove the organic matter considerably decreases the boiler failure and clogging of the injection wells.

In order to study the application of SKL to surface modification of PES UF membranes, SKL was coated on the surface of the membranes using the LBL technique with pDAC and SKL as the polycation and polyanion, respectively. The effect of PE concentration and number of PE BLs on the performance of the membranes was studied. The effect of PE concentration was studied by coating the pristine membrane with 2 PE BLs and PE concentrations of 0.1 wt%, 0.5 wt%, 1, and 2 wt%. To investigate the influence of the number of PE BLs, 4 membranes were synthesized with 1, 2, and 3 BLs and employing 2 wt% PE concentration. The presence of SKL on the surface of the LBL-assembled membranes was probed by XPS analysis. The antifouling characteristics of

the membranes were evaluated through the filtration of oil-in-water emulsion using n-hexadecane as the oil. The results of the tests to find the effect of the PE concentrations showed that the hydrodynamic permeability of the fabricated membranes decreased from 3.8 LMH/psi for the pristine membrane to 3.1 LMH/psi for the membrane fabricated with 2 PE BLs and 2 wt% PE concentration. The pristine membrane possessed the largest flux decline ratio of 44.2% and the lowest flux recovery ratio of 76.0% during filtration of an oil-in-water emulsion. The lowest flux decline ratio of 28.3% and the largest flux recovery ratio of 92.4% were observed for the membrane coated with 2 PE BLs and 2 wt% PE concentration. Investigating the effect of PE BL number revealed that the permeability of the membranes reduced from 3.8 LMH/psi for the pristine membrane to 1.6 LMH/psi for the membrane coated with 3 BLs and 2 wt% PE concentration. This membrane also possessed the lowest flux decline ratio of 23.1% and the highest flux recovery of 93.8% as compared to the pristine membrane with the lowest antifouling properties. This observation was rationalized by the surface hydrophilicity of the membranes. Evaluating the surface wettability of the membranes by measuring the under-water oil contact angle exhibited that the water contact angle of the oil drop decreased from $71.1° \pm 0.7°$ for the pristine membrane to $22.6° \pm 0.5°$ for the 3 BLs coated membrane. Accordingly, the improved antifouling propensities of the LbL-assembled membranes can be mainly attributed to the higher hydrophilicity of these membranes. The tighter structure of the LbL-assembled membranes relative to the pristine membrane can also contribute to the higher antifouling properties of these membranes due to the decrease of the pore blockage during the fouling test. Moreover, the results of the AFM test showed that the LbL-assembled membranes possessed a slightly smoother surface compared to the pristine membrane. The smoother surface of these membranes can be another contributor to their higher antifouling properties. The high antifouling properties of the membranes, LbL-assembled with SKL, show the possibility of these membranes for long-term and continuous operation with simple cleaning and back-flushing process without a need for frequent shut-down. The significantly high fouling resistance of the SKL-coated membranes towards oily wastewater treatment as one of the harsh foulants makes these membranes potent candidates for the treatment of process-affected waters, such as SAGD produced water.

Finally, to enhance the fouling resistance and permeation performances of the TFC membranes, SKL was employed as a hydrophilic additive to modify the characteristics of the PA layer. To study the effect of SKL concentration on the performance of the TFC membranes,

different SKL concentrations of 1 wt%, 3 wt%, and 6 wt% were incorporated into the MPD solution to modify the PA layer of the TFC membranes. The performance of these membranes was compared with the performance of a pristine TFC membrane, synthesized without SKL. It was observed that the PA layer of the SKL-modified membranes possessed more free volumes, larger ridges and valleys, and a rougher surface in comparison with the pristine membrane. The water in air contact angle technique was used to investigate the surface wettability. It was found that the water contact angle declined from 88.7° ± 2.7° for the pristine membrane to 70.6° ± 1.3° for the 6 wt% SKL-incorporated membrane. The results of FO permeation tests showed that the membrane, modified with the highest content of SKL additive, 6 wt%, possessed 33.5 LMH water flux which was two folds higher than the water flux of the pristine membrane, using 2 M NaCl draw solution. The reverse salt flux for all the membranes was less than 7 gMH indicating that the addition of SKL into the PA layer did not have an adverse effect on the selectivity of this layer. The antifouling properties of the fabricated TFC membranes were evaluated against sodium alginate and SAGD BFW. It was observed that during the filtration of sodium alginate, the 6 wt% SKL-modified membrane provided the lowest flux decline ratio of 11.5% compared to the largest flux decline ratio of 18.9% for the pristine membrane. The 6 wt% SKL-modified membrane also showed the highest antifouling properties against BFW by flux decline ratio of 21.9% compared to 36.5% flux decline ratio of the pristine membrane. The findings of this work provide a guideline for the synthesis of high-performance TFC membranes through incorporating hydrophilic additives into the amine-aqueous solution.

5.2 Future work

Studies on the application of SKL as a hydrophilic blending agent for the modification of the bulk properties of membranes can be further extended by conducting proper techniques for evaluating the effect of SKL concentration on the porosity of the fabricated membranes. Additionally, more experiments are required to quantify the amount of SKL, leaching out of the polymeric film during the phase inversion and in long-term application. Moreover, a systematic study is required to investigate the effect of influential parameters such as the temperature of the polymer solution, the temperature of the coagulation bath, concentration and type of co-additives, and solvent type on the performance of the SKL-blended membranes. Additionally, simple and straightforward chemical techniques can be performed to modify SKL to improve the

compatibility of SKL with the host PES polymer.

The investigation on the potential of SKL for surface modification of the membranes can be developed by studying the effect of other parameters such as polyelectrolyte pH, deposition time, washing time, and support type. Moreover, employing different chemical modification techniques can increase the possibility of coating the surface of various supports and fabricating membranes with different properties. For instance, quaternary ammonium can be embedded on SKL, or silver nanoparticles can be coated on the SKL-modified membranes to introduce antibacterial properties to these membranes. Furthermore, proper techniques need to be employed to characterize the coating layer in terms of the thickness, surface charge, etc.

The studies on the application of SKL for improving the performance of the PA TFC membranes can be extended by investigating the effect of other parameters, including MPD concentration, surfactant concentration, impregnation time, TMC concentration, and monomer type, to improve the permeation and separation performance of the synthesized membranes. Further characterization is also required to quantify the amount of SKL entrapped inside the PA film. Additionally, various pretreatment techniques such as electrocoagulation and coagulation can be employed to investigate the effect of the pretreatment on the antifouling resistance of the TFC membranes.

5.3 List of contributions

5.3.1 Journal papers

1. L. Shamaei,P. Karami, B. Khorshidi, M. Sadrzadeh, Novel Lignin-modified Thin Film Composite Forward Osmosis Membranes: Waste Material for Wastewater Treatment, J. Memb. Sci. Under review.
2. L. Shamaei, B. Khorshidi, M.A. Islam, M. Sadrzadeh, Development of antifouling membranes using agro-industrial waste lignin for the treatment of Canada's oil sands produced water, J. Memb. Sci. 611 (2020) 118326. doi:10.1016/j.memsci.2020.118326.
3. L. Shamaei, B. Khorshidi, M.A. Islam, M. Sadrzadeh, Industrial waste lignin as an antifouling coating for the treatment of oily wastewater: creating wealth from waste, J. Clean. Prod. 256 (2020) 120304. doi:10.1016/j.jclepro.2020.120304.

5.3.2 Conference presentations

1. L. Shamaei, B. Khorshidi, M.A. Islam, M. Sadrzadeh, Development of antifouling membranes using agro-industrial waste lignin for the treatment of Canada's oil sands produced water, 12th International Congress on Membranes and Membrane Processes (ICOM), London, England, December 2020.
2. L. Shamaei, B. Khorshidi, M.A. Islam, M. Sadrzadeh, Industrial waste lignin as an antifouling coating for the treatment of oily wastewater: creating wealth from waste, 16th International Conference on Environmental Science and Technology (CEST), Rhodes, Greece, September 2019.
3. L. Shamaei, B. Khorshidi, B. Perdicakis, M. Sadrzadeh, Treatment of oil sands produced water using combined electrocoagulation and chemical coagulation techniques, 3rd International Conference on Desalination Using Membrane Technology, Gran Canaria, Spain, April 2019.

References

[1] WHO, Water, Sanitation and Hygiene, 2018.

[2] G.R. Xu, S.H. Wang, H.L. Zhao, S.B. Wu, J.M. Xu, L. Li, X.Y. Liu, Layer-by-layer (LBL) assembly technology as promising strategy for tailoring pressure-driven desalination membranes, J. Memb. Sci. 493 (2015) 428–443. doi:10.1016/j.memsci.2015.06.038.

[3] WWAP, The United Nations world water development report 2015: water for a sustainable world (WWAP), UNESCO, Paris, 2015.

[4] OECD, OECD environmental outlook to 2050 : the consequences of inaction., OECD Publishing, Paris, 2012.

[5] NRTEE, Changing currents: water sustainability and the future of Canada's natural resource sectors, The National Round Table on the Environment and Economy (NRTEE), 2010. doi:10.1108/ebr.2000.05412bab.008.

[6] S.M. Jordaan, Land and water impacts of oil sands production in Alberta, Environ. Sci. Technol. 46 (2012) 3611–3617. doi:10.1021/es203682m.

[7] NRCan, Water use by the natural resource sectors-facts, Natural Resources: Canada, 2010.

[8] AER, ST98: Alberta energy outlook, 2020.

[9] A. Orellana, I.J. Laurenzi, H.L. Maclean, J.A. Bergerson, Statistically enhanced model of in situ oil sands extraction operations: An evaluation of variability in greenhouse gas emissions, Environ. Sci. Technol. 52 (2018) 947–954. doi:10.1021/acs.est.7b04498.

[10] C. Atallah, A.Y. Tremblay, S. Mortazavi, Silane surface modified ceramic membranes for the treatment and recycling of SAGD produced water, J. Pet. Sci. Eng. 157 (2017) 349–358. doi:10.1016/j.petrol.2017.07.007.

[11] B. Khorshidi, Advanced Thin Film Composite and Nanocomposite Polyamide Membrane for Water Treatment, University of Alberta, 2017.

[12] M.A. Farrukh, Nanofiltration, IntechOpen, London, 2018.

[13] S.G. Thakurta, A. Maiti, D.J. Pernitsky, S. Bhattacharjee, Dissolved organic matter in steam assisted gravity drainage boiler blow-down water, Energy & Fuels. 27 (2013) 3883−3890. doi:10.1021/ef4002154.

[14] D.W. Jennings, A. Shaikh, B. Petrolite, W. Airport, V. Boule, S. Land, Heat-exchanger deposition in an inverted steam-assisted gravity drainage operation . Part 1 . Inorganic and organic analyses of deposit samples, Energy & Fuels. 21 (2007) 176–184. doi:10.1021/ef060109d.

[15] W.F. Heins, Technical advancements in SAGD evaporative produced water treatment, J. Can. Pet. Technol. 48 (2009) 27–32. doi:10.2118/130442-PA.

[16] L. Shamaei, B. Khorshidi, M.A. Islam, M. Sadrzadeh, Development of antifouling membranes using agro-industrial waste lignin for the treatment of Canada's oil sands produced water, J. Memb. Sci. 611 (2020) 118326. doi:10.1016/j.memsci.2020.118326.

[17] M. Mulder, Basic Principles of Membrane Technology, 1996.

[18] I. Pinnau, B.D. Freeman, Membrane formation and modification, 1999. doi:10.1021/bk-2000-

0744.ch001.

[19] Nidal Hilal Mohamed Khayet Chris J. Wright, ed., Membrane modification Technology and applications, Taylor & Francis Group, 2012.

[20] A. Lee, J.W. Elam, S.B. Darling, Membrane materials for water purification: Design, development, and application, Environ. Sci. Water Res. Technol. 2 (2016) 17–42. doi:10.1039/c5ew00159e.

[21] R.W. Baker, I.N. (Membrane Technology and Research, Membrane technology and applications, third, John Wiley and Sons Ltd, California, 2012.

[22] M.E. Ngai Yin Yip, Alberto Tiraferri, William A. Philip, Jessica D. Schiffman, High performance thin-film composite forward osmosis membrane, Environ. Sci. Technol. 44 (2010) 3812–3818.

[23] R.Y.S. Ho Kyong Shon, Sherub Phuntsho, Tian C. Zhang, Forward osmosis: Fundamentals and applications, Am. Soc. Civ. Eng. (2015) 505.

[24] S.S. Manickam, J.R. McCutcheon, Understanding mass transfer through asymmetric membranes during forward osmosis: A historical perspective and critical review on measuring structural parameter with semi-empirical models and characterization approaches, Desalination. 421 (2017) 110–126. doi:10.1016/j.desal.2016.12.016.

[25] Z. Wang, S. Dong, N. Li, X. Cao, M. Sheng, R. Xu, B. Wang, H. Wu, C. Ma, Y. Yuan, H. Xu, F. Chen, S. Zhao, CO2-selective membranes: How easy is their moving from laboratory to industrial scale?, Elsevier Inc., 2018. doi:10.1016/B978-0-12-813645-4.00003-9.

[26] S. Thomas, R. Wilson, A.K. S., S.C. George, Transport properties of polymeric membranes, Mathew Deans, 2018.

[27] H. Strathmann, K. Kock, The formation mechanism of phase inversion membranes, Desalination. 21 (1977) 241–255. doi:10.1016/S0011-9164(00)88244-2.

[28] P.A. H Strathman, K Kock, The formation mechanism of asymmetric membranes, Desulmurion. 16 (1975) 2746–2749.

[29] J.R. Fanchi, Integrated reservoir asset management, Elsevier Inc., 2010. doi:10.1016/C2009-0-62240-6.

[30] B. Kim, G. Gwak, S. Hong, Review on methodology for determining forward osmosis (FO) membrane characteristics: Water permeability (A), solute permeability (B), and structural parameter (S), Desalination. 422 (2017) 5–16. doi:10.1016/j.desal.2017.08.006.

[31] J.R. Mccutcheon, M. Elimelech, Influence of concentrative and dilutive internal concentration polarization on flux behavior in forward osmosis, J. Memb. Sci. 284 (2006) 237–247. doi:10.1016/j.memsci.2006.07.049.

[32] G.T. Gray, J.R. McCutcheon, M. Elimelech, Internal concentration polarization in forward osmosis: role of membrane orientation, Desalination. 197 (2006) 1–8. doi:10.1016/j.desal.2006.02.003.

[33] N.Y. Yip, A. Tiraferri, W.A. Phillip, J.D. Schi, L.A. Hoover, Y.C. Kim, M. Elimelech, Thin-film composite pressure retarded osmosis membranes for sustainable power generation from salinity gradients, Environ. Sci. Technol. 45 (2011) 4360–4369.

[34] A. Tiraferri, N.Y. Yip, A.P. Straub, S. Romero-Vargas Castrillon, M. Elimelech, A method for the simultaneous determination of transport and structural parameters of forward osmosis membranes, J. Memb. Sci. 444 (2013) 523–538. doi:10.1016/j.memsci.2013.05.023.

[35] N. Hilal, M. Khayet, C.J. Wright, eds., Membrane modifcation Technology and application, Taylor & Francis Group, 2012.

[36] K. Kimura, Y. Hane, Y. Watanabe, G. Amy, N. Ohkuma, Irreversible membrane fouling during ultrafiltration of surface water, Water Res. 38 (2004) 3431–3441. doi:10.1016/j.watres.2004.05.007.

[37] J.H. Jhaveri, Z.V.P. Murthy, A comprehensive review on anti-fouling nanocomposite membranes for pressure driven membrane separation processes, Desalination. 379 (2016) 137–154. doi:10.1016/j.desal.2015.11.009.

[38] F.A. et al. Escobar, Isabel C; Hoek, Eric M; Gabelich, Christopher J; DiGiano, Committee report: Recent advances and research needs in membrane fouling, Am. Water Work. Assoc. 97 (2005) 79–89.

[39] C. Das, K.A. Gebru, Polymeric membrane synthesis, modification, and applications electro-spun and phase inverted membranes, New York, 2019.

[40] B. Khorshidi, T. Thundat, B.A. Fleck, M. Sadrzadeh, A novel approach toward fabrication of high performance thin film composite polyamide membranes, Sci. Rep. 6 (2016) 1–10. doi:10.1038/srep22069.

[41] Z. Xu, L. Wan, X. Huang, Surface engineering of polymer membranes, 2009. doi:10.1007/978-3-540-88413-2.

[42] D.S. Wavhal, E.R. Fisher, Modification of polysulfone ultrafiltration membranes by CO2 plasma treatment, Desalination. 172 (2005) 189–205. doi:10.1016/j.desal.2004.06.201.

[43] E.S. Kim, Q. Yu, B. Deng, Plasma surface modification of nanofiltration (NF) thin-film composite (TFC) membranes to improve anti organic fouling, Appl. Surf. Sci. 257 (2011) 9863–9871. doi:10.1016/j.apsusc.2011.06.059.

[44] K.S. Kim, K.H. Lee, K. Cho, C.E. Park, Surface modification of polysulfone ultrafiltration membrane by oxygen plasma treatment, J. Memb. Sci. 199 (2002) 135–145. doi:10.1016/S0376-7388(01)00686-X.

[45] A.P. Straub, E. Asa, W. Zhang, T.H. Nguyen, M. Herzberg, In-situ graft-polymerization modification of commercial ultrafiltration membranes for long-term fouling resistance in a pilot-scale membrane bioreactor, Chem. Eng. J. 382 (2020) 122865. doi:10.1016/j.cej.2019.122865.

[46] T. Hong Anh Ngo, K. Dinh Do, D. Thi Tran, Surface modification of polyamide TFC membranes via redox-initiated graft polymerization of acrylic acid, J. Appl. Polym. Sci. 134 (2017) 1–8. doi:10.1002/app.45110.

[47] R. Lu, C. Zhang, M. Piatkovsky, M. Ulbricht, M. Herzberg, T.H. Nguyen, Improvement of virus removal using ultrafiltration membranes modified with grafted zwitterionic polymer hydrogels, Water Res. 116 (2017) 86–94. doi:10.1016/j.watres.2017.03.023.

[48] Y. Gu, B. Zhang, Z. Fu, J. Li, M. Yu, L. Li, J. Li, Poly (vinyl alcohol) modification of poly(vinylidene fluoride) microfiltration membranes for oil/water emulsion separation via an unconventional radiation method, J. Memb. Sci. 619 (2021). doi:10.1016/j.memsci.2020.118792.

[49] F. Liu, C.H. Du, B.K. Zhu, Y.Y. Xu, Surface immobilization of polymer brushes onto porous poly(vinylidene fluoride) membrane by electron beam to improve the hydrophilicity and fouling resistance, Polymer (Guildf). 48 (2007) 2910–2918. doi:10.1016/j.polymer.2007.03.033.

[50] L. Shen, H. Wang, Y. Zhang, R. Li, B. Fabien, G. Yu, H. Lin, B.Q. Liao, New strategy of grafting hydroxyethyl acrylate (HEA) via Γ ray radiation to modify polyvinylidene fluoride (PVDF) membrane: Thermodynamic mechanisms of the improved antifouling performance, Sep. Purif. Technol. 207 (2018) 83–91. doi:10.1016/j.seppur.2018.06.044.

[51] S.Y. Park, Y.J. Kim, S.Y. Kwak, Versatile surface charge-mediated anti-fouling UF/MF membrane comprising charged hyperbranched polyglycerols (HPGs) and PVDF membranes, RSC Adv. 6

(2016) 88959–88966. doi:10.1039/c6ra19020k.

[52] D.S. Wavhal, E.R. Fisher, Membrane surface modification by plasma-induced polymerization of acrylamide for improved surface properties and reduced protein fouling, Langmuir. 19 (2003) 79–85. doi:10.1021/la020653o.

[53] X. Chen, G. Huang, C. An, R. Feng, Y. Wu, C. Huang, Plasma-induced PAA-ZnO coated PVDF membrane for oily wastewater treatment: Preparation, optimization, and characterization through Taguchi OA design and synchrotron-based X-ray analysis, J. Memb. Sci. 582 (2019) 70–82. doi:10.1016/j.memsci.2019.03.091.

[54] H. Ju, B.D. McCloskey, A.C. Sagle, Y.H. Wu, V.A. Kusuma, B.D. Freeman, Crosslinked poly(ethylene oxide) fouling resistant coating materials for oil/water separation, J. Memb. Sci. 307 (2008) 260–267. doi:10.1016/j.memsci.2007.09.028.

[55] E. Igbinigun, Y. Fennell, R. Malaisamy, K.L. Jones, V. Morris, Graphene oxide functionalized polyethersulfone membrane to reduce organic fouling, J. Memb. Sci. 514 (2016) 518–526. doi:10.1016/j.memsci.2016.05.024.

[56] H. Susanto, M. Balakrishnan, M. Ulbricht, Via surface functionalization by photograft copolymerization to low-fouling polyethersulfone-based ultrafiltration membranes, J. Memb. Sci. 288 (2007) 157–167. doi:10.1016/j.memsci.2006.11.013.

[57] M.S.S.A. Saraswathi, D. Rana, S. Alwarappan, S. Gowrishankar, P. Vijayakumar, A. Nagendran, Polydopamine layered poly (ether imide) ultrafiltration membranes tailored with silver nanoparticles designed for better permeability, selectivity and antifouling, J. Ind. Eng. Chem. 76 (2019) 141–149. doi:10.1016/j.jiec.2019.03.014.

[58] M.A. Islam, J.-Y. Cho, K. Azyat, F. Mohammadtabar, F. Gao, M.J. Serpe, A.J. Myles, Y.-H. La, M. Sadrzadeh, Highly efficient antifouling coating of star-shaped block copolymers with variable sizes of hydrophobic cores and charge-neutral hydrophilic arms, ACS Appl. Polym. Mater. 3 (2021) 1116–1134. doi:10.1021/acsapm.0c01334.

[59] Q. Li, G.Q. Chen, L. Liu, S.E. Kentish, Spray assisted layer-by-layer assembled one-bilayer polyelectrolyte reverse osmosis membranes, J. Memb. Sci. 564 (2018) 501–507. doi:10.1016/j.memsci.2018.07.047.

[60] H. Zhang, J. Duan, C. Wang, Z. Wang, F. Yang, D. Jia, Cross-linked polyvinyl alcohol microspheres (PVA-MS) for modification of terylene microporous membranes self-assembled by a dynamic layer-by-layer technique, Microporous Mesoporous Mater. 132 (2010) 72–79. doi:10.1016/j.micromeso.2009.12.003.

[61] L. Liu, D.Y.W. Di, H. Park, M. Son, H. Hur, H. Choi, Improved antifouling performance of polyethersulfone (PES) membrane via surface modification by CNTs bound polyelectrolyte multilayers, R. Soc. Chem. Adv. 5 (2015) 7340–7348. doi:10.1039/c4ra14113j.

[62] J. Diep, A. Tek, L. Thompson, J. Frommer, R. Wang, V. Piunova, J. Sly, Y. La, Layer-by-layer assembled core-shell star block copolymers for fouling resistant water purification membranes, Polymer (Guildf). 103 (2016) 468–477. doi:10.1016/j.polymer.2015.11.048.

[63] by Z.D. Forshomi, Investigation of water treatment and steam generation alternatives for SAGD operations using process integration and optimization, UNIVERSITY OF CALGARY, 2015.

[64] B. Díez, R. Rosal, A critical review of membrane modification techniques for fouling and biofouling control in pressure-driven membrane processes, Nanotechnol. Environ. Eng. 5 (2020) 1–21. doi:10.1007/s41204-020-00077-x.

[65] A. Bhattacharya, B.N. Misra, Grafting: A versatile means to modify polymers: Techniques, factors

and applications, Prog. Polym. Sci. 29 (2004) 767–814. doi:10.1016/j.progpolymsci.2004.05.002.

[66] Z. Wang, X. Jiang, X. Cheng, C.H. Lau, L. Shao, Mussel-inspired hybrid coatings that transform membrane hydrophobicity into high hydrophilicity and underwater superoleophobicity for oil-in-water emulsion separation, ACS Appl. Mater. Interfaces. 7 (2015) 9534–9545. doi:10.1021/acsami.5b00894.

[67] P. Zhang, J. Qian, Y. Yang, Q. An, X. Liu, Z. Gui, Polyelectrolyte layer-by-layer self-assembly enhanced by electric field and their multilayer membranes for separating isopropanol – water mixtures, J. Memb. Sci. 320 (2008) 73–77. doi:10.1016/j.memsci.2008.03.055.

[68] Y. Huang, J. Sun, D. Wu, X. Feng, Layer-by-layer self-assembled chitosan/PAA nanofiltration membranes, Sep. Purif. Technol. 207 (2018) 142–150.

[69] J. Kochan, T. Wintgens, J.E. Wong, T. Melin, Properties of polyethersulfone ultrafiltration membranes modified by polyelectrolytes, Desalination. 250 (2010) 1008–1010. doi:10.1016/j.desal.2009.09.092.

[70] Z. Zhao, Z. Wang, S. Wang, Formation , charged characteristic and BSA adsorption behavior of carboxymethyl chitosan / PES composite MF membrane, J. Memb. Sci. 217 (2003) 151–158. doi:10.1016/S0376-7388(03)00105-4.

[71] S. Liang, P. Gao, X. Gao, K. Xiao, X. Huang, Improved blending strategy for membrane modification by virtue of surface segregation using surface-tailored amphiphilic nanoparticles, Front. Environ. Sci. Eng. 10 (2016) 1–9. doi:10.1007/s11783-016-0875-5.

[72] J. Zhang, Q. Wang, Z. Wang, C. Zhu, Z. Wu, Modification of poly(vinylidene fluoride)/polyethersulfone blend membrane with polyvinyl alcohol for improving antifouling ability, J. Memb. Sci. 466 (2014) 293–301. doi:10.1016/j.memsci.2014.05.006.

[73] A. Rahimpour, S.S. Madaeni, S. Mehdipour-Ataei, Synthesis of a novel poly(amide-imide) (PAI) and preparation and characterization of PAI blended polyethersulfone (PES) membranes, J. Memb. Sci. 311 (2008) 349–359. doi:10.1016/j.memsci.2007.12.038.

[74] Y. Kakihana, L. Cheng, L.F. Fang, S.Y. Wang, S. Jeon, D. Saeki, S. Rajabzadeh, H. Matsuyama, Preparation of positively charged PVDF membranes with improved antibacterial activity by blending modification: Effect of change in membrane surface material properties, Colloids Surfaces A Physicochem. Eng. Asp. 533 (2017) 133–139. doi:10.1016/j.colsurfa.2017.08.039.

[75] D. Liu, D. Li, D. Du, X. Zhao, A. Qin, X. Li, C. He, Antifouling PVDF membrane with hydrophilic surface of terry pile-like structure, J. Memb. Sci. 493 (2015) 243–251. doi:10.1016/j.memsci.2015.07.005.

[76] A. Behboudi, Y. Jafarzadeh, R. Yegani, Polyvinyl chloride/polycarbonate blend ultrafiltration membranes for water treatment, J. Memb. Sci. 534 (2017) 18–24. doi:10.1016/j.memsci.2017.04.011.

[77] T. Ahmad, C. Guria, A. Mandal, Enhanced performance of salt-induced Pluronic F127 and bentonite blended polyvinyl chloride ultrafiltration membrane for the processing of oilfield produced water, J. Water Process Eng. 34 (2020) 101144. doi:10.1016/j.jwpe.2020.101144.

[78] C. Cheng, L. Ma, D. Wu, J. Ren, W. Zhao, J. Xue, S. Sun, C. Zhao, Remarkable pH-sensitivity and anti-fouling property of terpolymer blended polyethersulfone hollow fiber membranes, J. Memb. Sci. 378 (2011) 369–381. doi:10.1016/j.memsci.2011.05.028.

[79] Q. Wu, G.E. Chen, W.G. Sun, Z.L. Xu, Y.F. Kong, X.P. Zheng, S.J. Xu, Bio-inspired GO-Ag/PVDF/F127 membrane with improved anti-fouling for natural organic matter (NOM) resistance, Chem. Eng. J. 313 (2017) 450–460. doi:10.1016/j.cej.2016.12.079.

[80] P. Kaner, E. Rubakh, D.H. Kim, A. Asatekin, Zwitterion-containing polymer additives for fouling resistant ultrafiltration membranes, J. Memb. Sci. 533 (2017) 141–159. doi:10.1016/j.memsci.2017.03.034.

[81] R. Kumar, A.M. Isloor, A.F. Ismail, S.A. Rashid, A. Al Ahmed, Permeation, antifouling and desalination performance of TiO2 nanotube incorporated PSf/CS blend membranes, Desalination. 316 (2013) 76–84. doi:10.1016/j.desal.2013.01.032.

[82] R.A. Damodar, S.J. You, H.H. Chou, Study the self cleaning, antibacterial and photocatalytic properties of TiO2 entrapped PVDF membranes, J. Hazard. Mater. 172 (2009) 1321–1328. doi:10.1016/j.jhazmat.2009.07.139.

[83] Y. Yang, H. Zhang, P. Wang, Q. Zheng, J. Li, The influence of nano-sized TiO2 fillers on the morphologies and properties of PSF UF membrane, J. Memb. Sci. 288 (2007) 231–238. doi:10.1016/j.memsci.2006.11.019.

[84] J. nan Shen, H. min Ruan, L. guang Wu, C. jie Gao, Preparation and characterization of PES-SiO2 organic-inorganic composite ultrafiltration membrane for raw water pretreatment, Chem. Eng. J. 168 (2011) 1272–1278. doi:10.1016/j.cej.2011.02.039.

[85] A.L. Ahmad, M.A. Majid, B.S. Ooi, Functionalized PSf/SiO2 nanocomposite membrane for oil-in-water emulsion separation, Desalination. 268 (2011) 266–269. doi:10.1016/j.desal.2010.10.017.

[86] S. Liang, K. Xiao, Y. Mo, X. Huang, A novel ZnO nanoparticle blended polyvinylidene fluoride membrane for anti-irreversible fouling, J. Memb. Sci. 394–395 (2012) 184–192. doi:10.1016/j.memsci.2011.12.040.

[87] C.P. Leo, W.P. Cathie Lee, A.L. Ahmad, A.W. Mohammad, Polysulfone membranes blended with ZnO nanoparticles for reducing fouling by oleic acid, Sep. Purif. Technol. 89 (2012) 51–56. doi:10.1016/j.seppur.2012.01.002.

[88] I. Akin, E. Zor, H. Bingol, M. Ersoz, Green synthesis of reduced graphene oxide/polyaniline composite and its application for salt rejection by polysulfone-based composite membranes, J. Phys. Chem. B. 118 (2014) 5707–5716. doi:10.1021/jp5025894.

[89] Z. Wang, H. Yu, J. Xia, F. Zhang, F. Li, Y. Xia, Y. Li, Novel GO-blended PVDF ultrafiltration membranes, Desalination. 299 (2012) 50–54. doi:10.1016/j.desal.2012.05.015.

[90] J. Huang, G. Arthanareeswaran, K. Zhang, Effect of silver loaded sodium zirconium phosphate (nanoAgZ) nanoparticles incorporation on PES membrane performance, Desalination. 285 (2012) 100–107. doi:10.1016/j.desal.2011.09.040.

[91] J. Huang, H. Wang, K. Zhang, Modification of PES membrane with Ag-SiO2: Reduction of biofouling and improvement of filtration performance, Desalination. 336 (2014) 8–17. doi:10.1016/j.desal.2013.12.032.

[92] T.A. Otitoju, A.L. Ahmad, B.S. Ooi, Recent advances in hydrophilic modification and performance of polyethersulfone (PES) membrane via additive blending, RSC Adv. 8 (2018) 22710–22728. doi:10.1039/c8ra03296c.

[93] N. Nady, M.C.R. Franssen, H. Zuilhof, M.S.M. Eldin, R. Boom, K. Schroën, Modification methods for poly(arylsulfone) membranes: A mini-review focusing on surface modification, Desalination. 275 (2011) 1–9. doi:10.1016/j.desal.2011.03.010.

[94] S. Bharathiraja, J. Suriya, M. Krishnan, P. Manivasagan, S.K. Kim, Production of enzymes from agricultural wastes and their potential industrial applications, 1st ed., Elsevier Inc., 2017. doi:10.1016/bs.afnr.2016.11.003.

[95] S. I., L. F., S. Martins, J. A., Use of agro-industrial wastes in solid-state fermentation processes, in:

Ind. Waste, 2012. doi:10.5772/36310.

[96] L. Manjarrez Nevárez, L. Ballinas Casarrubias, O.S. Canto, A. Celzard, V. Fierro, R. Ibarra Gómez, G. González Sánchez, Biopolymers-based nanocomposites: Membranes from propionated lignin and cellulose for water purification, Carbohydr. Polym. 86 (2011) 732–741. doi:10.1016/j.carbpol.2011.05.014.

[97] B.B. Mehta, R.N. Joshi, H.D. Raval, A novel ultra-low energy reverse osmosis membrane modified by chitosan with glutaraldehyde crosslinking, J. Appl. Polym. Sci. 135 (2018) 1–7. doi:10.1002/app.45971.

[98] R. Xu, P. Jiang, C. Wei, Z. Lü, S. Yu, M. Liu, C. Gao, Depositing sericin on partially degraded polyamide reverse osmosis membrane for restored salt rejection and simultaneously enhanced resistance to both fouling and chlorine, J. Memb. Sci. 545 (2018) 196–203. doi:10.1016/j.memsci.2017.09.073.

[99] Y.Z. Song, X. Kong, X. Yin, Y. Zhang, C.C. Sun, J.J. Yuan, B. Zhu, L.P. Zhu, Tannin-inspired superhydrophilic and underwater superoleophobic polypropylene membrane for effective oil/water emulsions separation, Colloids Surfaces A Physicochem. Eng. Asp. 522 (2017) 585–592. doi:10.1016/j.colsurfa.2017.03.023.

[100] Y.C. Xu, Y.P. Tang, L.F. Liu, Z.H. Guo, L. Shao, Nanocomposite organic solvent nanofiltration membranes by a highly-efficient mussel-inspired co-deposition strategy, J. Memb. Sci. 526 (2017) 32–42. doi:10.1016/j.memsci.2016.12.026.

[101] P. Qu, H. Tang, Y. Gao, L.P. Zhang, S. Wang, Polyethersulfone composite membrane blended With cellulose fibrils, BioResources. 5 (2010) 2323–2336. doi:10.15376/biores.5.4.2323-2336.

[102] Y. Manawi, V. Kochkoda, E. Mahmoudi, D.J. Johns, A. Wahab, Characterization and separation performance of a novel polyethersulfone membrane blended with acacia gum, Sci. Rep. 7 (2017) 1–12. doi:10.1038/s41598-017-14735-9.

[103] R.S. Kumar, G. Arthanareeswaran, D. Paul, J. Hyang, Effective removal of humic acid using xanthan gum incorporated polyethersulfone membranes, Ecotoxicol. Environ. Saf. 121 (2015) 223–228.

[104] G.P.S. Ibrahim, A.M. Isloor, A. Moslehyani, A.F. Ismail, Bio-inspired, fouling resistant, tannic acid functionalized halloysite nanotube reinforced polysulfone loose nanofiltration hollow fiber membranes for efficient dye and salt separation, J. Water Process Eng. 20 (2017) 138–148. doi:10.1016/j.jwpe.2017.09.015.

[105] M. Han, Q. Liu, B. Su, S. Sun, C. Zhao, Bioinspired polyethersulfone membrane design via blending with functional polyurethane, Int. J. Polym. Sci. 2017 (2017). doi:10.1155/2017/2158124.

[106] J.H. Jiang, L.P. Zhu, H.T. Zhang, B.K. Zhu, Y.Y. Xu, Improved hydrodynamic permeability and antifouling properties of poly(vinylidene fluoride) membranes using polydopamine nanoparticles as additives, J. Memb. Sci. 457 (2014) 73–81. doi:10.1016/j.memsci.2014.01.043.

[107] J. Tafreshi, H. Fashandi, Environmentally friendly modification of polysulfone ultrafiltration membrane using organic plant-derived nanoparticles prepared from basil seed gum (BSG) and Ar/O2 low-pressure plasma, J. Environ. Chem. Eng. 7 (2019) 103245. doi:10.1016/j.jece.2019.103245.

[108] M. Yong, Y. Zhang, S. Sun, W. Liu, Properties of polyvinyl chloride (PVC) ultra filtration membrane improved by lignin : Hydrophilicity and antifouling, J. Memb. Sci. 575 (2019) 50–59. doi:10.1016/j.memsci.2019.01.005.

[109] O. Gordobil, I. Egüés, R. Llano-ponte, J. Labidi, Physicochemical properties of PLA lignin blends,

Polym. Degrad. Stab. 108 (2014) 330–338. doi:10.1016/j.polymdegradstab.2014.01.002.

[110] E. Sjöström, Wood chemistry : fundamentals and applications, second, Harcourt Brace Jovanovich, 1993.

[111] T.P. Schultz, D.D. Nicholas, Lignin: Historical, Biological, and Materials Perspectives, American Chemical Society, Washington, DC, 1999. doi:10.1021/bk-2000-0742.

[112] F. Kong, S. Wang, W. Gao, P. Fatehi, Novel pathway to produce high molecular weight kraft lignin – acrylic acid polymers in acidic suspension systems, RSC Adv. 8 (2018) 12322–12336. doi:10.1039/C7RA12971H.

[113] S. Kubo, J.F. Kadla, Hydrogen bonding in lignin: A fourier transform infrared model compound study, Biomacromolecules. 6 (2005) 2815–2821. doi:10.1021/bm050288q.

[114] M.R. Barzegari, A. Alemdar, Y. Zhang, D. Rodrigue, Mechanical and rheological behavior of highly filled polystyrene with lignin, Polym. Compos. 33 (2012) 353–361. doi:10.1002/pc.

[115] N. Mahmood, Z. Yuan, J. Schmidt, C.C. Xu, Production of polyols via direct hydrolysis of kraft lignin: Optimization of process parameters, J-For. 4 (2014) 44–51. doi:10.1016/j.biortech.2013.03.199.

[116] M.N. Belgacem, A.E. Rodrigues, An integrated process to produce vanillin and lignin-based polyurethanes from Kraft lignin, Chem. Eng. Res. Des. 7 (2009) 1276–1292. doi:10.1016/j.cherd.2009.05.008.

[117] K.M. Davis, M. Rover, R.C. Brown, X. Bai, Z. Wen, L.R. Jarboe, Recovery and utilization of lignin monomers as part of the biorefinery approach, Energies. 9 (2016) 1–28. doi:10.3390/en9100808.

[118] A. Duval, S. Molina-Boisseau, C. Chirat, Comparison of kraft lignin and lignosulfonates addition to wheat gluten-based materials: Mechanical and thermal properties, Ind. Crops Prod. 49 (2013) 66–74. doi:10.1016/j.indcrop.2013.04.027.

[119] G. Chatel, R.D. Rogers, Review: Oxidation of lignin using ionic liquids-an innovative strategy to produce renewable chemicals, ACS Sustain. Chem. Eng. 2 (2014) 322–339. doi:10.1021/sc4004086.

[120] O. Ajao, J. Jeaidi, M. Benali, A.M. Restrepo, N. El Mehdi, Y. Boumghar, Quantification and variability analysis of lignin optical properties for colour-dependent industrial applications, Molecules. 23 (2018). doi:10.3390/molecules23020377.

[121] L. Shamaei, B. Khorshidi, M.A. Islam, M. Sadrzadeh, Industrial waste lignin as an antifouling coating for the treatment of oily wastewater: creating wealth from waste, J. Clean. Prod. 256 (2020) 120304. doi:10.1016/j.jclepro.2020.120304.

[122] M. Yong, Y. Zhang, S. Sun, W. Liu, Properties of polyvinyl chloride (PVC) ultrafiltration membrane improved by lignin: Hydrophilicity and antifouling, J. Memb. Sci. 575 (2019) 50–59. doi:10.1016/j.memsci.2019.01.005.

[123] A. Hasan, P. Fatehi, Synthesis and characterization of lignin–poly(acrylamide)–poly(2-methacryloyloxyethyl) trimethyl ammonium chloride copolymer, J. Appl. Polym. Sci. 135 (2018). doi:10.1002/app.46338.

[124] L. Zhang, J. Huang, Effects of nitrolignin on mechanical properties of polyurethane – nitrolignin films, J. Appl. Polym. Sci. 80 (2001) 1213–1219.

[125] V.K. Thakur, M.K. Thakur, P. Raghavan, M.R. Kessler, Progress in green polymer composites from lignin for multifunctional applications: A review, ACS Sustain. Chem. Eng. 2 (2014) 1072–1092. doi:10.1021/sc500087z.

[126] S.C. Gordts, G. Férir, T. D'Huys, M.I. Petrova, S. Lebeer, R. Snoeck, G. Andrei, D. Schols, The low-cost compound lignosulfonic acid (LA) exhibits broad-spectrum anti-HIV and anti-HSV activity and has potential for microbicidal applications, PLoS One. 10 (2015) 1–30. doi:10.1371/journal.pone.0131219.

[127] J. Gil-Chávez, P. Gurikov, X. Hu, R. Meyer, W. Reynolds, I. Smirnova, Application of novel and technical lignins in food and pharmaceutical industries: structure-function relationship and current challenges, Biomass Convers. Biorefinery. (2019). doi:10.1007/s13399-019-00458-6.

[128] Y. Hasegawa, Y. Kadota, C. Hasegawa, S. Kawaminami, Lignosulfonic acid-induced inhibition of intestinal glucose absorption, J. Nutr. Sci. Vitaminol. (Tokyo). 61 (2015) 449–454. doi:10.3177/jnsv.61.449.

[129] C. Lai, Z. Zhou, L. Zhang, X. Wang, Q. Zhou, Y. Zhao, Y. Wang, X.F. Wu, Z. Zhu, H. Fong, Free-standing and mechanically flexible mats consisting of electrospun carbon nanofibers made from a natural product of alkali lignin as binder-free electrodes for high-performance supercapacitors, J. Power Sources. 247 (2014) 134–141. doi:10.1016/j.jpowsour.2013.08.082.

[130] M. Ago, M. Borghei, J.S. Haataja, O.J. Rojas, Mesoporous carbon soft-templated from lignin nanofiber networks: Microphase separation boosts supercapacitance in conductive electrodes, RSC Adv. 6 (2016) 85802–85810. doi:10.1039/c6ra17536h.

[131] W. Zhang, M. Zhao, R. Liu, X. Wang, H. Lin, Hierarchical porous carbon derived from lignin for high performance supercapacitor, Colloids Surfaces A Physicochem. Eng. Asp. 484 (2015) 518–527. doi:10.1016/j.colsurfa.2015.08.030.

[132] M.J. Uddin, P.K. Alaboina, L. Zhang, S.J. Cho, A low-cost, environment-friendly lignin-polyvinyl alcohol nanofiber separator using a water-based method for safer and faster lithium-ion batteries, Mater. Sci. Eng. B Solid-State Mater. Adv. Technol. 223 (2017) 84–90. doi:10.1016/j.mseb.2017.05.004.

[133] S. V. Gnedenkov, D.P. Opra, S.L. Sinebryukhov, A.K. Tsvetnikov, A.Y. Ustinov, V.I. Sergienko, Hydrolysis lignin: Electrochemical properties of the organic cathode material for primary lithium battery, J. Ind. Eng. Chem. 20 (2014) 903–910. doi:10.1016/j.jiec.2013.06.021.

[134] M. Li, X. Jiang, D. Wang, Z. Xu, M. Yang, In situ reduction of silver nanoparticles in the lignin based hydrogel for enhanced antibacterial application, Colloids Surfaces B Biointerfaces. 177 (2019) 370–376. doi:10.1016/j.colsurfb.2019.02.029.

[135] D. Spasojević, D. Zmejkoski, J. Glamočlija, M. Nikolić, M. Soković, V. Milošević, I. Jarić, M. Stojanović, E. Marinković, T. Barisani-Asenbauer, R. Prodanović, M. Jovanović, K. Radotić, Lignin model compound in alginate hydrogel: A strong antimicrobial agent with high potential in wound treatment, Int. J. Antimicrob. Agents. 48 (2016) 732–735. doi:10.1016/j.ijantimicag.2016.08.014.

[136] J. Domínguez-Robles, N.K. Martin, M.L. Fong, S.A. Stewart, N.J. Irwin, M.I. Rial-Hermida, R.F. Donnelly, E. Larrañeta, Antioxidant pla composites containing lignin for 3D printing applications: A potential material for healthcare applications, Pharmaceutics. 11 (2019) 5–7. doi:10.3390/pharmaceutics11040165.

[137] Y. Wu, S. Zhang, X. Guo, H. Huang, Adsorption of chromium (III) on lignin, Bioresour. Technol. 99 (2008) 7709–7715. doi:10.1016/j.biortech.2008.01.069.

[138] T. Zhang, G. Cai, S. Liu, Application of lignin-based by-product stabilized silty soil in highway subgrade : A field investigation, J. Clean. Prod. 142 (2017) 4243–4257. doi:10.1016/j.jclepro.2016.12.002.

[139] T. Zhang, G. Cai, S. Liu, Assessment of mechanical properties in recycled lignin-stabilized silty soil as base fill material, J. Clean. Prod. 172 (2018) 1788–1799. doi:10.1016/j.jclepro.2017.12.011.

[140] T. Zhang, D. Ph, G. Cai, D. Ph, S. Liu, D. Ph, Application of lignin-stabilized silty soil in highway subgrade : A macroscale laboratory study, 30 (2018) 1–16. doi:10.1061/(ASCE)MT.1943-5533.0002203.

[141] G.D. Vilakati, E.M.V. Hoek, B.B. Mamba, Probing the mechanical and thermal properties of polysulfone membranes modified with synthetic and natural polymer additives, Polym. Test. 34 (2014) 202–210.

[142] G.D. Vilakati, E.M. V Hoek, B.B. Mamba, Investigating the structure and water permeation of membranes modified with natural and synthetic additives using tensile , porosity , and glass transition temperature studies, J. Appl. POLYMEIi Sci. (2014) 1–9. doi:10.1002/app.40616.

[143] Z. Ding, X. Liu, Y. Liu, L. Zhang, Enhancing the compatibility, hydrophilicity and mechanical properties of polysulfone ultrafiltration membranes with lignocellulose nanofibrils, Polymers (Basel). 8 (2016). doi:10.3390/polym8100349.

[144] Z. Ding, L. Zhong, X. Wang, L. Zhang, Effect of lignin-cellulose nanofibrils on the hydrophilicity and mechanical properties of polyethersulfone ultrafiltration membranes, High Perform. Polym. 28 (2016) 1192–1200. doi:10.1177/0954008315621611.

[145] R.J. Beck, Y. Zhao, H. Fong, T.J. Menkhaus, Electrospun lignin carbon nanofiber membranes with large pores for highly efficient adsorptive water treatment applications, J. Water Process Eng. 16 (2017) 240–248. doi:10.1016/j.jwpe.2017.02.002.

[146] M. Esmaeili, I. Anugwom, M. Mänttäri, M. Kallioinen, Utilization of DES-lignin as a bio-based hydrophilicity promoter in the fabrication of antioxidant polyethersulfone membranes, Membranes (Basel). 8 (2018) 1–16. doi:10.3390/membranes8030080.

[147] X. Zhang, J. Benavente, R. Garcia-Valls, Lignin-based membranes for electrolyte transference, J. Power Sources. 145 (2005) 292–297. doi:10.1016/j.jpowsour.2005.02.052.

[148] A. Zhou, C. Shi, X. He, Y. Fu, A.W. Anjum, J. Zhang, W. Li, Polyarylester nanofiltration membrane prepared from monomers of vanillic alcohol and trimesoyl chloride, Sep. Purif. Technol. 193 (2018) 58–68. doi:10.1016/j.seppur.2017.10.047.

[149] A. Colburn, R.J. Vogler, A. Patel, M. Bezold, J. Craven, C. Liu, D. Bhattacharyya, Composite membranes derived from cellulose and lignin sulfonate for selective separations and antifouling aspects, Nanomaterials. 9 (2019) 867. doi:10.3390/nano9060867.

[150] F. Zhang, Y. Wu, W. Li, W. Xing, Y. Wang, Depositing lignin on membrane surfaces for simultaneously upgraded reverse osmosis performances: An upscalable route, AIChE J. 63 (2017) 2221–2231. doi:10.1002/aic.15628.

[151] J. Marchese, M. Ponce, N.A. Ochoa, P. Prádanos, L. Palacio, A. Hernández, Fouling behaviour of polyethersulfone UF membranes made with different PVP, Membr. Sci. 211 (2003) 1–11.

[152] G.R. Guillen, Y. Pan, M. Li, E.M. V. Hoek, Preparation and characterization of membranes formed by nonsolvent induced phase separation: A review, Ind. Eng. Chem. Res. 50 (2011) 3798–3817. doi:10.1021/ie101928r.

[153] M. Hopp-Hirschler, U. Nieken, Modeling of pore formation in phase inversion processes: Model and numerical results, J. Memb. Sci. 564 (2018) 820–831. doi:10.1016/J.MEMSCI.2018.07.085.

[154] B. Khorshidi, A. Bhinder, T. Thundat, D. Pernitsky, M. Sadrzadeh, Developing high throughput thin film composite polyamide membranes for forward osmosis treatment of SAGD produced water, J. Memb. Sci. 511 (2016) 29–39. doi:10.1016/j.memsci.2016.03.052.

[155] M. Sadrzadeh, S. Bhattacharjee, Rational design of phase inversion membranes by tailoring thermodynamics and kinetics of casting solution using polymer additives, J. Memb. Sci. 441 (2013)

31–44. doi:10.1016/j.memsci.2013.04.009.

[156] N. Helali, M. Rastgar, M. Farhad Ismail, M. Sadrzadeh, Development of underwater superoleophobic polyamide-imide (PAI) microfiltration membranes for oil/water emulsion separation, Sep. Purif. Technol. 238 (2020) 116451. doi:10.1016/j.seppur.2019.116451.

[157] C.G. Boeriu, D. Bravo, R.J.A. Gosselink, J.E.G. Van Dam, Characterisation of structure-dependent functional properties of lignin with infrared spectroscopy, Ind. Crops Prod. 20 (2004) 205–218. doi:10.1016/j.indcrop.2004.04.022.

[158] F.H. Nour-Eddine El Mansouri, Qiaolong Yuan, Synthesis and characterization of kraft lignin-based epoxy resins, BioResources. 6 (2011) 2492–2503.

[159] O. Derkacheva, D. Sukhov, Investigation of lignins by FTIR spectroscopy, Macromol. Symp. 265 (2008) 61–68. doi:10.1002/masy.200850507.

[160] C. Crestini, H. Lange, M. Sette, D.S. Argyropoulos, On the structure of softwood kraft lignin, Green Chem. 19 (2017) 4104–4121. doi:10.1039/c7gc01812f.

[161] W. Gao, J.P.W. Inwood, P. Fatehi, Sulfonation of phenolated kraft lignin to produce water soluble products, J. Wood Chem. Technol. 39 (2019) 225–241. doi:10.1080/02773813.2019.1565866.

[162] J.P.W. Inwood, L. Pakzad, P. Fatehi, Production of sulfur containing kraft lignin products, BioResources. 13 (2018) 53–70. doi:10.15376/biores.13.1.53-70.

[163] H. Lou, H. Lai, M. Wang, Y. Pang, D. Yang, X. Qiu, B. Wang, H. Zhang, Preparation of lignin-based superplasticizer by graft sulfonation and investigation of the dispersive performance and mechanism in a cementitious system, Ind. Eng. Chem. Res. 52 (2013) 16101–16109.

[164] B. Khorshidi, J. Hajinasiri, G. Ma, S. Bhattacharjee, M. Sadrzadeh, Thermally resistant and electrically conductive PES/ITO nanocomposite membrane, J. Memb. Sci. 500 (2016) 151–160. doi:10.1016/j.memsci.2015.11.015.

[165] M. Han, S. Nam, Thermodynamic and rheological variation in polysulfone solution by PVP and its effect in the preparation of phase inversion membrane, J. Memb. Sci. 202 (2002) 55–61.

[166] A. Rahimpour, S.S. Madaeni, Polyethersulfone (PES)/cellulose acetate phthalate (CAP) blend ultrafiltration membranes: Preparation, morphology, performance and antifouling properties, J. Memb. Sci. 305 (2007) 299–312. doi:10.1016/j.memsci.2007.08.030.

[167] E. Saljoughi, M. Amirilargani, T. Mohammadi, Effect of PEG additive and coagulation bath temperature on the morphology, permeability and thermal/chemical stability of asymmetric CA membranes, DES. 262 (2010) 72–78. doi:10.1016/j.desal.2010.05.046.

[168] V.R.S.S. Mokkapati, D.Y. Koseoglu-Imer, N. Yilmaz-Deveci, I. Mijakovic, I. Koyuncu, Membrane properties and anti-bacterial/anti-biofouling activity of polysulfone-graphene oxide composite membranes phase inversed in graphene oxide non-solvent, RSC Adv. 7 (2017) 4378–4386. doi:10.1039/C6RA25015G.

[169] A. Karkooti, A. Zehtab, P. Chen, M. Mcgregor, N. Nazemifard, Development of advanced nanocomposite membranes using graphene nanoribbons and nanosheets for water treatment, J. Memb. Sci. 560 (2018) 97–107. doi:10.1016/j.memsci.2018.04.034.

[170] E. Saljoughi, M. Sadrzadeh, T. Mohammadi, Effect of preparation variables on morphology and pure water permeation flux through asymmetric cellulose acetate membranes, J. Memb. Sci. 326 (2009) 627–634.

[171] M. Amirilargani, M. Sadrzadeh, T. Mohammadi, Synthesis and characterization of polyethersulfone membranes, J. Polym. Res. 17 (2009) 363–377. doi:10.1007/s10965-009-9323-6.

[172] S. Salg, U. Salgı, N. Soyer, Streaming potential measurements of polyethersulfone ultrafiltration membranes to determine salt effects on membrane zeta potential, Int. J. Electrochem. Sci. 8 (2013) 4073–4084.

[173] G.B. T, R.H. Davisb, A.L. Zydney, The behavior of suspensions and macromolecular solutions in crossflow microfiltration, Membr. Sci. 96 (1994) 1–58.

[174] H.D. and A.L. A. Abdelrasoul, Fouling in membrane filtration and remediation methods, in: H. Nakajima (Ed.) (Ed.), Mass Transf. - Adv. Sustain. Energy Environ. Oriented Numer. Model., InTech, 2013.

[175] S. Huang, R.H.A. Ras, X. Tian, Antifouling membranes for oily wastewater treatment: Interplay between wetting and membrane fouling, Curr. Opin. Colloid Interface Sci. 36 (2018) 90–109. doi:10.1016/j.cocis.2018.02.002.

[176] B. Khorshidi, S.A. Hosseini, G. Ma, M. McGregor, M. Sadrzadeh, Novel nanocomposite polyethersulfone- antimony tin oxide membrane with enhanced thermal, electrical and antifouling properties, Polymer (Guildf). 163 (2019) 48–56. doi:10.1016/j.polymer.2018.12.058.

[177] V. Kochkodan, N. Hilal, A comprehensive review on surface modified polymer membranes for biofouling mitigation, Desalination. 356 (2015) 187–207. doi:10.1016/j.desal.2014.09.015.

[178] J. Tröger, K. Lunkwitz, W. Bürger, Determination of the surface tension of microporous membranes using contact angle measurements, J. Colloid Interface Sci. 286 (1997) 281–286.

[179] M. Hayatbakhsh, M. Sadrzadeh, D. Pernitsky, S. Bhattacharjee, J. Hajinasiri, Treatment of an in situ oil sands produced water by polymeric membranes, Desalin. Water Treat. 57 (2016) 14869–14887. doi:10.1080/19443994.2015.1069216.

[180] T.V. Nguyen, M.T.M. Pendergast, M.T. Phong, X. Jin, F. Peng, M.L. Lind, E.M.V. Hoek, Relating fouling behavior and cake layer formation of alginic acid to the physiochemical properties of thin film composite and nanocomposite seawater RO membranes, Desalination. 338 (2014) 1–9. doi:10.1016/j.desal.2014.01.013.

[181] A. Karkooti, M. Rastgar, N. Nazemifard, M. Sadrzadeh, Study on antifouling behaviors of GO modified nanocomposite membranes through QCM-D and surface energetics analysis, Colloids Surfaces A Physicochem. Eng. Asp. 588 (2020) 124332. doi:10.1016/j.colsurfa.2019.124332.

[182] S. Kasemset, Z. He, D.J. Miller, B.D. Freeman, M.M. Sharma, Effect of polydopamine deposition conditions on polysulfone ultrafiltration membrane properties and threshold flux during oil/water emulsion filtration, Polym. (United Kingdom). 97 (2016) 247–257. doi:10.1016/j.polymer.2016.04.064.

[183] F. Li, J. Meng, J. Ye, B. Yang, Q. Tian, C. Deng, Surface modification of PES ultrafiltration membrane by polydopamine coating and poly(ethylene glycol) grafting: Morphology, stability, and anti-fouling, Desalination. 344 (2014) 422–430. doi:10.1016/j.desal.2014.04.011.

[184] Z. Zhu, X. Feng, A. Penlidis, Layer-by-layer self-assembled polyelectrolyte membranes for solvent dehydration by pervaporation, Mater. Sci. Eng. 27 (2007) 612–619. doi:10.1016/j.msec.2005.12.002.

[185] D. Saeki, M. Imanishi, Y. Ohmukai, T. Maruyama, Stabilization of layer-by-layer assembled nano filtration membranes by crosslinking via amide bond formation and siloxane bond formation, J. Memb. Sci. 447 (2013) 128–133. doi:10.1016/j.memsci.2013.07.022.

[186] L. Wang, N. Wang, J. Li, J. Li, W. Bian, S. Ji, Layer-by-layer self-assembly of polycation/GO nanofiltration membrane with enhanced stability and fouling resistance, Sep. Purif. Technol. 160 (2016) 123–131. doi:10.1016/j.seppur.2016.01.024.

[187] H. Li, L. Peng, Antimicrobial and antioxidant surface modification of cellulose fibers using layer-by-layer deposition of chitosan and lignosulfonates, Carbohydr. Polym. 124 (2015) 35–42. doi:10.1016/j.carbpol.2015.01.071.

[188] F. Mohammadtabar, B. Khorshidi, A. Hayatbakhsh, M. Sadrzadeh, Integrated coagulation-membrane processes with zero liquid discharge (ZLD) configuration for the treatment of oil sands produced water, Water. 11 (2019) 1348.

[189] M.F. Ismail, B. Khorshidi, M. Sadrzadeh, New insights into the impact of nanoscale surface heterogeneity on the wettability of polymeric membranes, J. Memb. Sci. 590 (2019) 117270. doi:10.1016/J.MEMSCI.2019.117270.

[190] P. Kaner, D.J. Johnson, E. Seker, N. Hilal, S. Alsoy, Layer-by-layer surface modification of polyethersulfone membranes using polyelectrolytes and AgCl/TiO2 xerogels, J. Memb. Sci. 493 (2015) 807–819.

[191] T. Ishigami, K. Amano, A. Fujii, Y. Ohmukai, E. Kamio, T. Maruyama, H. Matsuyama, Fouling reduction of reverse osmosis membrane by surface modification via layer-by-layer assembly, Sep. Purif. Technol. 99 (2012) 1–7. doi:10.1016/j.seppur.2012.08.002.

[192] L. Deng, Q. Wang, X. An, Z. Li, Y. Hu, Towards enhanced antifouling and flux performances of thin-film composite forward osmosis membrane via constructing a sandwich-like carbon nanotubes-coated support, Desalination. 479 (2020) 114311. doi:10.1016/j.desal.2020.114311.

[193] B. Khorshidi, B. Soltannia, T. Thundat, M. Sadrzadeh, Synthesis of thin film composite polyamide membranes: Effect of monohydric and polyhydric alcohol additives in aqueous solution, J. Memb. Sci. 523 (2017) 336–345. doi:10.1016/j.memsci.2016.09.062.

[194] K.Y. Wang, T.-S. Chung, G. Amy, Developing thin-film-composite forward osmosis membranes on the PES/SPSf substrate through interfacial polymerization, AIChE J. 58 (2012) 770–781. doi:10.1002/aic.12635.

[195] T.D. and I.F.J.V. Chalida Klaysom, Tazhi Y. Cath, Forward and pressure retarded osmosis: potential solutions for global challenges in energy and water supply, Chem. Soc. Rev. 42 (2013) 6959–6989. doi:10.1039/c3cs60051c.